

**SILICEOUS DOLOMITES IN THE HORSETHIEF CREEK**

**AUREOLE, S.E. BRITISH COLUMBIA:**

**FLUID INFILTRATION AND MINERAL REACTIONS**

by

**MARIA C. NIERMANN**

A THESIS SUBMITTED IN PARTIAL FULFILLMENT OF THE REQUIREMENTS FOR

THE DEGREE OF MASTER OF SCIENCE

in

THE FACULTY OF GRADUATE STUDIES

(Department of Earth and Ocean Sciences)

We accept this thesis as conforming to the required standard

THE UNIVERSITY OF BRITISH COLUMBIA

November, 1998

© Maria C. Niermann, 1998

In presenting this thesis in partial fulfilment of the requirements for an advanced degree at the University of British Columbia, I agree that the Library shall make it freely available for reference and study. I further agree that permission for extensive copying of this thesis for scholarly purposes may be granted by the head of my department or by his or her representatives. It is understood that copying or publication of this thesis for financial gain shall not be allowed without my written permission.

Department of EOS - Geology

The University of British Columbia  
Vancouver, Canada

Date Nov. 9, 1998

## ABSTRACT

Potassic siliceous dolomites in the Horsethief Creek aureole, S.E. British Columbia, Canada record peak contact-metamorphic conditions of  $\approx 2.2$  kbars and  $650^\circ\text{C}$  in the inner aureole. The protolithic dolostones have varying but small amounts of disseminated quartz ( $\leq 5$  volume percent) and K-feldspar ( $\leq 15$  volume percent) but have interbedded numerous chert nodules and layers. Subvertical joints and veins cut across layering. Six isograds can be identified: phlogopite; tremolite+K-feldspar; diopside; diopside+phlogopite; diopside+dolomite; and at highest grade forsterite.

The prevalence of isobarically divariant mineral assemblages, paucity of high  $X_{\text{CO}_2}$  mineral assemblages, widespread development of hydrous minerals often in high abundance (up to 65 volume percent) and a  $\approx 7$  per mill (‰) depletion (from  $\approx 23$  ‰ to  $\approx 16$  ‰) in  $\delta^{18}\text{O}$  are all evidence for substantial syn-metamorphic fluid flow. The almost complete de-dolomization of the inner and middle aureole suggests that metamorphism was not isochemical and that silica-metasomatism took place. Heterogeneity in the distribution of index minerals and the potassic phases reflect varying bulk composition as well as variable fluid infiltration. Infiltration-driven near-isothermal reactions are documented in the rocks in form of numerous samples showing a texture interpreted to record prograde reaction of diopside to tremolite.

A petrographic break is observed at the tremolite+K-feldspar isograd. While rocks up-grade of this isograd are dominated by isobarically divariant assemblages, rocks down-grade are characterized by isobarically univariant assemblages. This break may record a sudden change in infiltration character.

The proposed model of contact metamorphism in the impure siliceous dolomites of the Horsethief Creek aureole is: 1) Intrusion of the Horsethief pluton triggered metamorphic reactions in the siliceous dolomites and the underlying pelitic rocks. 2) Buoyant fluids evolving in the metapelites at temperatures  $>530^\circ\text{C}$  rose along subvertical joints in and across the different

lithologies and infiltrated the dolostone. 3) Infiltration of silica-bearing aqueous fluids triggered pervasive reaction in the siliceous dolomites. Rocks in the outer aureole did not experience significant infiltration because temperatures were too low to trigger the dehydration reaction in the underlying metapelites. Plutonic fluids may only have played a minor role, and bedding parallel flow likely was also only minor.

## TABLE OF CONTENTS

ABSTRACT.....	ii
TABLE OF CONTENTS.....	iv
LIST OF TABLES .....	vii
LIST OF FIGURES.....	viii
LIST OF PLATES.....	ix
ACKNOWLEDGEMENTS.....	x
<b><u>1.0 INTRODUCTORY STATEMENTS</u></b>	<b><u>1</u></b>
1.1 Structure of Thesis.....	1
1.2 Introduction .....	1
1.3 The T-X <sub>CO2</sub> Diagram.....	7
<b><u>2.0 GEOLOGICAL SETTING</u></b>	<b><u>10</u></b>
2.1 Regional Geology.....	10
2.2 Local Geology.....	12
<b><u>3.0 MINERALOGY AND MINERAL CHEMISTRY</u></b>	<b><u>18</u></b>
3.1 Introduction .....	18
3.2 Metamorphic Zones.....	20
3.2.1 Phlogopite zone.....	20
3.2.2 Tremolite + K-feldspar zone.....	28
3.2.3 Diopside zone.....	30
3.2.4 Diopside + Phlogopite zone.....	30

3.2.5 Diopside + Dolomite zone.....	32
3.2.6 Forsterite zone.....	34
<b>3.3 Mineral Chemistry.....</b>	<b>36</b>
<b><u>4.0 CONTROLLING FACTORS ON THE DEVELOPMENT OF</u></b>	
<b><u>THE METAMORPHIC MINERAL ASSEMBLAGES</u></b>	<b>40</b>
<hr/>	
<b>4.1 Introduction .....</b>	<b>40</b>
<b>4.2 Effects of Bulk-Compositional Variations .....</b>	<b>40</b>
<b>4.3 Thermal Controls .....</b>	<b>44</b>
<b>4.4 Fluid Infiltration .....</b>	<b>51</b>
4.4.1 Nominally retrograde assemblages .....	52
4.4.2 Reaction of diopside to tremolite - Textural evidence for infiltration- triggered near-isothermal reaction .....	52
4.4.3 $\delta^{18}\text{O}$ whole rock carbonate data .....	54
4.4.4 Silica metasomatism and intensity of infiltration .....	58
<b>4.5 Discussion of Possible Fluid Flow Direction(s), Fluid Source(s)     and Heat Advection .....</b>	<b>60</b>
4.5.1 Heat flow - conductive or advective? .....	60
4.5.2 Discussion of the possibility of horizontal fluid flow in the direction of increasing temperature .....	62
4.5.3 Discussion of the possibility of horizontal fluid flow in the direction of decreasing temperature .....	65
4.5.4 Discussion of the possibility of vertical fluid flow .....	67
4.5.4.1 <i>Metamorphism of the pelite and its implication for                 the siliceous dolomite.....</i>	68
4.5.4.2 <i>Metamorphism of the siliceous dolomite in the middle aureole.....</i>	69
4.5.4.3 <i>Metamorphism of the siliceous dolomite in the                 tremolite + K-feldspar zone.....</i>	71
4.5.4.4 <i>The <math>T_{max}</math> - profile.....</i>	71

4.5.4.5 <i>The inner aureole - a special case</i> .....	72
<b>4.6 The Petrographic Break - A Change in Infiltration Character</b> .....	<b>73</b>
4.6.1 A model of diachronous heat and (horizontal) fluid flow.....	75
4.6.2 A model of vertical fluid flow.....	79
<b>5.0 SUMMARY AND CONCLUSION</b> .....	<b>82</b>
<b>REFERENCES</b> .....	<b>85</b>
<b>APPENDICES</b>	
<b>Appendix A:</b> Electronmicroprobe Data and Geothermometry Results .....	91
<b>Appendix B:</b> XRF Data .....	108
<b>Appendix C:</b> Stable Isotope Data .....	113
Appendix C1: Stable Isotopes- Methods, Data and $\delta^{13}\text{C}$ - Signature .....	114
Appendix C2: Silica Weight Percent (whole rock) versus $\delta^{18}\text{O}$ data	
- Evidence for Silica Metasomatism .....	116
<b>Appendix D:</b> Mineral Formulas and Molar Volumes .....	117
<b>Appendix E:</b> Sample Number Conversion .....	119

## LIST OF TABLES

Table	Page
1. List of peak metamorphic assemblages .....	22
2. Selected results of quantitative analyses of silicates and carbonates .....	37
3. List of maximum stability ranges and .....	45

## LIST OF FIGURES

Figure	Page
1. Introductory T-X <sub>CO2</sub> diagram .....	8
2. Map of the regional geology of the Horsethief Creek area .....	11
3. Geological map of the working area .....	13
4. T-X <sub>CO2</sub> diagram for KCMAS-HC system at P=2.2kb .....	19
5. Map showing the six isograds .....	21
6. F-content in phlogopites .....	39
7. Major element whole rock analyses .....	41
8. Mineral facies diagrams (projected on Qtz-Dol-Ksp plane) .....	43
9. Map showing situation after elimination of bulk compositional effects .....	46
10. T-X <sub>CO2</sub> diagram illustrating effects of thermal controls .....	47
11. Geothermometry data .....	49
12. T-X <sub>CO2</sub> diagram illustrating isothermal reaction .....	53
13. Oxygen isotope analyses.....	56
14. Oxygen isotope ranges of selected geological materials.....	57
15. Diagrams showing the process of 'annealing' of low-grade rocks.....	76

## LIST OF PLATES

Plate	Page
1. View of the field area.....	15
2. Typical veining observed in siliceous dolomites.....	17
3. Phlogopite zone rock with normal low phlogopite abundance.....	24
4. a and b) High abundance phlogopite in deformed phlogopite zone rock .....	25
5. Phlogopite concentration in vein in rock from phlogopite zone.....	26
6. Typical 'protolithic' rock with chert nodules and veining.....	27
7. Typical tremolite - calcite - K-feldspar assemblage.....	29
8. a and b) Reaction texture of diopside to tremolite.....	31
9. Bleaching along chert layer.....	33
10. a and b) Cross cut of a vein with mineral assemblages indicating local silica enrichment.....	35

## ACKNOWLEDGMENTS

I like to thank the members of my supervisory committee Greg Dipple, Tom Brown, Kelly Russell and Lori Kennedy for their support and discussions during my time at UBC. Special thanks to my main supervisor Greg Dipple whose door was always open and from whom I learned a lot over the years.

Thanks to the MDRU for letting me use their facilities, to UBC-geochron people namely Jim Mortenson and Rich Friedman for their ready help on thesis work, and to Mati Raudsepp for his patience with me during my S.E.M. and microprobe work.

Thanks also to Terry Gordon and Dave Pattison who, from the beginning on, shared their enthusiasm for this project with me, the former adding a lot of extra fun to my first field season. Many thanks to my field assistants, especially Anne Bagley who probably was the best field assistant one can have in a rainy, snowy and physically very challenging season. The 'pain' of this hard season, as well as the second season in 1996, was significantly eased by the extra effort of 'Helicopter-John' and the fabulous support by the Madsons out of Invermere.

I also like to express my thanks to Nathalie Marchildon, without whose help my start at UBC would have been so much more difficult, and to Peter Alt-Epping, Art Calderwood and Mathias Westphal for the interesting discussions and the phantastic support during the last 'hot' phase of writing this thesis. Many thanks also to my mother, especially for the financial support for my 'round the globe trips'.

'Danke' also to my friends back in / from Germany for their never-ending support and concern, especially to Magdalena & Michael. Very special thanx for the 'personal' support also to Susannah, Art, Shin Yi, Mathias and especially Peter who kept me going

- Ta and Good Luck to you!

# CHAPTER 1

## INTRODUCTORY STATEMENTS

### 1.1 Structure of Thesis

Most of the thesis addresses the petrography of mineral assemblages that developed in siliceous dolomites in a contact aureole adjacent to the Horsethief Creek pluton and the analysis of oxygen isotope data from these rocks. These data are used to develop a model of contact metamorphism in the Horsethief Creek siliceous dolomites. Additional data - carbon stable isotopes and whole rock compositions - are used in support of a model involving local, pervasive silica metasomatism as briefly discussed in Appendices B and C.

I first discuss a few basics of the interpretation of contact-metamorphic siliceous dolomites in paragraph 1.3 by explaining some of the principles of the temperature (T) -  $X_{\text{CO}_2}$  diagram, where  $X_{\text{CO}_2}$  is the mole fraction of  $\text{CO}_2$  in a binary  $\text{H}_2\text{O} - \text{CO}_2$  fluid. This diagram is routinely used in the interpretation of the metamorphic evolution of siliceous dolomites.

### 1.2 Introduction

The mineralogy developing in chemically simple siliceous dolomites during metamorphism is sensitive to the amount and composition of fluid they interact with. Mineral abundance and composition commonly allow for determination of the amount of influx, fluid source(s) and possible metasomatic changes (e.g., Bucher-Nurminen 1982, Hover Granath *et al.* 1983, Ferry

1991, Holness 1992, Ferry 1994). Stable isotope analyses in combination with petrographic observations provide an additional powerful tool to decipher the infiltration history of these rocks (Lattanzi *et al.* 1980; Nabalek *et al.* 1984, Bowman 1994, Holness and Fallick 1997).

The succession of mineral assemblages in siliceous dolomites of different contact aureoles is often observed to be different from each other. Assemblages vary in spatial distribution and/or can be of different variances depending on amounts of fluid infiltration and/or differences in flow direction. Ferry (1994) and Dipple and Ferry (1996) showed in a systematic way which mineral assemblage successions are expected to develop in an aureole depending on (a) whether the fluid flow is in direction of increasing temperature (up-T) or in the direction of decreasing temperature (down-T), and (b) the absolute amount of infiltration. They used a 1-dimensional model of coupled fluid flow and mineral reaction (and heat flow in Dipple and Ferry 1996) in rocks with 10 mol% quartz and 90 mol% dolomite, a bulk composition similar to that observed in many contact-metamorphic siliceous dolomites.

In numerous contact aureoles siliceous dolomites with predominantly isobarically univariant assemblages are observed (Rice, 1977a,b; Suzuki, 1977). This makes it possible to trace reaction paths, and in many cases progressive metamorphism is proposed for these aureoles (i.e., high grade assemblages developed through all the lower grade stages that are now found in the aureole). These aureoles are interpreted to have experienced up-T fluid flow (Ferry, 1994).

Other aureoles exhibit a change in the prevalent variance of assemblages over distance. Predominantly isobarically univariant or isobarically univariant 'key' ('key' with respect to the determination of fluid flow direction) and divariant assemblages are found throughout the aureole, except for the innermost part (usually <150 m from the contact with the intrusion). Here rocks contain periclase or forsterite in predominantly isobarically divariant assemblages (Holness 1992, Moore and Kerrick 1977, Bowman *et al.* 1994). The observed mineral assemblages in aureoles like these require down-T flow in the inner aureole and possibly up-T flow in (at least parts of) the rest of the aureole (Ferry 1994, Dipple and Ferry 1996). Interestingly the observed  $\delta^{18}\text{O}$  isotope

signature sometimes allows for an interpretation of down-T flow in all of the aureole (Bowman *et al.* 1994).

In contrast, mineral assemblages in the siliceous dolomites of the Elkhorn aureole are dominantly isobarically divariant assemblages throughout the aureole except for the periclase zone (<20 m). Here, generally isobarically univariant periclase assemblages are developed (Bowman and Essene 1982). Fluid flow is interpreted to have been vertical in the periclase zone and down-T in the rest of the aureole (Ferry 1994). This interpretation of vertical fluid flow in the inner aureole is in accordance with observations in massive garnet-pyroxen skarns that formed in reentrants of the pluton-wallrock contact. These were also interpreted to have experienced vertical fluid flow (Bowman *et al.* 1985).

The special character of the zone closest to the contact is underlined by the occasional observation of signs of (silica-) metasomatism in this area. For example, forsterite in the inner part of the Adamallo aureole was formed in significantly higher abundance than metamorphic silicates in the outer aureole. It was suggested that the forsterite formed by reaction of dolomite with SiO<sub>2</sub> dissolved in fluid emanating from the igneous body (Bucher-Nurminen 1994).

In most of these aureoles, independent of flow direction, the fluid flow is interpreted to have been heterogeneous. The scatter in isotope values and in the spatial distribution of mineral assemblages commonly cannot be explained if total influx was the same in all areas (Ferry 1994). However, these heterogeneities can be reproduced by models of fluid flow in rocks with heterogeneous permeability (Gerdes *et al.*, 1995; Marchildon and Dipple, 1998). In summary it can be said that hydrologic models for fluid flow in contact aureoles are diverse and potentially very complex.

The complexity of the issue of fluid flow in carbonate rocks is underlined by the problems of understanding infiltration mechanism. Massive, pure carbonate rocks are generally not susceptible to pervasive grain-boundary flow of H<sub>2</sub>O-CO<sub>2</sub> fluids under normal metamorphic pressure-temperature conditions. Experiments with monomineralic carbonates (under static

conditions) showed that pervasive fluid flow along grain boundaries is essentially impossible in dolomites and restricted to low pressure (<1.5 kilobars (kbar)) and fluids with intermediate H<sub>2</sub>O-CO<sub>2</sub> compositions or strong brines in calcite; the dihedral angle theta is always larger than the critical angle of 60° (Holness and Graham 1995, Hay and Evans 1988).

Experiments with monomineralic quartz show similar results. The dihedral angle for grains in equilibrium with a H<sub>2</sub>O fluid is only smaller than 60° at low temperatures (<350 °C) or at high pressures (>8 kbar) (Holness 1993). In the presence of a CO<sub>2</sub> fluid theta is always larger than 60°.

The experimental results are generally confirmed by field observations. Massive, pure limestone in metamorphic terrains show no or only small isotopic alteration even if they are adjacent to lithologies that experienced large influxes and show significant isotope depletion (e.g., Nabalek *et al.* 1984, Schliestedt and Matthews 1987, Jamtveit *et al.* 1992). Quartz or chert layers are occasionally interpreted to be permeable (e.g., Heinrich 1993) but infiltration might have been channeled mostly along the lithologic boundaries (Jamtveit *et al.* 1992, Walther 1996).

Consequently, in rocks similar to the monomineralic samples used in experiments, fluid flow under metamorphic conditions is interpreted to occur only or predominantly along fractures. It is not clear however, what percentage of for example carbonate minerals in a rock is sufficient to give the rock the overall permeability behavior of a pure (dolo)marble. Some authors suggest that minerals that make up only about 30 - 40 percent of a rock determine its overall (grain boundary) permeability behavior (Holness and Graham 1991, and citations therein). These values appear to be low. With up to 70 volume percent other material in the rock the possibility of the formation of a interconnected network of fluid 'channels' along grain boundaries seems possible.

In nature, most rocks are not monomineralic but exhibit at least low abundances of other minerals, and many natural (impure) carbonate rocks in metamorphic terrains show signs of fluid infiltration. For example all the above mentioned contact-metamorphic siliceous dolomites have quartz contents of about 5 - 15 volume percent (vol%) in the protolithic rocks and show (with

increasing metamorphic grade) mineral reactions and isotopic depletion that generally require low to moderate amounts of fluid infiltration (Dipple and Ferry 1996). Hence, some processes must enhance permeability of these rocks. Etheridge et al. (1983, p.219) noted that the "main controls on permeability are rock type and structure. The lithological influence will result largely from differences in microstructural behaviour and rate of fluid production, rather than of primary porosity."

There are at least three very potent mechanisms, which are coupled to some degrees, that can cause permeability enhancement in massive rocks. These are (a) reaction-enhanced permeability, (b) hydrofracturing, and (c) deformation.

Reaction often enhances permeability because the volume of the produced minerals is (usually) smaller than the volume of the reactants. This leads to an increase in porosity which, if it (at least partially) can be kept open against the pressure of compaction, leads to an increase in permeability (Etheridge *et al.* 1983, Ortoleva *et al.* 1987). Additionally if the reactions are devolatilisation reactions, large volumes of volatiles are liberated. This either is supportive of keeping the increased porosity open (against the pressure of compaction), or, if volume reduction of the solids is small, devolatilisation would lead to hydrofracturing. Fluid pressure increases up to or above lithostatic pressure (or, the least compressive stress  $\sigma_3$ ) at which point the pores crepitate and the fluids are expelled into the surrounding area by hydro-fracturing (e.g., Fyfe *et al.* 1978). This in turn can lead to further reaction in the infiltrated region, if fluid infiltration is able to speed up the rate limiting process of reaction. Rocks in which no (devolatilisation) reaction occurs would experience only minor hydro-fracturing. With a sufficient increase in temperature the very small amounts of pore fluids can reach fluid pressures larger than the lithostatic pressure of the rocks. If these two rock types are interlayered, for example in form of "permeable" pelites and "impermeable" carbonates, the carbonate could be affected by the enhanced infiltration in the more permeable pelites. This can lead to increased advective-diffusive infiltration into the

carbonate near the lithologic contact (e.g., Bickle and Baker 1990, Jamtveit *et al.* 1992, Cartwright and Weaver 1997).

Deformation is another process interpreted to be effective in enhancing permeability by crystal plastic mechanisms or some other mass transport mechanism (Etheridge *et al.* 1983, Holness 1997).

In recent years studies have increasingly focused on the complexity in the interplay between heating, structural influences, fluid flow and reaction and their effects on the permeability structure (e.g., Etheridge *et al.* 1983, Nabalek *et al.* 1992, Dutrow and Norton 1995, Holness 1997, and in a review by Ferry 1994).

In this study I describe the mineralogy, mineral chemistry and isotope signature of siliceous dolomites in the Horsethief Creek contact-metamorphic aureole in south-eastern British Columbia, Canada. The siliceous dolomites show a normal prograde sequence of isograds but some features are of special interest and attest to the complexity of the contact-metamorphic process. Throughout the mid to inner aureole ( $\leq 1250$  m from contact) almost all assemblages are isobarically divariant and most rocks are completely de-dolomized. Metamorphic minerals occur in unusually high abundance and pervasive distribution, and index minerals are heterogeneously distributed. An abrupt change from predominantly isobarically divariant assemblages in the inner and middle aureole to isobarically univariant assemblages in the outermost aureole is observed in the Horsethief Creek siliceous dolomites. The peak temperature profile and the isotope signature of the aureole also are unusual.

The development of the mineral assemblages in the Horsethief Creek aureole must have been influenced by varying bulk composition, temperature, and spatially and temporally heterogeneous fluid infiltration. An attempt is made to outline a model that satisfactorily explains the distribution of mineral assemblages and most of the features special to this aureole.

### 1.3 The T- $X_{\text{CO}_2}$ diagram

Mineral assemblages in contact-metamorphic siliceous dolomites are commonly used to interpret fundamental aspects of metamorphic fluid flow. Carbonate rocks are particularly useful for this purpose because they are chemically and mineralogically simple and sensitive to the amount and composition of an infiltrating fluid. This leads to the development of only a small number of characteristic mineral assemblages in the temperature range typical for metamorphism. The developed mineral assemblages commonly are the result of infiltration-triggered reaction.

Two reaction paths in a T- $X_{\text{CO}_2}$  diagram are used to illustrate the interaction of siliceous carbonitic rocks and a  $\text{H}_2\text{O}-\text{CO}_2$  fluid. These diagrams are commonly used to depict mineral assemblages and reaction paths for impure carbonate rocks. Fluid pressure (P) is assumed to be constant. Hence, they should be applied with caution in regional metamorphic rocks but are generally considered to be applicable on the small scale of a contact aureole.

Figure 1 shows a simple T- $X_{\text{CO}_2}$  diagram at  $P=1\text{kbar}$ . The  $X_{\text{CO}_2}$  is the  $X_{\text{CO}_2}$  of a fluid in contact with the rock. If the protolithic dolomite - quartz rock is heated without infiltration, the reaction path will follow reaction curves (path 1). This results in the formation of isobarically univariant assemblages where usually only small amounts of products are found besides the reactants. Little reaction progress of the devolatilisation reactions is sufficient to change the fluid composition of the small amount of fluid present in the pore space. As soon as rock and fluid are in equilibrium reaction ceases for a given temperature. This kind of reaction is referred to as an internally (by the rock) buffered reaction (Greenwood 1975).

If on the other hand the rocks are infiltrated by an infinite amount of  $\text{H}_2\text{O}$ -fluid during heating the  $\text{CO}_2$  produced during reaction is not sufficient to change the fluid- $X_{\text{CO}_2}$  and the reactions will continue at the  $X_{\text{CO}_2}$  of the infiltrating fluid until at least one of the reactants is completely exhausted (path 2). This is followed by a temperature increase at constant  $X_{\text{CO}_2}$ . The resulting assemblages are referred to as isobarically divariant assemblages as they are represented

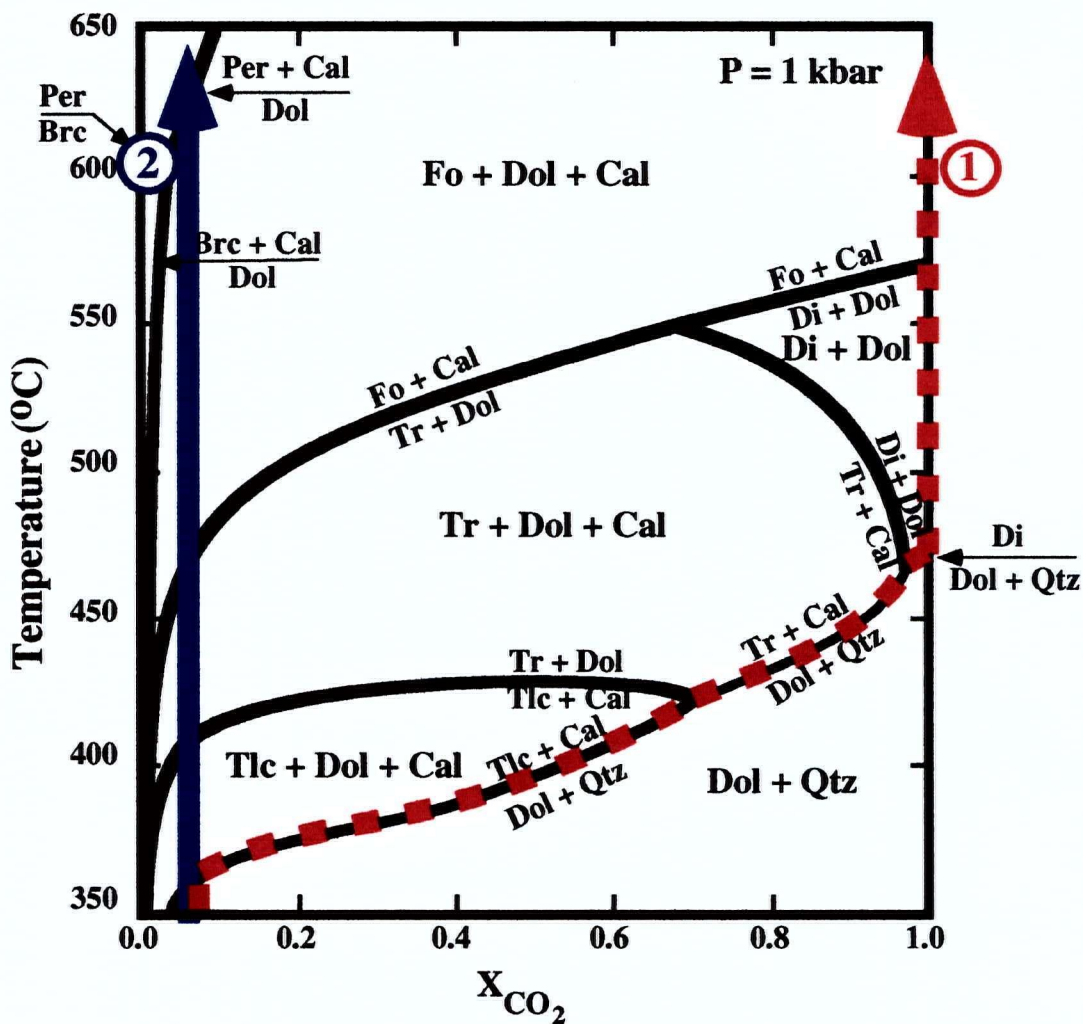


**Figure 1:** T-X<sub>CO2</sub> diagram illustrating the influence of H<sub>2</sub>O-CO<sub>2</sub> fluids on the development of mineral assemblages in siliceous dolomites at P<sub>fluid</sub> = const = 1kb. Path 1 (red dashed line) shows the reaction path for a rock that is not infiltrated during heating. Path 2 (blue solid line) shows the reaction path for a rock that is infiltrated by an infinite amount of a nearly pure H<sub>2</sub>O fluid. Mineral abbreviation according to Kretz (1983).

by a stability field rather than a reaction line in the  $T-X_{\text{CO}_2}$  diagram. The  $X_{\text{CO}_2}$  in this case is governed by the externally derived fluid.

## CHAPTER 2

### GEOLOGIC SETTING

#### 2.1 Regional Geology

The quartz monzonitic Horsethief Creek pluton is located in the Purcell Mountains of southeastern British Columbia, Canada (Figure 2). The Purcell Mountains are part of the 'Purcell Anticlinorium' which is dominated by a thick sequence of Proterozoic to upper Paleozoic sedimentary rocks that were deposited on or near the western edge of the North American craton (Cook and Van der Velden 1995).

During the Mesoproterozoic, the area was part of an intracratonic basin into which predominately shallow water sediments were deposited, leading to the formation of the Belt Purcell Supergroup. This sequence is unconformably overlain by the Neoproterozoic Windermere Supergroup. Reesor (1973) attributed the lower Windermere rocks to reflect a rifted margin setting and the upper part to comprise continental margin strata. Warren and Price (1992, p.15) noted that in more detail the "stratigraphic relationships within and between Upper Proterozoic and Lower Cambrian rocks show that this interval was punctuated by several tectonic events, related to extension and/or rifting of the North American continental margin.". This led "to the emergence of 'the Windermere High' (Reesor, 1973) as a high-standing continental block."

During the mid-Mesozoic the area experienced extensive tectonic activity when the allochthonous Intermontane Superterrane was accreted to the western side of the North American craton. This caused widespread deformation as recorded in N-NW trending folds and faults, regional scale metamorphism and the intrusion of late- to synkinematic mid-Jurassic plutons

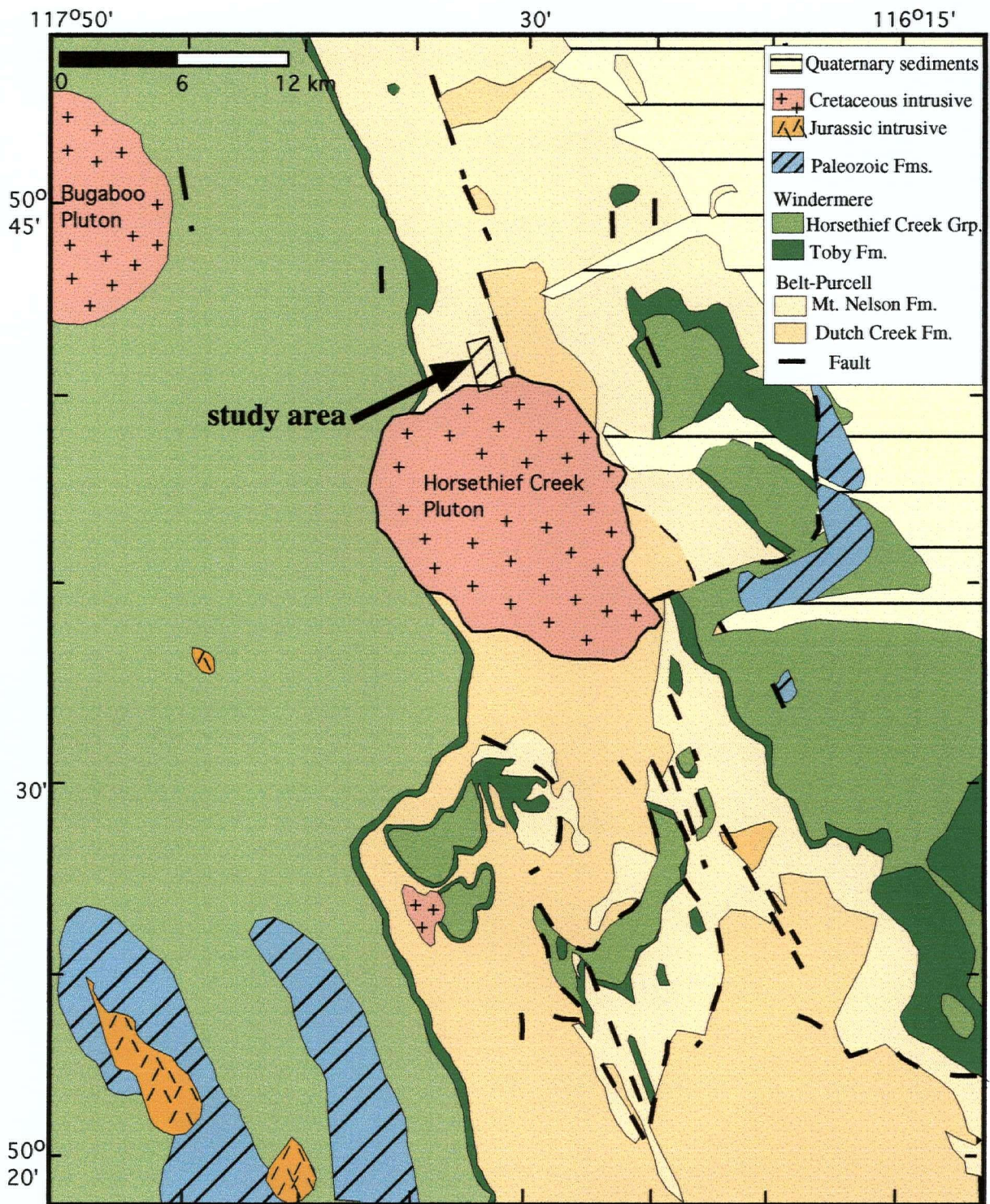


**Figure 2:** Simplified map of the regional geology (after Reesor 1973)

(Figure 2) in the suture zone that forms today's Omineca Belt (Archibald *et al.* 1983).

A second episode of plutonism occurred during the mid-Cretaceous leading to the intrusion of several post-kinematic and hence discordant igneous bodies (Reesor, 1973). This plutonism is interpreted to be the result of crustal thickening (Archibald *et al.*, 1984). Geochemical characterization of various of the mid-Cretaceous plutons confirms this hypothesis. Brandon and Lambert (1993) invoke crustal anatexis of Precambrian basement gneisses and/or Proterozoic metapelites to produce these later intrusions. The Horsethief Creek Batholith (HCB) belongs to this later group of discordant mid-Cretaceous intrusions. K-Ar dating (biotite) revealed one age of 108 Ma (Reesor 1973) and Rb-Sr dating an age of 109 Ma (Brandon and Lambert 1993) for the HCB.

After slow cooling from mid- to late-Cretaceous time the area was thrust eastwards moving "over a step-like ramp in the basement corresponding to the ancient rifted margin of the continent" (Archibald *et al.* 1984, p.578). This convergence during Late Cretaceous to Paleocene time is attributed to the accretion of the Insular Belt to the west. Seismic data confirms that the Anticlinorium formed when up to 15 km Belt-Purcell to Paleozoic margin sediments were carried eastward over a prominent basement ramp by means of imbricate thrust faults (Cook and Van der Velden 1995). During the Eocene the area was affected by crustal extension and tectonic denudation (Archibald *et al.* 1984).

## **2.2 Local Geology**

This study focuses on the contact metamorphism of siliceous-potassic dolomites from the Mount Nelson Formation of the Belt-Purcell Supergroup along the northern margin of the Horsethief Creek pluton (Figure 3).

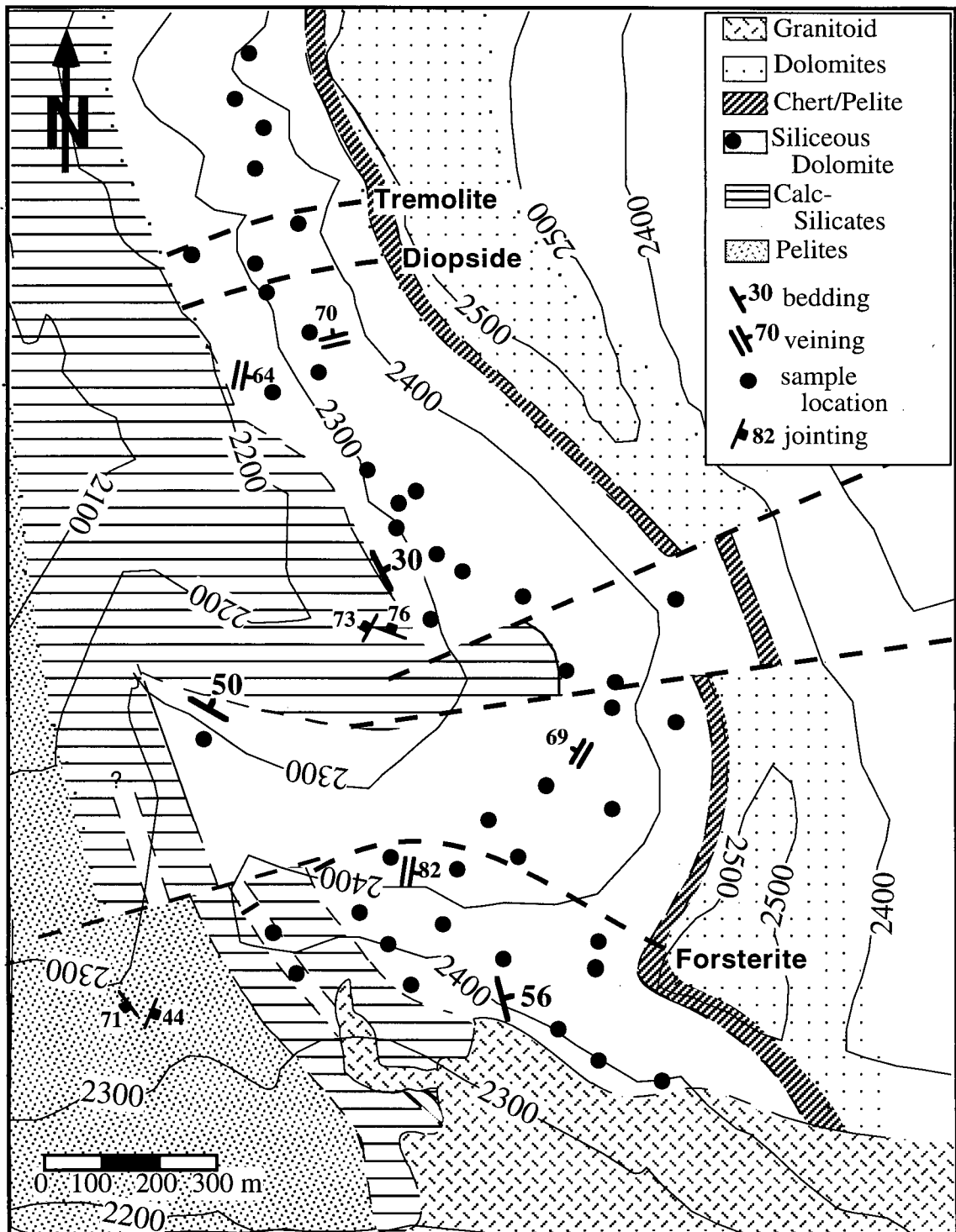


**Figure 3:** Geological map of the northern flank of the Horsethief Batholith showing main units, topography (altitudes in meters), sample locations and isograds (for sample location numbers see Figure 5). Isograds as defined within the siliceous dolomite system ( $\text{CaO-MgO-SiO}_2\text{-H}_2\text{O-CO}_2$ ) considering index minerals that can be observed in the field.

The intrusion is  $\approx 15$  km in diameter and is one of several discordant mid-Cretaceous igneous bodies that intruded the Proterozoic to early Paleozoic clastic and carbonate sediments of the Belt-Purcell and Windermere Supergroups in mid-Cretaceous time (Archibald *et al.*, 1984). Close to the intrusion, within a 1 - 2 km wide contact aureole, low-grade regionally metamorphosed rocks are overprinted with high-grade mineral assemblages. The regional metamorphism is coeval with Jurassic deformation and is of sub-chlorite grade in the study area (Reesor 1973). The development of systems of steeply dipping joints in all lithologies of the working area is believed to be associated with the folding (Twiss and Moores 1992).

The Mount Nelson Formation in the working area consists of a sequence of cliff-forming (siliceous and potassic) dolomitic marbles underlain by calc-silicates and pelites (Figure 3) and with numerous chert interlayers of various thickness (centimeter - decimeters). The thickness of the underlying pelitic layer can only be estimated as  $>300$  m because the contacts are outside the mapped area. Pelitic interlayers in the siliceous dolomites are rare and very thin (cm). The whole sequence dips  $\approx 35^\circ$  ENE (Figure 3), and is part of the west flank of a NNW-trending anticline (Reesor 1973).

Most of the inner two-thirds of the study-area contains good exposures along a west-facing cliff that radiates northward from the batholith (Plate 1). Exposure deteriorates considerably at the perimeter of the aureole. The irregular map pattern of parts of the inner aureole is due to a combination of irregular topography within a NW draining cirque (Figure 3) and block faulting resulting in poor exposure. The rocks closest to the contact are exposed along an approximately E-W trending ridge that parallels the pluton-wallrock contact.

Siliceous and potassic dolomite dominates a coherent stratigraphic package  $\approx 160$  m in thickness that can be mapped from the inner to outer aureole. Individual beds within this package range in thickness from  $\approx 1$  - 50 cm but cannot be traced with confidence through the aureole because of mm to m offset on E-W trending high angle faults. These faults appear to be post-contact-metamorphic as no (infiltration-driven) development of metamorphic minerals along



**Plate 1:** Photograph of the field area showing the middle part of the aureole (looking North).

them is observed. Thin (cm) chert interlayers are common, and in some localities dolomite is characterized by dark, discontinuous elongated chert lenses or nodules that are arranged parallel to bedding. Sets of closely (cm - dm) spaced joints that are roughly perpendicular to the bedding are found in the low-grade rocks of all lithologies in the working area and beyond the extent of the aureole further north. At higher grades, in rocks where abundant metamorphic minerals were produced, the rocks are generally massive. In the siliceous dolomites veins roughly perpendicular to bedding are common (Plate 2). They are thought to be related to the pre-contact metamorphic joint system. The length of the veins is in most cases determined by the width of the sedimentary layers in which they are contained. The width of the veins is usually a few millimeters (mm) and they are spaced on a cm - dm scale.

This study focuses on iron-poor, silicic-potassic dolomites which form the bulk of the mappable unit. Scapolite-bearing or iron-rich dolomitic marble is present in  $\approx 5\%$  of the samples examined. These samples are not considered further in this study. Sample localities are shown in Figure 3.



**Plate 2:** Photograph of an outcrop near sample location 19/3 (looking South). The rocks show typical veins trending vertical and parallel to bedding. The amount and form of veining differs between the individual layers; sledgehammer for scale. Parts of the inner aureole can be seen in the background.

## CHAPTER 3

### MINERALOGY AND MINERAL CHEMISTRY

#### 3.1 Introduction

Mineral assemblages were examined in thin section by optical microscopy and back-scattered electron imaging. Carbonate minerals were identified by staining with the method of Dickson as described in Hutchison (1974). Very fine grained carbonate minerals were identified with scanning electron microscopy (SEM), using a Philips XL30 with back-scattered electron (BSE) imaging. All dolomite occurrences were confirmed with SEM.

A T-X<sub>CO<sub>2</sub></sub> phase diagram for potassic siliceous dolomites was constructed using endmember compositions of the minerals: quartz (Qtz), dolomite (Dol), calcite (Cal), talc (Tlc), tremolite (Tr), diopside (Di), forsterite (Fo), brucite (Br), periclase (Per), wollastonite (Wo), K-feldspar (Ksp), and phlogopite (Phl) (Figure 4). The PTAX program by Perkins *et al.* (1980) which is based on the thermodynamic data set by Berman (1988) and H<sub>2</sub>O-CO<sub>2</sub> mixing properties of Kerrick and Jacobs (1984) was used for the calculation and plotting of the mineral reactions. This use of endmember compositions is justified by the general occurrence of colorless phlogopite which is indicative for very iron poor conditions. The iron poor character of the rocks was qualitatively confirmed by SEM and quantified by microprobe analyses (see paragraph 3.3 below). Fluid pressure was assumed to be ≈2.2 kbar in accordance with PT estimates derived from mineral assemblages observed in metapelites. (Floriet 1996). Peak metamorphic conditions in the inner aureole are estimated to be ≈2.1 - 2.5 kbar and ≈610 °C based on the observation of the breakdown of muscovite + quartz to andalusite + K-feldspar and the occurrence of fibrolite in a

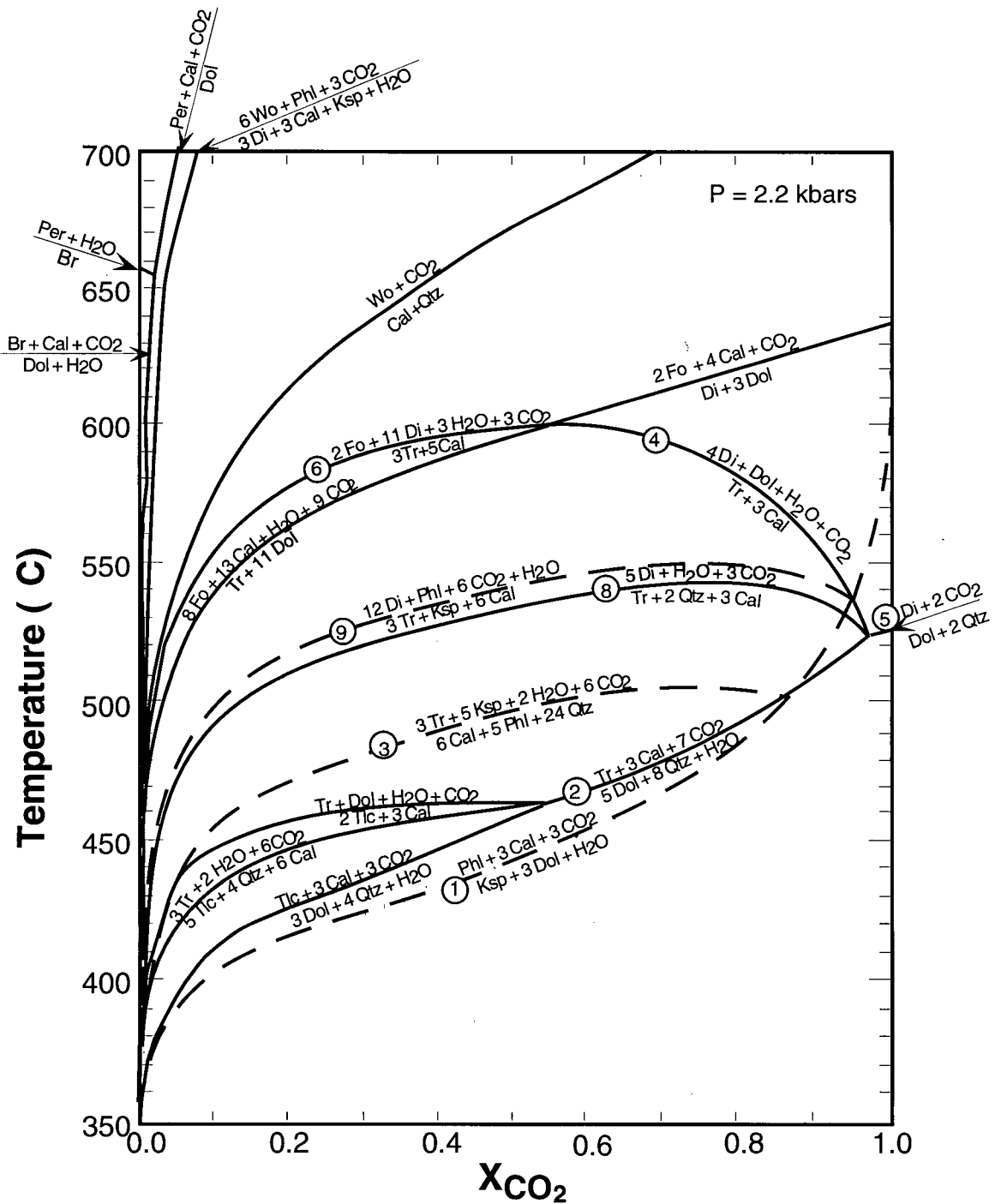


**Figure 4:** T- $X_{CO_2}$  diagram depicting phase equilibria in the potassic siliceous dolomite system [KCMAS-HC ( $K_2O$ - $CaO$ - $MgO$ - $Al_2O_3$ - $SiO_2$ - $H_2O$ - $CO_2$ )] at  $P = 2.2$  kb. Calculated for endmembers with the PTAX program (Perkins *et al.* 1980). Fluorine-substitution was not considered. It would cause some changes in the low-temperature area. The thermal stability of (OH-F) minerals increases at the expense of anhydrous breakdown products with increasing F-content (e.g. Abercombie *et al.* 1987). Reactions are numbered according to their order of appearance in the text. Mineral abbreviations after Kretz (1983).

few of the highest grade samples, with no partial melting of the metapelites.

In the siliceous dolomites, six isograds are identified based on the first appearance of index minerals: phlogopite; tremolite + K-feldspar; diopside; diopside + phlogopite; diopside+dolomite and forsterite (Figure 5).

The identified assemblages and isograds are listed in order of increasing proximity to the pluton in Table 1. Mineralogical variations on the sub-thin section scale are frequently found. Samples with two distinct layers or large lenses with assemblages different from those in the matrix are indicated by the suffices 'A' and 'B' to the respective sample number in Table 1.

### **3.2 The Six Metamorphic Zones**

Following is a description of the 6 metamorphic zones in prograde sequence. Typical mineral assemblages and textures are described and possible reactions listed. The assemblages are listed in Table 1. Almost all rocks outside the phlogopite zone show static recrystallisation and mineral formation. Few samples showed a preferred mineral orientation.

#### 3.2.1 The Phlogopite Zone

This zone cannot be identified in the field because phlogopite is found only in very low abundance - typically 1 - 3 volume percent (vol%). Furthermore, the lack of outcrop in the outermost aureole prohibits the collection of unmetamorphosed rocks and therefore, although there is a phlogopite zone, the phlogopite *isograd* cannot be traced. The outermost outcrop lies 1515 m from the pluton and contains phlogopite. The phlogopite isograd must occur at a distance equal or greater than 1515 m away from the pluton. The phlogopite zone rocks are composed of

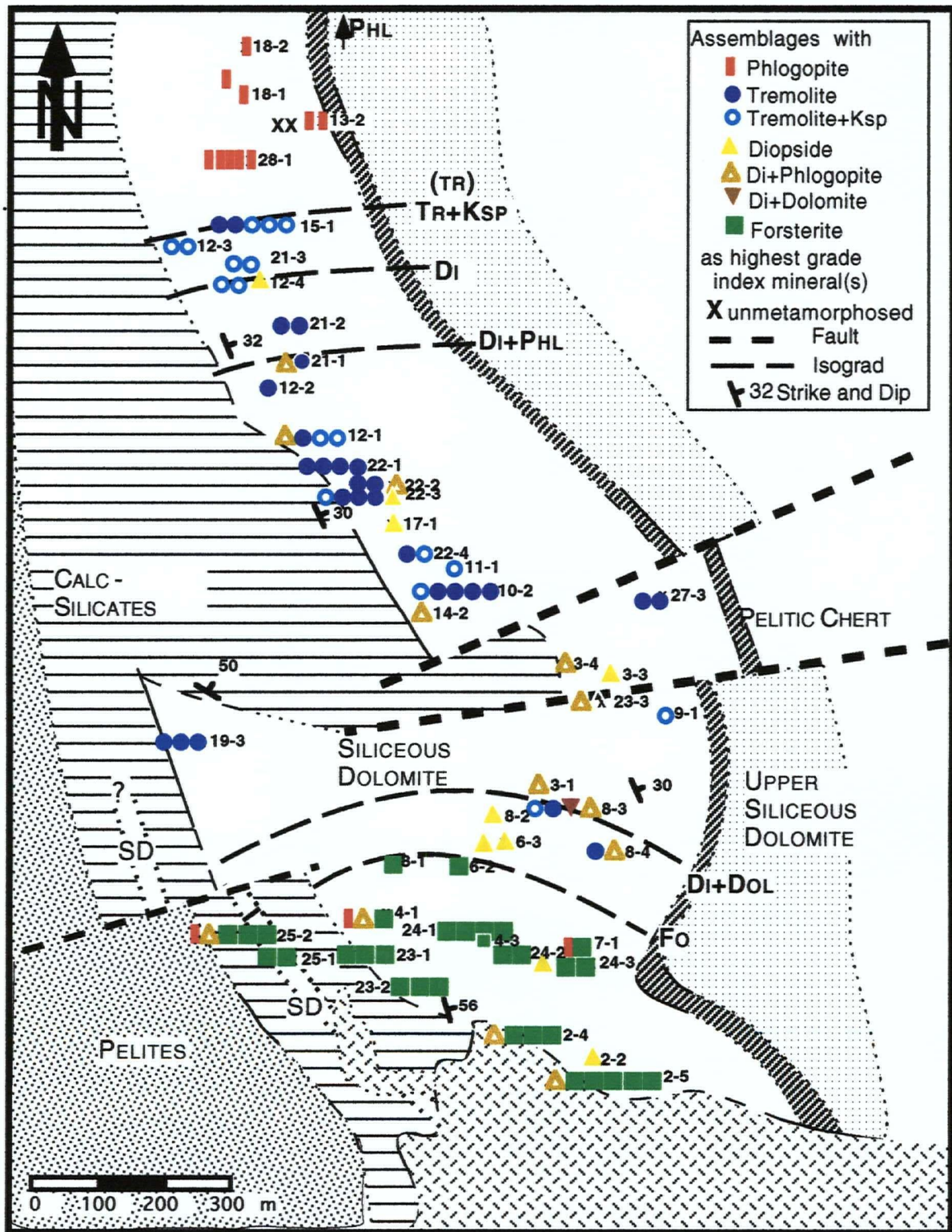


**Figure 5:** Map showing all isograds and assemblages as defined by the KCMAS-HC system. Note the very heterogeneous distribution of assemblages within the metamorphic zones. The exact outcrop location is at the symbol nearest to the outcrop number.

**Table1: Peak metamorphic assemblages in increasing proximity to pluton.**

Note: X=present; (X)=traces; C=isolated core, XC=cores with contact to matrix minerals; n/d=not detected (only used in phlogopite zone rocks, where calcite is expected if phlogopite is of metamorphic origin).

	Dol	Qtz	Tr	Cal	Di	Fo	Ksp	Phl		Dol	Qtz	Tr	Cal	Di	Fo	Ksp	Phl
18/2 - 1	X	X		n/d			X	(X)				X	X				X
18/1 - 1	X	(X)		(X)			X	(X)				X	X				X
18/1 - 2	X	X		n/d			X	(X)				X	X	X			X
13/2 - 1	X	X					X					X	X			X	
13/2 - 2	X	X					X					X	X			X	
13/2 - 3	X	X		(X)			X	(X)				X	X				X
13/2 - 4	X	X		(X)			X	(X)				X	X				X
28/1 - 1	X	X		(X)			X	(X)				X	X				X
28/1 - 2	X	X		(X)			X	(X)				X	X			X	X
28/1 - 3	X	X		(X)			X	(X)				X	X			X	X
28/1 - 4	X	X		n/d			X	(X)				X	X				X
28/1 - 5	X	(X)		X		Tr + Ksp	X	(X)				X	X				X
15/1 - 3			X	X			X					X	X				X
15/1 - 4		X	X	X			X					X	X				X
15/1 - 5			X	X								X	X				X
15/1 - 6		X	X	X			X					X	X				X
15/1 - 7			X	X								X	X				X
12/3 - 1			X	X			X					X	X				X
12/3 - 2			X	X			X					X	X				X
21/3 - 1			X	X			X					X	X				X
21/3 - 2			X	X		Di	X	X				X	X				X
12/4 - 1		X	X	(X)	X		X					X	X				X
12/4 - 2			X	X								X	X			(X)	X
12/4 - 3			X	X	C							X	X			(X)	X
21/2 - 1			X	X								X	X				X
21/2 - 2			X	X	C							X	X				X
21/1 - 1	X		X	X		Di + Phl	X					X	X				X
21/1 - 3			X	X	XC							X	X				X
12/2 - 1			X	X								X	X				X
12/1 - 1			X	X								X	X				X
12/1 - 3			X	X	XC							X	X				X
12/1 - 4			X	X			X	(X)				X	X				X
12/1 - 5			X	X			X					X	X				X
22/1 - 1	X		X	X								X	X				X
22/1 - 2	X		X	X								X	X				X
22/1 - 3A			X	X								X	X				X
22/1 - 3B	X		X	X								X	X				X
22/2 - 1			X	X								X	X			(X)	X
22/2 - 2			X	(X)			X	(X)				X	X				X
22/2 - 3				X	X		X	X				X	X				X
22/3 - 1			X	X								X	X				X
22/3 - 2A			X	X								X	X				X
22/3 - 2B				X	X		X	X				X	X				X
22/3 - 3	X		X	X								X	X				X
22/3 - 4			X	X								X	X				X
17/1 - 1			X	X	X		X					X	X				X
22/4 - 1			X	X								X	X				X
22/4 - 2			X	X								X	X			X	X
11/1 - 1			X	X								X	X				X
10/2 - 1			X	X								X	X				X
10/2 - 2			X	X								X	X				X
10/2 - 3			X	X								X	X				X
10/2 - 4			X	X								X	X			(X)	X
10/2 - 5			X	X			X					X	X				X
19/3 - 1			X	X								X	X				X
19/3 - 2A			X	X								X	X				X
19/3 - 2B	X		X	X								X	X			X	X
14/2 - 1				X	X							X	X				X
27/3 - 1												X	X				X
27/3 - 2												X	X				X
3/4 - 1												X	X	X			X
3/3 - 1												X	X	X		X	
9/1 - 2												X	X			X	
23/3 - 1												X	X	X			X
23/3 - 2												X	X	X			X
3/1 - 1												X	X	X			X
8/3 - 1												X	X			X	X
8/3 - 2	X											X	X	Di + Dol		X	X
8/3 - 3A	X											X	X	XC			X
8/3 - 3B												X	X	X			X
8/4 - 1A												X	X				X
8/4 - 1B												X	X	X			(X)
8/2 - 1												X	X		Fo		X
8/1 - 1												X	X	X			X
25/2 - 1												X	X	X			X
25/2 - 2												X	X	X			X
25/2 - 3A												X	X	X			X
25/2 - 3B	X											X	X	X			X
25/2 - 4												X	X	X			X
25/1 - 1												X	X	X			X
25/1 - 2												X	X	X			X
6/3 - 1												X	X			X	
6/3 - 2												(X)	X			X	
6/2 - 1												X	X	X			X
4/1 - 1A	X											X	X	X			X
4/1 - 1B												X	X	X			X
4/1 - 2												X	X	X			X
23/1 - 1												X	X	X			X
23/1 - 2												X	X	X			X
23/1 - 4												X	X	X			X
24/1 - 1												X	X	X			X
24/1 - 2												X	X	X			X
24/1 - 3												X	X	X			X
24/1 - 4												X	X	X			X
7/1 - 1A												X	X	X			X
7/1 - 1B	X											X	X	X			X
24/3 - 1												X	X	X			X
24/3 - 2	X											X	X	X			X
24/3 - 3												X	X	X			X
4/3 - 2												X	X	X			X
23/2 - 1												X	X	X			X
23/2 - 2												X	X	X			X
23/2 - 3												X	X	X			X
24/2 - 1	X											X	X	X			X
24/2 - 2												X	X	X			X
2/5 - 1												X	X	X			X
2/5 - 2												X	X	X			X
2/5 - 3												X	X	X			X
2/5 - 4												X	X	X			X
2/5 - 5												X	X	X			X
2/5 - 6												X	X	X			X
2/4 - 1A	X											X	X	X			X
2/4 - 1B												X	X	X			X
2/4 - 2												X	X	X			X
2/4 - 3												X	X	X			X
2/2 - 1												X	X	X			X

dolomite - quartz - K-feldspar  $\pm$  calcite and varying but generally small amounts of phlogopite.

In very fine grained, homogeneous rocks containing only traces ( $\leq 1-3$  vol%) of randomly orientated phlogopite are found (Plate 3). In small discrete zones (mm - cm scale) phlogopite is present in greater abundance (as high as  $\approx 8$  vol%) and with preferred mineral orientation (Plate 4 a and b). In one thin section phlogopite is found in the center of a quartz vein (Plate 5). If the phlogopite is of contact-metamorphic origin, it most likely formed by the reaction:



at  $0.00 > X_{\text{CO}_2} < \approx 0.86$  (cf. Figure 4). The fact that there are usually only small amounts of calcite found in the matrix and that the amount of calcite increases proportionally with the amount of phlogopite supports the assumption that the phlogopite formed by reaction (1). Calcite may be present but not identified in these samples because in BSE imaging the calcite shows a gray value very close to that of K-feldspar. It is easily possible that calcite which is expected in the presence of phlogopite was simply not detected. Based on these observations the protolith is presumed to be dolomite - quartz - K-feldspar and  $\pm$  calcite.

Chert lenses or nodules (Plate 6) are characteristic of rocks in the phlogopite zone. They are sometimes interconnected by bedding-parallel chert layers and/or sub-vertical quartz veins. Because they are more resistant to weathering they stand out of the more strongly weathered quartz-poor dolostones. The quartz content varies from just a few percent in a fine grained mainly dolomitic matrix up to  $\approx 50$  vol% in layers containing chert lenses. The potassic feldspar content ranges from trace up to  $\approx 15$  vol%. Calcite only occurs in trace amounts in the matrix but makes up for 10 - 90 vol% of the material in occasional small veins.

The effect of iron on mineral distribution is not considered in this study because most samples are Fe-poor. However, above sample locations 28/1 and 13/2 (in the Mg-phlogopite zone) is an outcrop that contains two adjacent layers (both  $\approx 40 - 50$  cm wide) with Fe-amphibole in high abundance ( $\approx 60$  vol%).

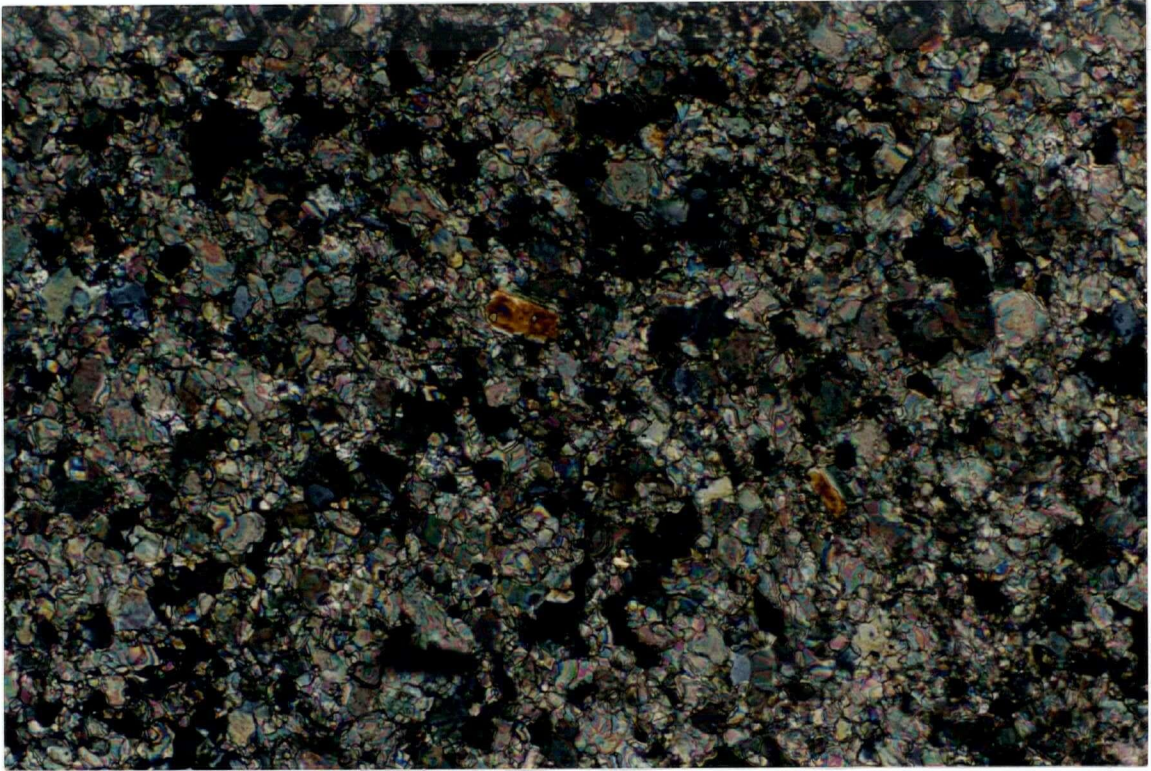


**Plate 3:** Photomicrograph of a mineral assemblage in the phlogopite zone in cross-polarized light (XPL) (sample 18/1-1). Field of view  $\approx 0.6$  mm wide. The assemblage shown is typical for this zone in that it shows very fine grained dolomite (very high interference colors (IC)) - K-feldspar (first order gray)) - and 3 flaky phlogopite crystals (first order gray-to second order purple interference colors (IC)). These crystals are larger than average and were chosen to ease identification.

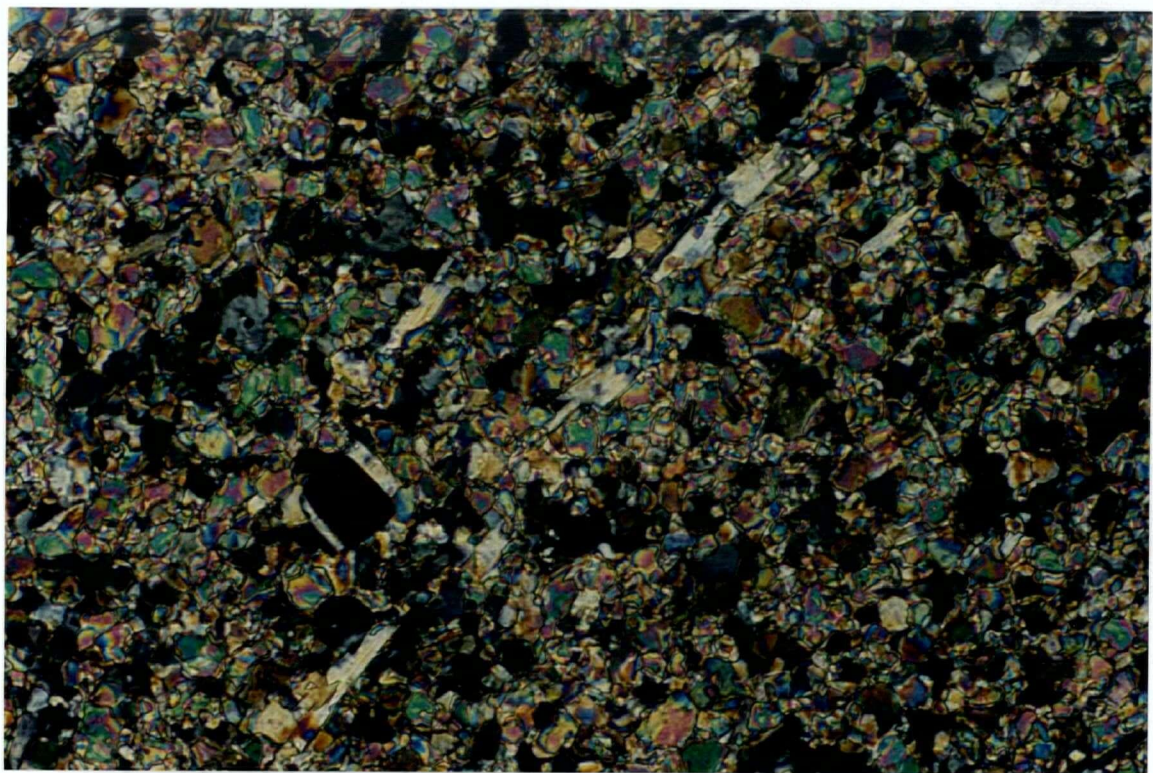
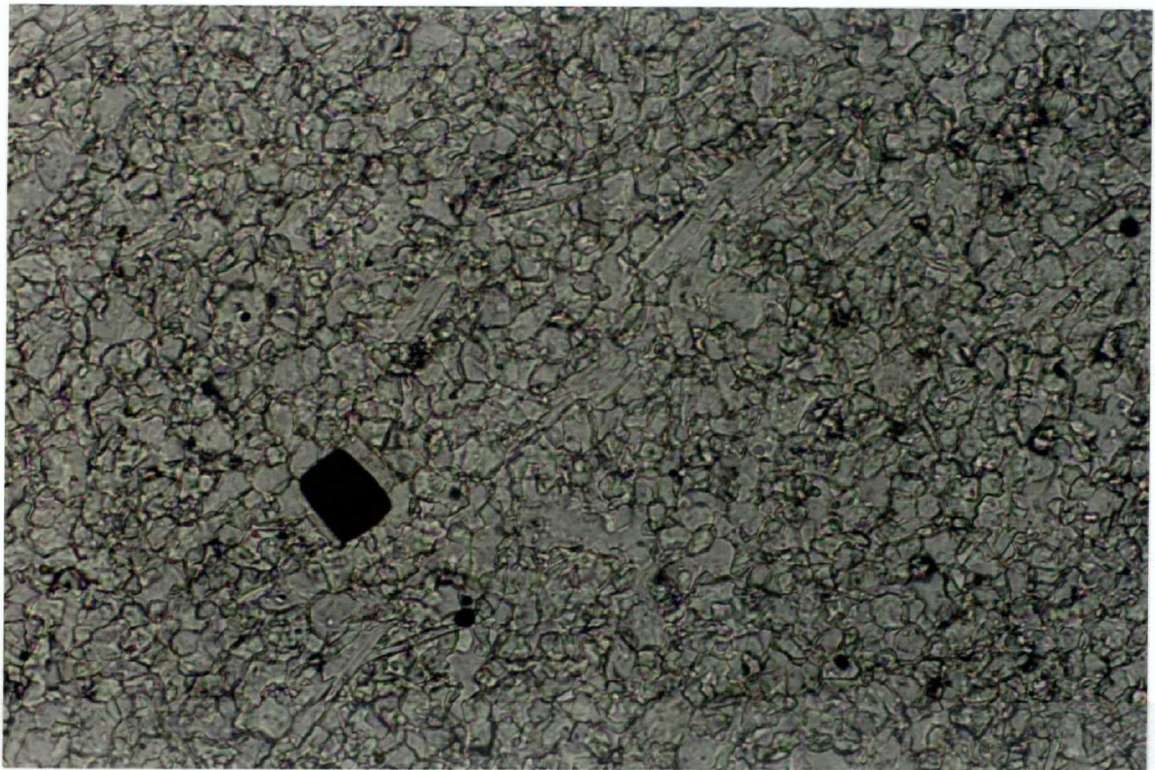


**Plate 4:** a) Plain-polarized light (PPL) and b) XPL photomicrograph respectively showing the higher abundance of orientated phlogopites (flakes) in deformed rocks of the phlogopite zone (sample 13/1-1). The cause of the small scale, local deformation is not clear. Note the growth of phlogopite grains perpendicular to the foliation in the pressure shadows of a pyrite grain. Field of view is  $\approx 0.3$  mm wide.

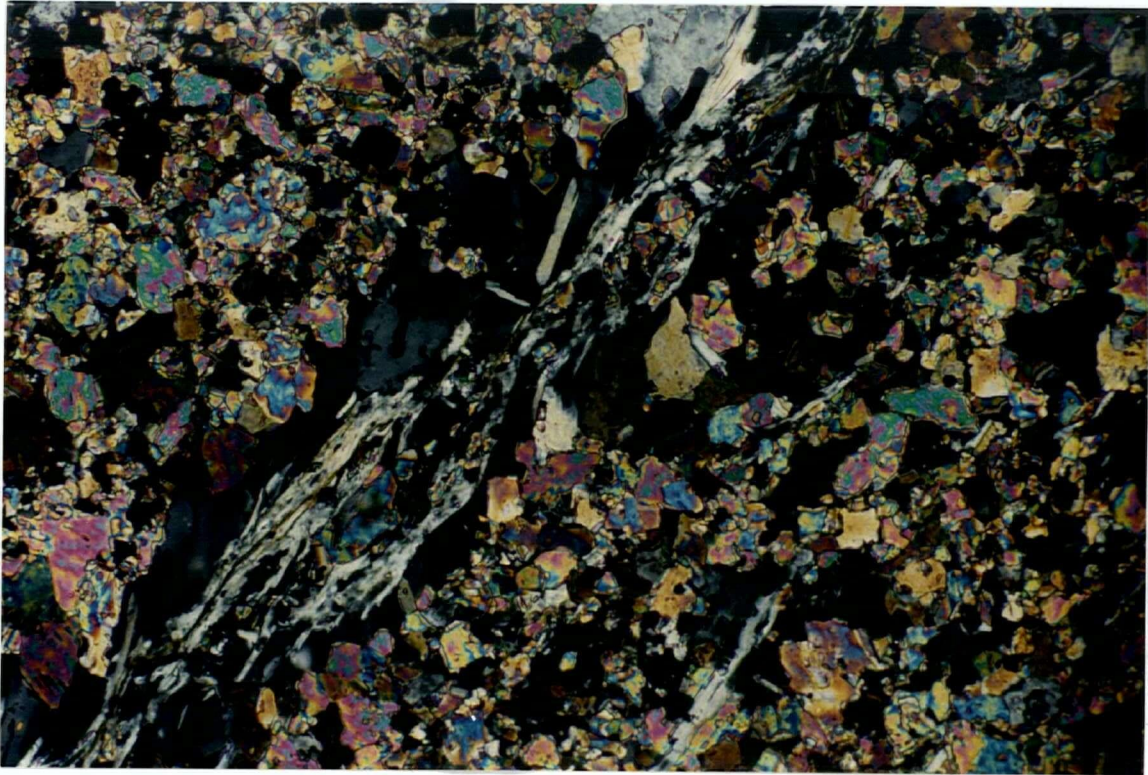


**Plate 5:** XPL photomicrograph of a phlogopite zone rock (sample 13/1-1) that shows a vein unusually rich in phlogopite. As K-feldspar veins are not observed the for reaction necessary potassium and aluminum was likely introduced by the fluid. Field of view  $\approx 0.3$  mm wide.

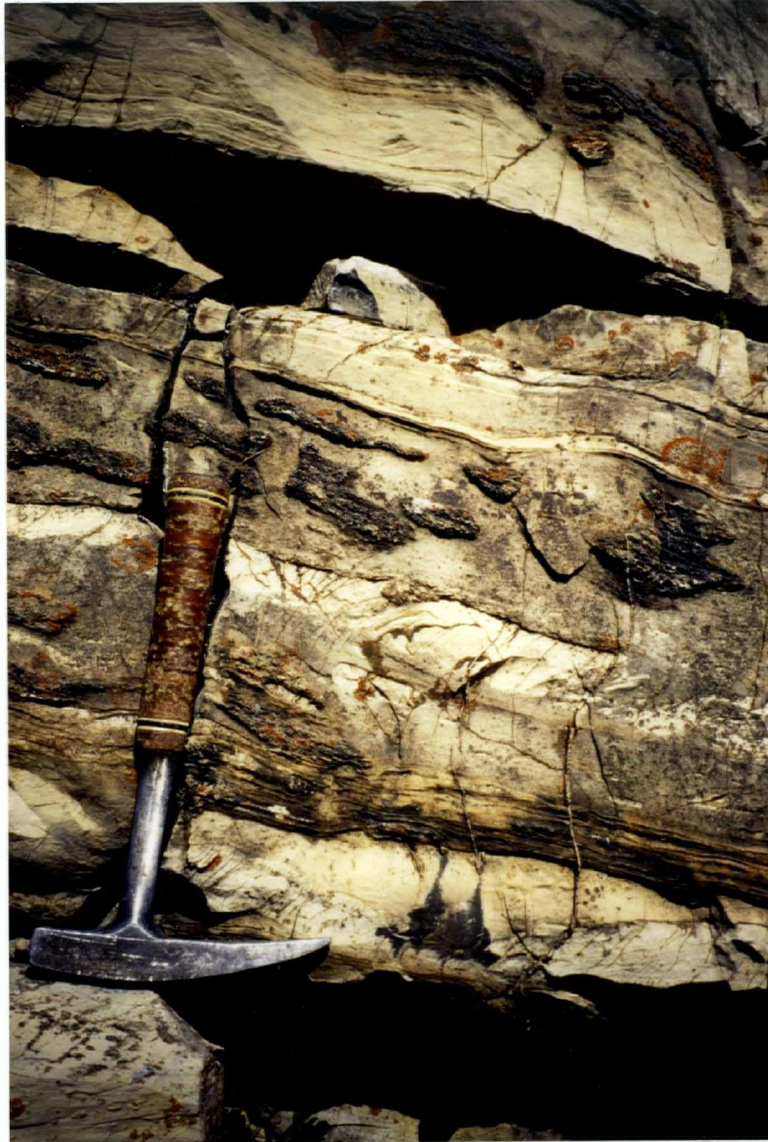
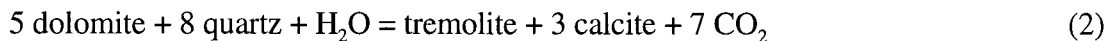


**Plate 6:** Photograph of a typical outcrop in the phlogopite zone (near 13/1) showing bedding parallel chert lenses or nodules and subvertical joints and veins cutting through single layers; hammer for scale.

### 3.2.2 The Tremolite+K-feldspar Zone

The tremolite + K-feldspar isograd is located at  $\approx 1250$  m from the pluton - wallrock contact. The first occurrence of tremolite is marked by cm - dm wide layers with 1 - 3 cm long tremolite crystals growing mostly in rosettes and by layers with very fine grained ( $\approx 1$  mm) pervasive tremolite. The latter layers tend to be more abundant and wider. The number and thickness of tremolite-bearing layers increases towards the diopside isograd. The large tremolite crystals are mostly found in layers that contain abundant veins approximately perpendicular or parallel to bedding. In a few samples tremolite growth can be observed to have started in points where veins intersect. A widespread assemblage is tremolite - calcite - K-feldspar, showing homogeneously sized and distributed minerals (Plate 7). The tremolite content can reach up to  $\approx 65$  vol%. Another common assemblage is tremolite - calcite - phlogopite. Both of these assemblages persist to the forsterite isograd.

It is not clear which reactions are responsible for the formation of the tremolite in the various assemblages. In potassium free rocks tremolite was likely formed by the reaction



if fluid infiltration occurred during heating. In potassic rocks the situation is more complex.

Combinations of reaction (1), (2) and the reaction



are possible depending on bulk composition and timing of heat- and fluid flow. This is discussed in more detail in chapter 4.

At around 1000 m ( $\pm 200$  m) some samples were found to contain albite grains and Ba-bearing K-feldspars (cf. Appendix B, Figure B1).

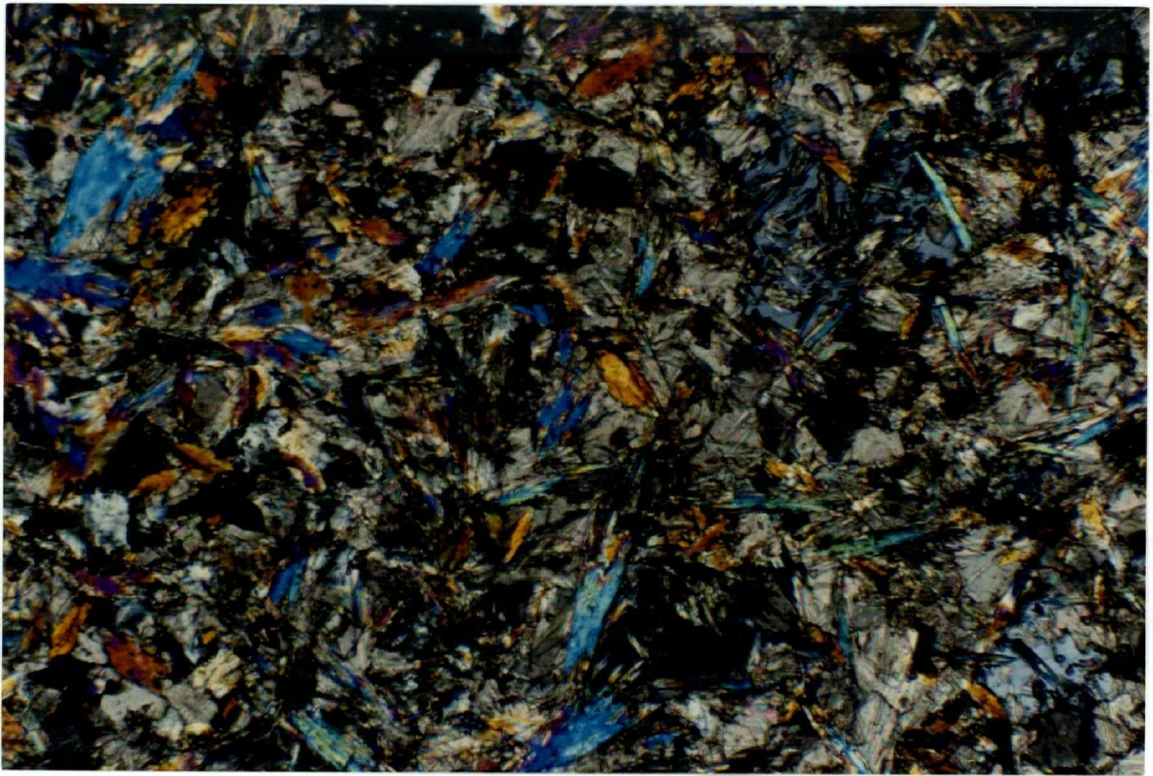


**Plate 7:** XPL photomicrograph of one of the most common assemblages in the Horsethief Creek aureole: tremolite (needles; second order IC) - calcite (very high order IC) - K-feldspar (first order gray IC). Note the even distribution of minerals throughout the rock. Field of view  $\approx 1.2$  mm wide( sample 12/3-2).

### 3.2.3 Diopside zone

The diopside isograd is placed  $\approx 1125$  m from the pluton. Only one sample in this narrow zone shows diopside in an equilibrium peak metamorphic assemblage. Samples 12/4-3 and 21/2-2 also contain diopside but the diopside was found only as cores within tremolite with no observed contact with the matrix minerals. In these two samples the diopside is listed with a "C" in the tabulation of peak metamorphic assemblages in Table 1.

### 3.2.4 Diopside+Phlogopite zone

The first appearance of a diopside + phlogopite bearing peak metamorphic equilibrium assemblage is in sample 12/4-1, approximately 1010 m from the pluton - wallrock contact. This sample and 12/1-3 (the next further sample up-grade) show diopside cores within tremolite but these diopsides are observed to be in contact with the matrix minerals. The samples do not show diopside in the fine grained matrix. It is conspicuous that almost all of the diopside bearing samples in the middle to outer aureole show diopside reacting to tremolite. Further up-grade this reaction texture between diopside and tremolite is less commonly observed. It does occur in rocks up-grade to near the forsterite isograd where the unambiguously isobarically univariant assemblage diopside - dolomite - tremolite - calcite (-phlogopite) in sample 8/3-2 shows this texture (Plates 8 a and b). The most common diopside bearing assemblage observed is diopside - tremolite - calcite - phlogopite with diopside often occurring in roundish, 0.3 - 0.7 mm large grains while tremolite forms 1 - 2 mm long needles. The rocks commonly have a uniform fine grained texture. Original chert nodules are often found completely replaced by diopside and/or (?) tremolite and calcite, and occasionally diopside rosettes are found to grow within chert layers. Tremolite often grows in or nucleates at veins and is also found to generally be coarser directly

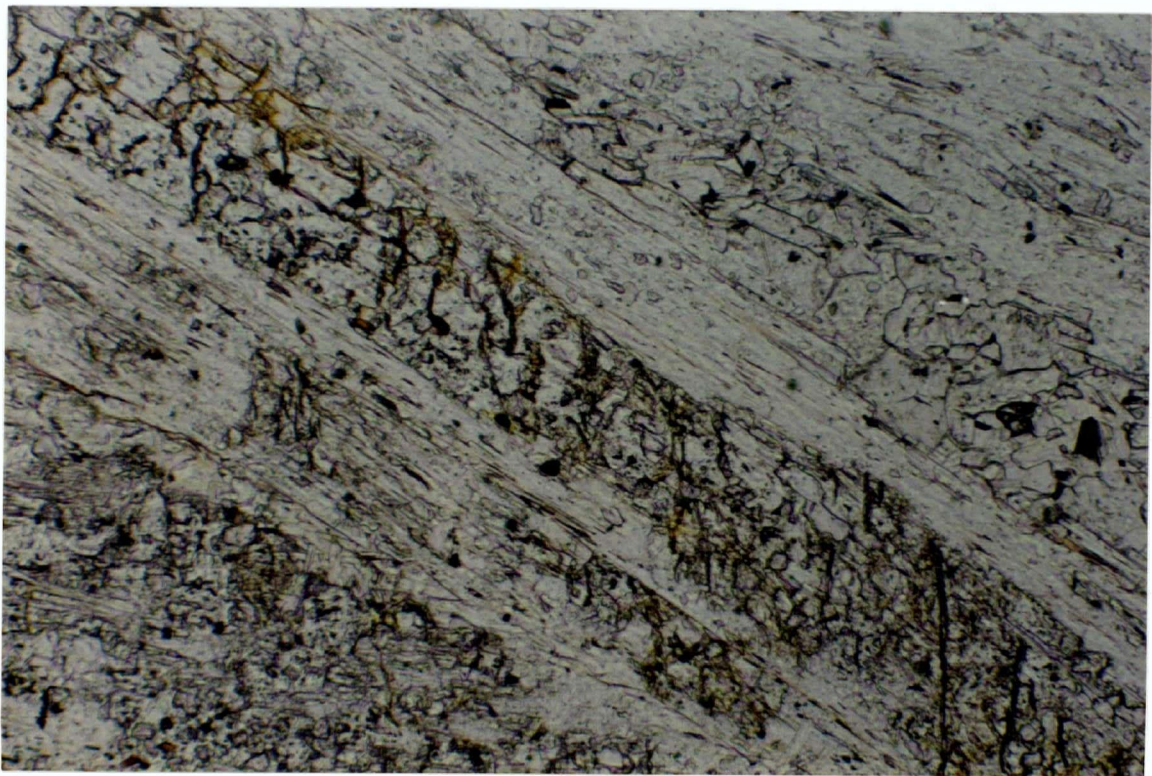
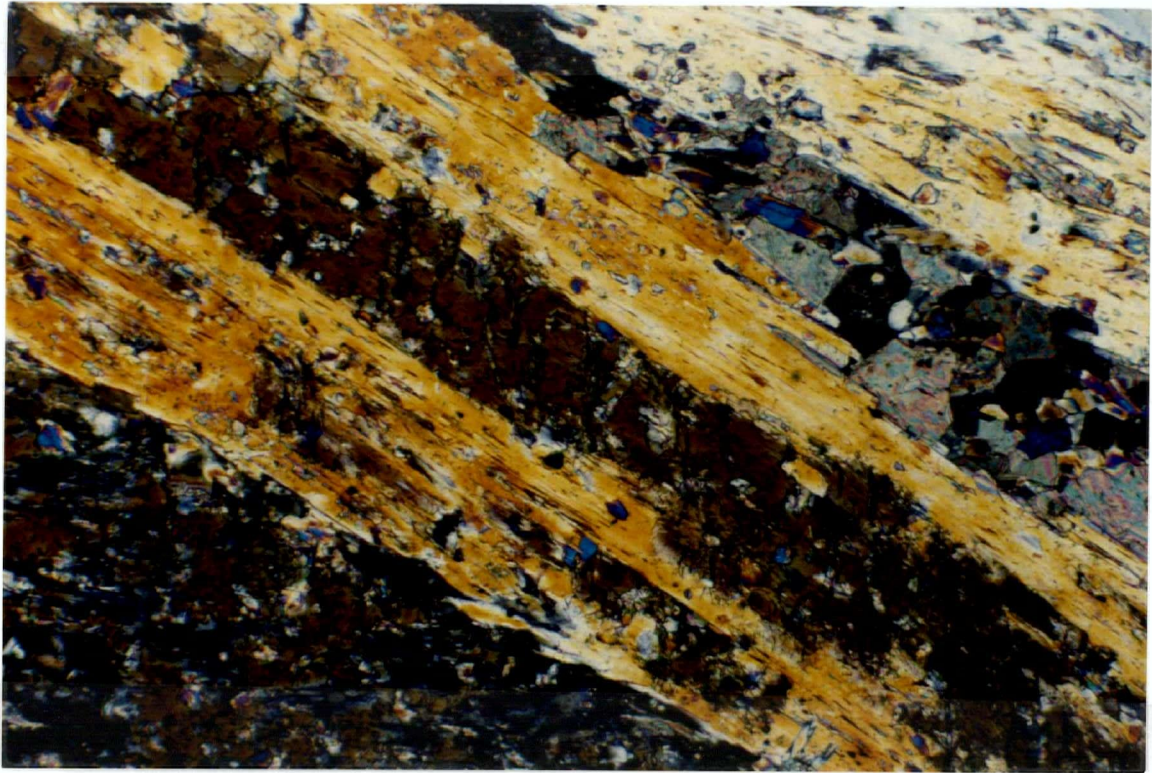


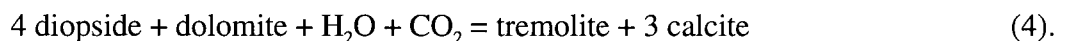
**Plate 8:** a) XPL photomicrograph showing a diopside core within a tremolite porphyroblast (sample 8/3-2). The diopside has brownish IC the tremolite first order IC or is extinct. b) Same as a) but in PPL showing the relief contrast between the diopside cores (high) and the tremolite (low). The orange spots are iron oxide staining around pyrites, the pink hue is a result of carbonate staining. Field of view  $\approx$  1.2 mm wide.

adjacent to chert layers. One sample (22/2-1) in this zone was found to have talc cores within tremolite, and another sample (21/1-1) contained a calcite - tremolite - talc - calcite (rim to core) vein.

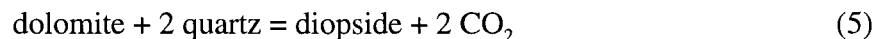
### 3.2.5. Diopside+ Dolomite zone

Sample 8/3-2 marks the beginning of the diopside + dolomite zone at about 360 m from the contact. This is the only sample recording diopside + dolomite in an isobarically univariant equilibrium assemblage. Sample 8/3-3 also contains diopside and dolomite but they are not found in mutual contact; they are in two different areas of the thin section with different bulk compositions. Close to sample location 8/4 a  $\approx 3$  cm wide bleached zone was observed below a chert layer. The bleached layer curves (keeping a constant width) around a diopside spray nucleating on the chert - marble boundary (Plate 9).

Diopside forming reactions cannot be determined from the observed textures. A possible exception is the case where diopside is found as cores to tremolite. This texture, observed in the isobarically univariant assemblages diopside - dolomite - tremolite - calcite (sample 8/3-2), suggests that the *tremolite* formed by reaction



The first developed *diopside* is concluded to have formed by reaction



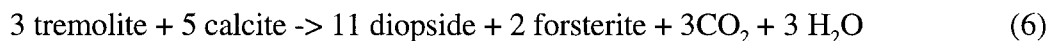
at  $X_{\text{CO}_2} > 0.95$ . In this case diopside would have formed without any significant amount of  $\text{H}_2\text{O}$ -fluid infiltrating the system up to that point.



**Plate 9:** Photograph from an rock outcrop close to sample location 8/4. It shows a bleached zone in a carbonate layer underneath a chert layer. Note how the bleached zone follows the diopside spray that nucleates at the chert - carbonate contact. Camera lens cover for scale.

### 3.2.6 The Forsterite Zone

The forsterite isograd is placed  $\approx 270$  m from the pluton. In hand sample, forsterite generally occurs as mm large, round, green crystals. Very few samples contain bladed forsterite next to also bladed diopside (e.g., sample 24/2-1). The most common mineral assemblage is forsterite - diopside - calcite  $\pm$  phlogopite. The relative abundance of forsterite and diopside varies considerably with both extremes of diopside-absent and forsterite-absent assemblages observed. These variations are observed on scales down to thin section size. Veins, or what seem to be more strongly recrystallized areas in rocks from this zone commonly have a higher abundance of diopside than the matrix assemblage - with only up to 30 vol% diopside in the matrix but up to 70 - 80 vol% in the veins (Plate 10 a and b). In a few thin sections (6/2-1, 2/5-5, all samples from outcrop 23/2) simultaneous growth of forsterite and diopside can be inferred from 'mutual' inclusions and small inclusions of tremolite in both kinds of porphyroblasts, suggesting that the reaction



took place at fluid  $X_{\text{CO}_2} < \approx 0.54$ . In most cases no specific reaction is recorded in the rocks.

The sample closest to the pluton that contains dolomite is 2/4-1 at a distance of 20 m. No periclase or brucite was detected in this thin section. With assumed maximum temperatures of 600 - 640 °C for that sample the  $X_{\text{CO}_2}$  must have been larger  $\approx 0.04$  to hinder the formation of periclase or brucite (cf. Figure 4).

Although there are some assemblages which are quite common in each of the zones as described above it is conspicuous that index minerals as well as the two potassic phases are not uniformly developed within the metamorphic zones and that the geometry of isograds is poorly constrained. The heterogeneity in observed mineral assemblages is evident in the tabulation of peak metamorphic mineral assemblages (Table 1) and also recognizable in Figure 5.

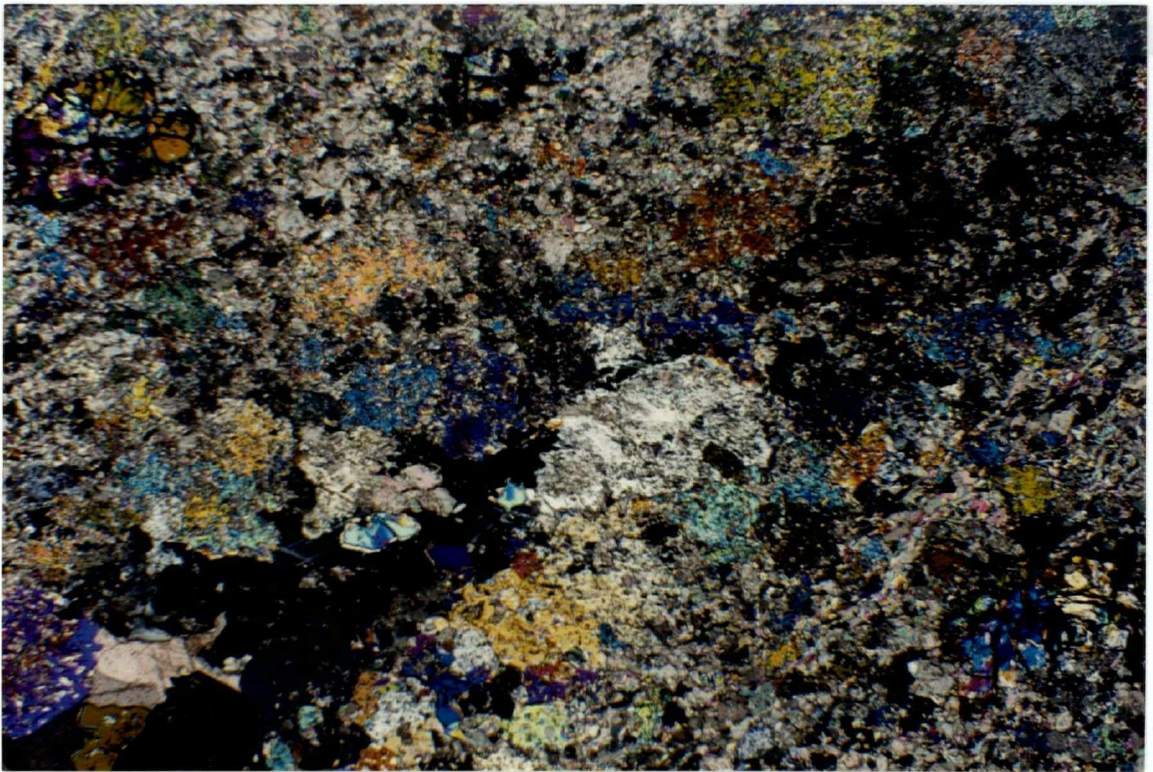
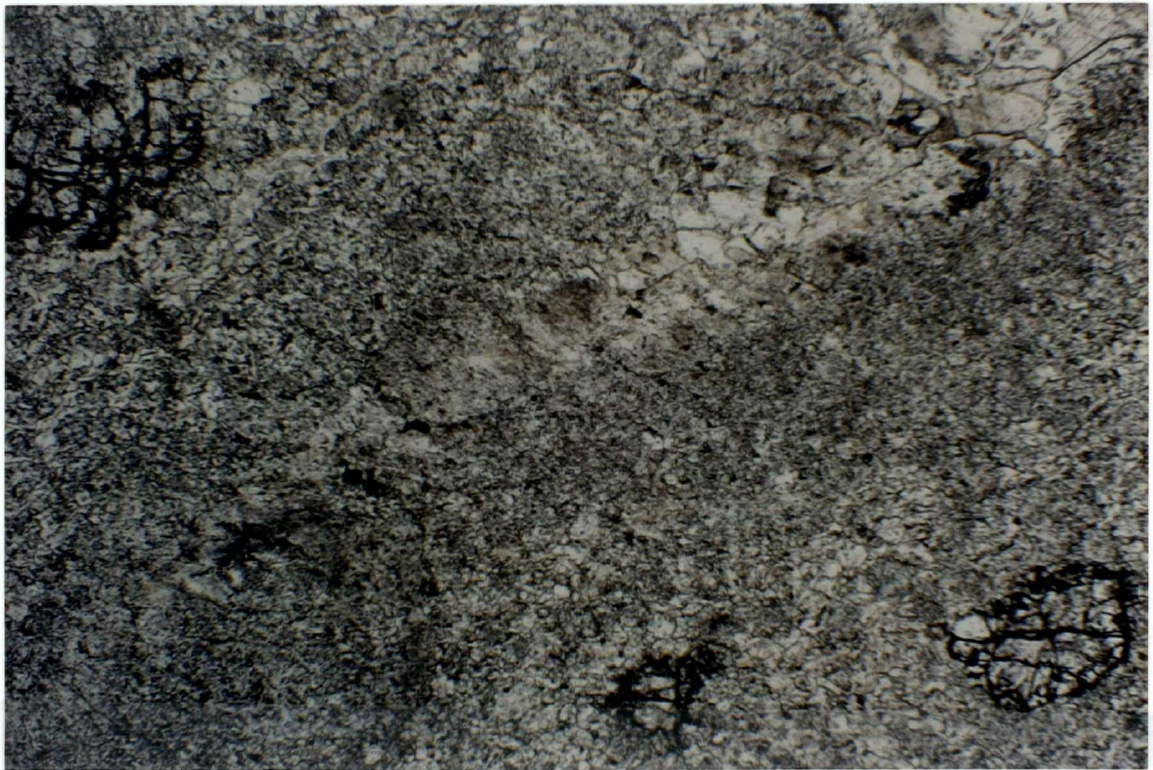


**Plate 10:** a) PPL and b) XPL photomicrograph respectively showing a cross-section of a vein in a forsterite zone rock. Note that the thin section is too thick. Forsterite in PPL with high relief and typical fracturing - diopside with relatively low relief (PPL) and here 1st to 3rd order IC (XPL). Note that the vein is virtually forsterite absent, and how diopside abundance and grain size decrease with increasing distance from the vein. Field of view  $\approx 5$  mm wide (sample 25/1-2).

### 3.3. Mineral Chemistry

Quantitative analyses of mineral compositions were obtained by Wavelength Dispersive Spectrometry (WDS) with a CAMECA SX-50 microprobe. Synthetic olivine and phlogopite and natural diopside and carbonate standards were used. Operation conditions for the silicates were excitation voltage, 15kV; beam current, 20nA; beam size 5 $\mu$ m, and for the carbonates 15 kV, 10nA and 10 $\mu$ m. Data reduction was done with the "PAP"  $\phi(\rho Z)$  method (Pouchou and Pichoir 1985).

Representative results are listed in Table 2 the complete data set is listed in Appendix A. In all minerals the Fe/(Fe+Mg) is very low. Other elements like for example Mn, Ti or Ni are only found in concentrations near or below the detection limit. This justifies the use of Mg-endmember thermodynamic data in the construction of the T-X<sub>CO<sub>2</sub></sub> diagram.

The degree of substitution of OH by F or Cl in phlogopites and tremolites varies. The chlorine content is below or at the detection limit in the Mg-endmember minerals. The fluorine content is higher and ranges from 0.079 - 0.233 (cations per 22 oxygens) in phlogopite and from 0.022 - 0.072 (cations per 23 oxygens) in tremolite. The interaction of F - Cl-bearing fluids and Mg - Fe solid solution minerals is quite complex but the observed trends seem to be in general agreement with the "Mg - Cl avoidance" rule (e.g. Zhu and Sverjensky, 1992). The distribution of fluorine contents in phlogopite (the only hydrous mineral found in all metamorphic zones) is plotted against distance in Figure 6. Throughout the aureole F-contents are relatively homogeneous with only two exceptions: The sample closest to the contact shows a F-content lower than average and the sample  $\approx$ 1250 m from the pluton in the upper phlogopite zone shows higher and more scattered F-contents. A description of the rocks with orientated phlogopite grains in the phlogopite zone is given in section 3.2.1. The significance of the data in Figure 6 is not clear. Moore and Kerrick (1976) interpreted the F-depletion near the contact to be the result of influx of igneous fluid while Rice (1977b) and Holness (1997) argue that high F-values in

**Table2:** Microprobe analyses of representative silicate and carbonate minerals <sup>a</sup>

a) Phlogopites<sup>b</sup>

Label	2/4-1	25/1-1	19/3-2	22/1-3	13/1-1	13/1-3	28/1-1	28/2-1
from zone:	Fo	Fo	Di+Phl	Di+Phl	Phl	Phl	Phl	Phl
K	1.788	1.866	1.878	1.769	1.764	1.506	1.823	1.846
Na	0.141	0.055	0.020	0.028	0.027	0.025	0.027	0.024
Mg	5.271	5.729	5.712	5.653	5.040	5.427	5.106	5.138
Fe	0.175	0.076	0.141	0.082	0.110	0.183	0.133	0.072
Ca	0.010	0.022	0.012	0.031	0.017	0.641	0.040	0.029
Mn	0.006	0.004	0.001	0.000	0.006	0.001	0.001	0.000
Ti	0.077	0.051	0.022	0.042	0.160	0.073	0.096	0.063
Si	5.462	5.912	5.941	6.129	5.776	5.841	5.747	5.741
Al	2.963	2.054	2.054	1.880	2.436	1.796	2.523	2.715
F	0.079	0.359	0.294	0.335	0.771	0.844	0.553	0.233
Cl	0.013	0.042	0.062	0.012	0.033	0.076	0.083	0.054
Oxide Sum	95.44	95.63	96.09	95.81	96.57	94.39	95.42	95.39
Fe/(Fe+Mg)	0.032	0.013	0.024	0.014	0.021	0.033	0.025	0.014

b) Tremolites<sup>c</sup>

Label	19/3-2	22/2-1	12/1-4
from zone:	Di+Phl	Di+Phl	Di+Phl
K	0.021	0.009	0.024
Na	0.043	0.017	0.072
Mg	4.860	4.926	4.834
Ca	1.946	1.989	1.964
Fe	0.090	0.072	0.116
Mn	0.004	0.005	0.002
Ti	0.006	0.002	0.004
Si	7.891	7.948	7.798
Al	0.160	0.037	0.270
F	0.044	0.072	0.047
Cl	0.024	0.008	0.007
Oxide sum	97.77	97.66	98.033
Fe/(Fe+Mg)	0.018	0.014	0.023

c) Diopsides<sup>d</sup>

sample	25/2-3	8/1-1
from zone:	Fo	Fo
Na	0.003	0.003
Mg	0.999	0.998
Fe	0.017	0.010
Ca	0.980	0.992
Mn	0.002	0.002
Ti	0.001	0.002
Al	0.009	0.012
Si	1.993	1.987
Oxide Sum	99.85	99.90
Fe/(Fe+Mg)	0.017	0.010

d) Forsterites<sup>e</sup>

sample	2/4-1	25/1-1	25/2-3	8/1-1
from zone:	Fo	Fo	Fo	Fo
Mg	1.918	1.935	1.899	1.957
Fe	0.076	0.057	0.096	0.052
Ca	0.002	0.001	0.001	0.000
Mn	0.004	0.003	0.004	0.002
Si	1.000	1.001	1.000	0.993
Oxide sum	100.14	99.98	99.90	100.73
Fe/(Fe+Mg)	0.038	0.029	0.048	0.026

a All mineral formulas assume Fe as Fe<sup>2+</sup>.

Oxide sum refers to the sum of metal oxide wt%.

b Phlogopites: cations per 22 oxygen atoms

c Tremolites: cations per 23 oxygen atoms

d Diopsides: cations per 6 oxygen atoms

e Forsterites: cations per 4 oxygen atoms

f Calcites: cation 1 oxygen atom;

minerals are the one that record maximum temperatures

e Dolomites cations per 2 oxygen atoms

minerals with maximum recorded Ca content

e) Calcites<sup>f</sup>

sample	2/4-1	2/5-1	24/3-2	4/1-1	8/3-2	8/3-3	22/3-3	22/1-1	22/1-3	21/1-1	13/1-3
from zone:	Fo	Fo	Fo	Fo	Di+Dol	Di+Dol	Di+Phl	Di+Phl	Di+Phl	Di+Phl	Phl
Ca	0.910	0.949	0.933	0.934	0.931	0.938	0.936	0.937	0.941	0.945	0.961
Mg	0.086	0.050	0.066	0.064	0.066	0.059	0.062	0.061	0.057	0.054	0.037
Fe	0.003	0.001	0.001	0.002	0.002	0.002	0.002	0.001	0.001	0.001	0.002
Mn	0.000	0.001	0.001	0.001	0.001	0.001	0.001	0.001	0.001	0.001	0.001
oxide sum	99.45	100.44	99.16	99.95	100.13	99.50	99.07	100.05	99.63	100.41	100.35
Fe/(Fe+Mg)	0.035	0.018	0.016	0.025	0.027	0.040	0.028	0.015	0.016	0.017	0.058

f) Dolomites<sup>g</sup>

sample	2/4-1	24/3-2	4/1-1	8/3-2	8/3-3	22/3-3	22/1-1	22/1-3	21/1-1	13/1-3
from zone:	Fo	Fo	Fo	Di+Phl	Di+Phl	Di+Phl	Di+Phl	Di+Phl	Di+Phl	Phl
Ca	1.031	1.032	1.034	1.019	1.023	1.021	1.025	1.020	1.020	1.007
Mg	0.950	0.957	0.956	0.960	0.954	0.963	0.962	0.970	0.964	0.968
Fe	0.016	0.008	0.009	0.021	0.020	0.013	0.010	0.010	0.016	0.024
Mn	0.003	0.002	0.001	0.001	0.003	0.003	0.003	0.000	0.001	0.001
oxide sum	99.23	99.41	100.22	99.10	99.40	99.85	99.63	99.59	99.65	99.22
Fe/(Fe+Mg)	0.017	0.008	0.009	0.021	0.020	0.013	0.010	0.011	0.016	0.024

minerals in all parts of the aureole are indicative for the involvement of igneous fluid, even in low-grade rocks. In this case the untypically high values in the outer aureole may reflect localized infiltration of fluid derived from an underlying igneous body of unknown shape or extent.

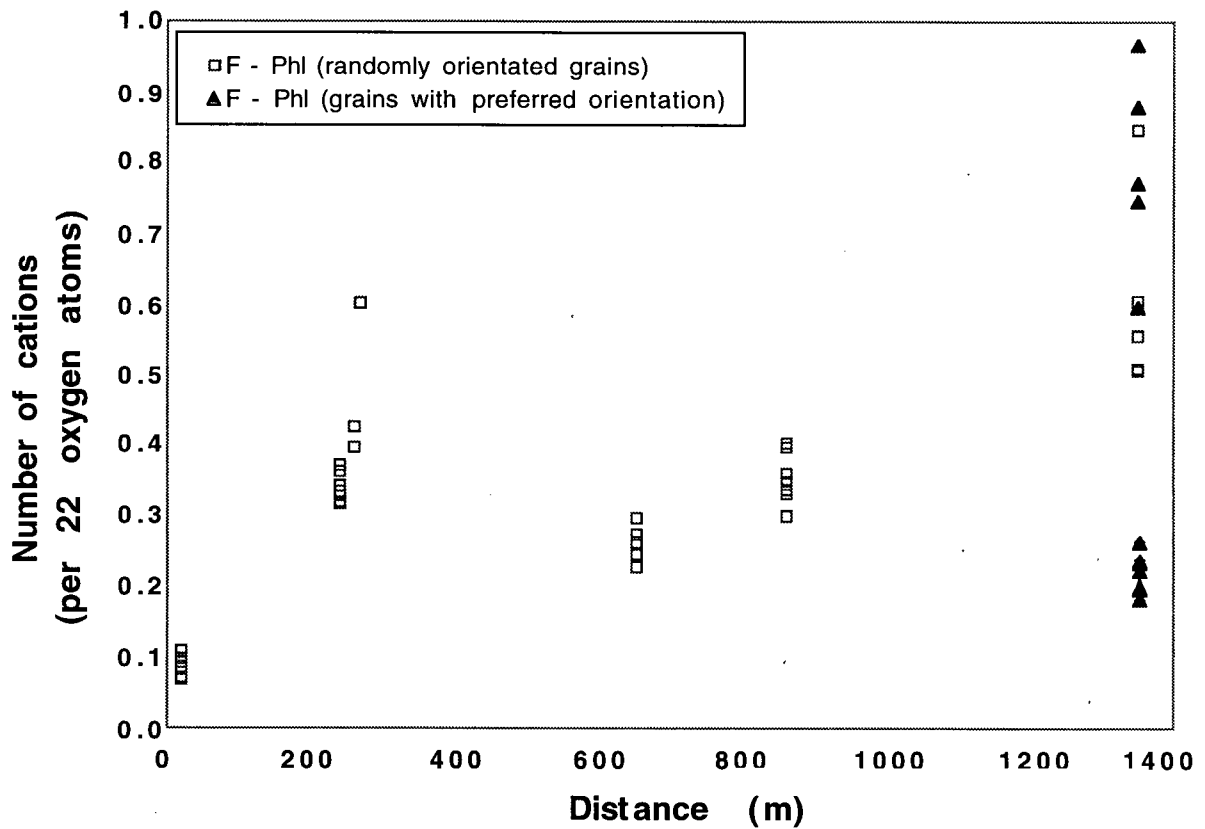


**Figure 6:** Fluorine content of phlogopites over the whole width of the aureole. The distinction between 'randomly orientated grains' and 'grains with preferred orientation' stems from the fact that in the phlogopite zones, phlogopite grains are significantly more abundant in parts of the rocks where the phlogopite grains show a preferred orientation..

## **CHAPTER 4**

### **CONTROLLING FACTORS ON THE DEVELOPMENT OF THE METAMORPHIC MINERAL ASSEMBLAGES**

#### **4.1 Introduction**

Metamorphic minerals and mineral assemblages commonly reflect peak metamorphic conditions and sometimes they preserve information on the reaction path. To identify the influences of contact metamorphic processes such as heating and fluid flow the effects of varying bulk compositions must be eliminated first. Below the effects of varying bulk composition on the development of the mineral assemblages in the Horsethief Creek aureole are addressed and the competing influences of heating and fluid infiltration discussed.

#### **4.2 Effects of Bulk Compositional Variations on Metamorphic Mineral Assemblages**

Part of the petrological complexity in the Horsethief Creek aureole as described above can be assumed to reflect variations in bulk composition. The extent of the variations becomes clear when looking at the results of whole rock analyses as shown for major elements only in Figure 7 a-f. MgO content for example varies from  $\approx 12 - 22$  weight percent (wt%), CaO from  $\approx 20 - 30$  wt% with a distribution pattern very similar to that of the MgO,  $K_2O$  varies from  $\approx 0 - 3.5$  wt% and  $SiO_2$  from  $\approx 10 - 48$  wt%. The complete data set for the whole rock analyses, plots of the distribution of some trace elements and a description of the methodology are listed in appendix B.

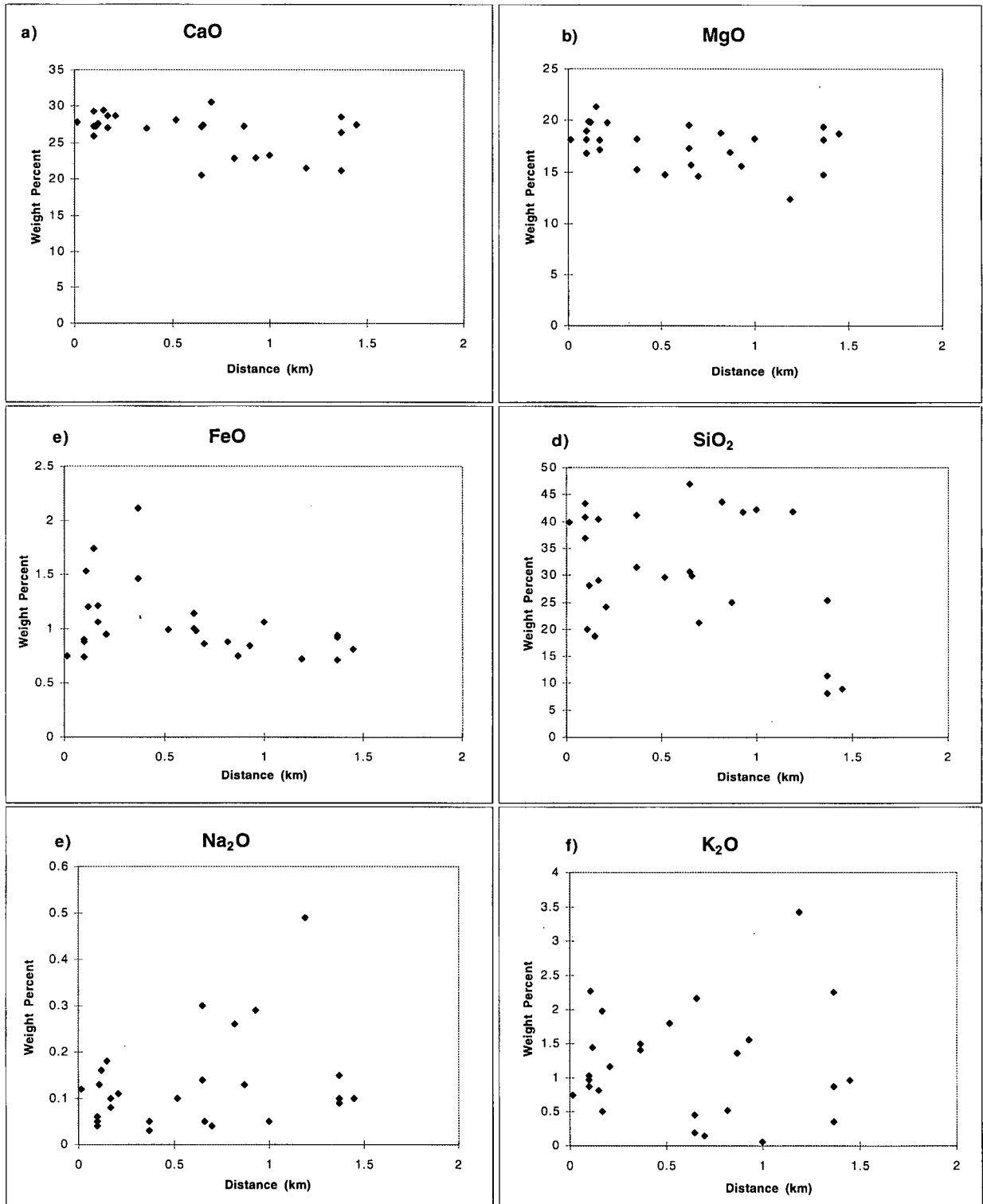
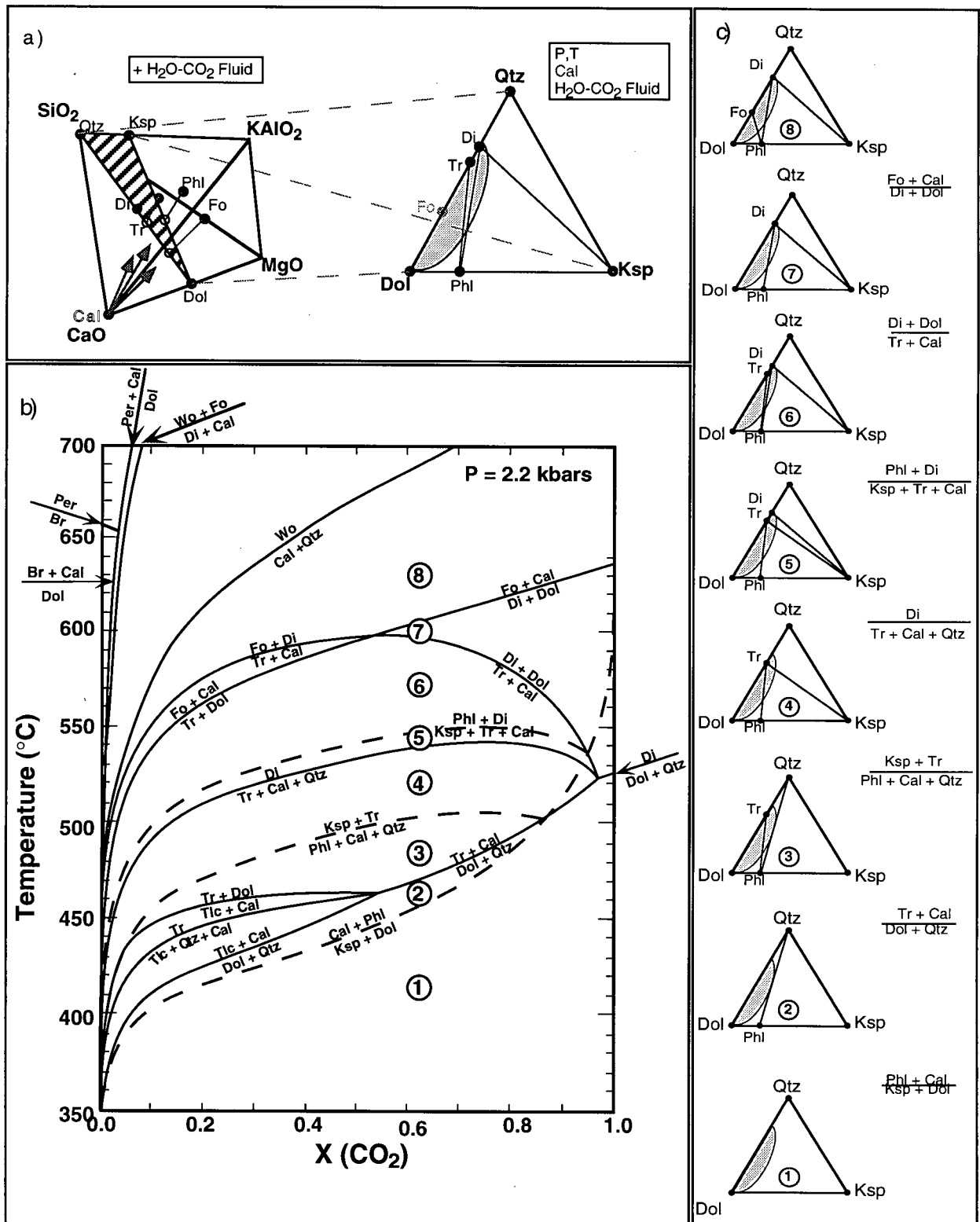


Figure 7: a-f) Major element whole rock XRF analyses.

An effective way to illustrate effects of varying bulk composition is by using ternary diagrams. The observed mineral assemblages in the potassic siliceous dolomites can be represented in the  $\text{SiO}_2$  - CaO - MgO -  $\text{KAlO}_2$  tetrahedron. As justified in section 3.2.1 it is assumed that prior to metamorphism the siliceous dolomites were composed of dolomite + quartz + K-feldspar  $\pm$  calcite. All higher grade rocks also contain calcite. This allows the simplification of the compositional phase diagrams by projecting from calcite onto the Qtz - Dol - Ksp plane (Figure 8a). Within the Qtz - Dol - Ksp ternary phase diagram, the effect of minor changes in bulk composition can be visualized. For example, the topology illustrated in figure 8a is for the diopside + phlogopite zone. It demonstrates that the sporadic development of diopside and the complex distribution of phlogopite and K-feldspar in part reflect bulk compositional variations. The mineral assemblages: Cal+Tr; Cal+Tr+Phl; Cal+Di+Phl; Cal+Di+Ksp; Cal+Di+Tr+Phl; Cal+Di+Phl+Ksp; Cal+Tr+Dol+Phl are all stable on this topology and are all observed in the diopside + phlogopite zone. Diopside-free rocks are not necessarily of tremolite grade but can be assigned to the diopside + phlogopite zone if the bulk composition prevents the formation of diopside. As an example, the assemblage tremolite - calcite - K-feldspar assemblage is stable in fields (4) and (5) of the T- $X_{\text{CO}_2}$  diagram (see Figure 8b and c). Diopside is produced at the reaction curve between fields (5) and (6). A silica rich sample with the assemblage tremolite - calcite - quartz is stable over fields (3) and (4) and starts producing diopside at lower temperatures along the reaction curve between fields (4) and (5). Hence, the potassic sample still shows tremolite as highest grade mineral in field (5) while the silicic sample already contains diopside in field (5). The stippled field on the ternary marks the approximate range of rock compositions observed in the Horsethief Creek aureole.

To systematically depict possible assemblages within and reactions between all the metamorphic zones, the relevant isobarically divariant fields in the T- $X_{\text{CO}_2}$  diagram were systematically numbered (Figure 8b) and a ternary projection for each of these zones was constructed (Figure 8c). In order to identify changes in mineral assemblages that require a change



**Figure 8:** a) Projection from Cal onto the Qtz-Ksp-Dol plane allowing an easier identification of stable assemblages, and example illustration of the diopside + phlogopite zone in the new simplified system. b) Simplified T- $X_{\text{CO}_2}$  diagram with the divariant fields systematically numbered for a clear representation of the different metamorphic zones. c) Phase compatibility diagrams for all the identified grades.

in temperature or  $X_{\text{CO}_2}$ , (and are not an effect of varying bulk composition) the maximum T- $X_{\text{CO}_2}$  stability range of each mineral assemblage was compiled (boxes in Table 3). New, higher grade metamorphic zones were defined by identifying samples with mineral assemblages that require an increase in metamorphic grade. For example, samples 12/4-2 through 21/1-1 were all assigned to the metamorphic zone (or grade) 5 (Table 3). Their stability fields allow an assignment to any one of the zones 3 through 6 but the down-grade sample 12/4-1 requires a minimum grade 5 and only sample 21/1-3 requires an increase in metamorphic grade above that, i.e. to grade 6.

The representative zone for each sample is indicated by the number within the boxes in table 3. Using this procedure we eliminate possible effects of bulk compositional variations, confirm the six earlier identified isograds and also identify what appear to be retrograde assemblages (r#). The upper stability limit of these samples lie below the peak metamorphic grade assigned to the respective areas. Note that these assemblages predominantly occur in samples in the intermediate (to high) temperature range. These "retrograde" assemblages may only appear to be retrograde. They can also be the result of fluid infiltration at or near peak metamorphic conditions as is explained below in section 4.4.

See Figure 9 for the spatial distribution of assemblages assigned to zones as described here.

### 4.3 Thermal Controls

If metamorphism is driven by heat flow alone, low-variance mineral assemblages with sharp isograds are expected (e.g., Rice 1977a,b, and section 1.3 this study). The assemblages in the Horsethief Creek aureole are predominantly isobarically divariant and the geometry of the isograds is not very well defined. Additionally, the concept of progressive metamorphism suggests that higher-grade assemblages develop from the lower-grade assemblages observed in an aureole (e.g., Rice 1977a,b). For example, during heating tremolite + calcite should react to

**Table3:** Maximum stability range and representative zone for each assemblage after elimination of bulk compositional effects, resulting in the identification of seemingly retrograde assemblages (r)

Note: The numbers in table 3 correspond to the numbers assigned to the stability fields in the T-X<sub>CO2</sub> in figure 3b.

	1	2	3	4	5	6	7	8
18/2 - 1	1→2							
18/1 - 1	1→2							
18/1 - 2	1→2							
13/2 - 1	1							
13/2 - 2	1							
13/2 - 3	1→2							
13/2 - 4	1→2							
28/1 - 1	1→2							
28/1 - 2	1→2							
28/1 - 3	1→2							
28/1 - 4	1→2							
28/1 - 5	1→2							
15/1 - 3				4				
15/1 - 4				4				
15/1 - 5				4				
15/1 - 6				4				
15/1 - 7				4				
12/3 - 1				4				
12/3 - 2				4				
21/3 - 1				4				
21/3 - 2				4				
12/4 - 1				4←5				
12/4 - 2				5				
12/4 - 3				5				
21/2 - 1				5				
21/2 - 2				5				
21/1 - 1				5				
21/1 - 3						6		
12/2 - 1						6		
12/1 - 1						6		
12/1 - 3						6		
12/1 - 4					r5			
12/1 - 5					r5			
22/1 - 1						6		
22/1 - 2						6		
22/1 - 3A						6		
22/1 - 3B						6		
22/2 - 1						6		
22/2 - 2					r5			
22/2 - 3						6		
22/3 - 1						6		
22/3 - 2A					r5			
22/3 - 2B						6		
22/3 - 3						6		
22/3 - 4						6		
17/1 - 1					r5			
22/4 - 1					r5			
22/4 - 2					r5			
11/1 - 1					r5			
10/2 - 1						6		
10/2 - 2						6		
10/2 - 3						6		
10/2 - 4						6		
10/2 - 5					r5			
19/3 - 1						6		
19/3 - 2A						6		
19/3 - 2B						6		
14/2 - 1						6		
27/3 - 1						6		
27/3 - 2						6		
3/4 - 1						6		
3/3 - 1					r5			
9/1 - 2					r5			
23/3 - 1						6		
23/3 - 2						6		
3/1 - 1						6		
8/3 - 1						r5		
8/3 - 2						6←7		
8/3 - 3A						r6		
8/3 - 3B						r6		
8/4 - 1A						r6		
8/4 - 1B						7		
8/2 - 1						7		
8/1 - 1							8	
25/2 - 1							8	
25/2 - 2							8	
25/2 - 3A							8	
25/2 - 3B							8	
25/2 - 4							8	
25/1 - 1							8	
25/1 - 2							8	
6/3 - 1							8	
6/3 - 2							8	
6/2 - 1							8	
4/1 - 1A							8	
4/1 - 1B							8	
4/1 - 2							8	
23/1 - 1							8	
23/1 - 2							8	
23/1 - 4							8	
24/1 - 1							8	
24/1 - 2							8	
24/1 - 3							8	
24/1 - 4							8	
7/1 - 1A							8	
7/1 - 1B							8	
24/3 - 1							8	
24/3 - 2							7→8	
24/3 - 3							8	
4/3 - 2							8	
23/2 - 1							8	
23/2 - 2							8	
23/2 - 3							8	
24/2 - 1							8	
24/2 - 2							8	
2/5 - 1							8	
2/5 - 2							8	
2/5 - 3							8	
2/5 - 4							8	
2/5 - 5							8	
2/5 - 6							8	
2/4 - 1A							8	
2/4 - 1B							8	
2/4 - 2							8	
2/4 - 3							8	
2/2-1							8	

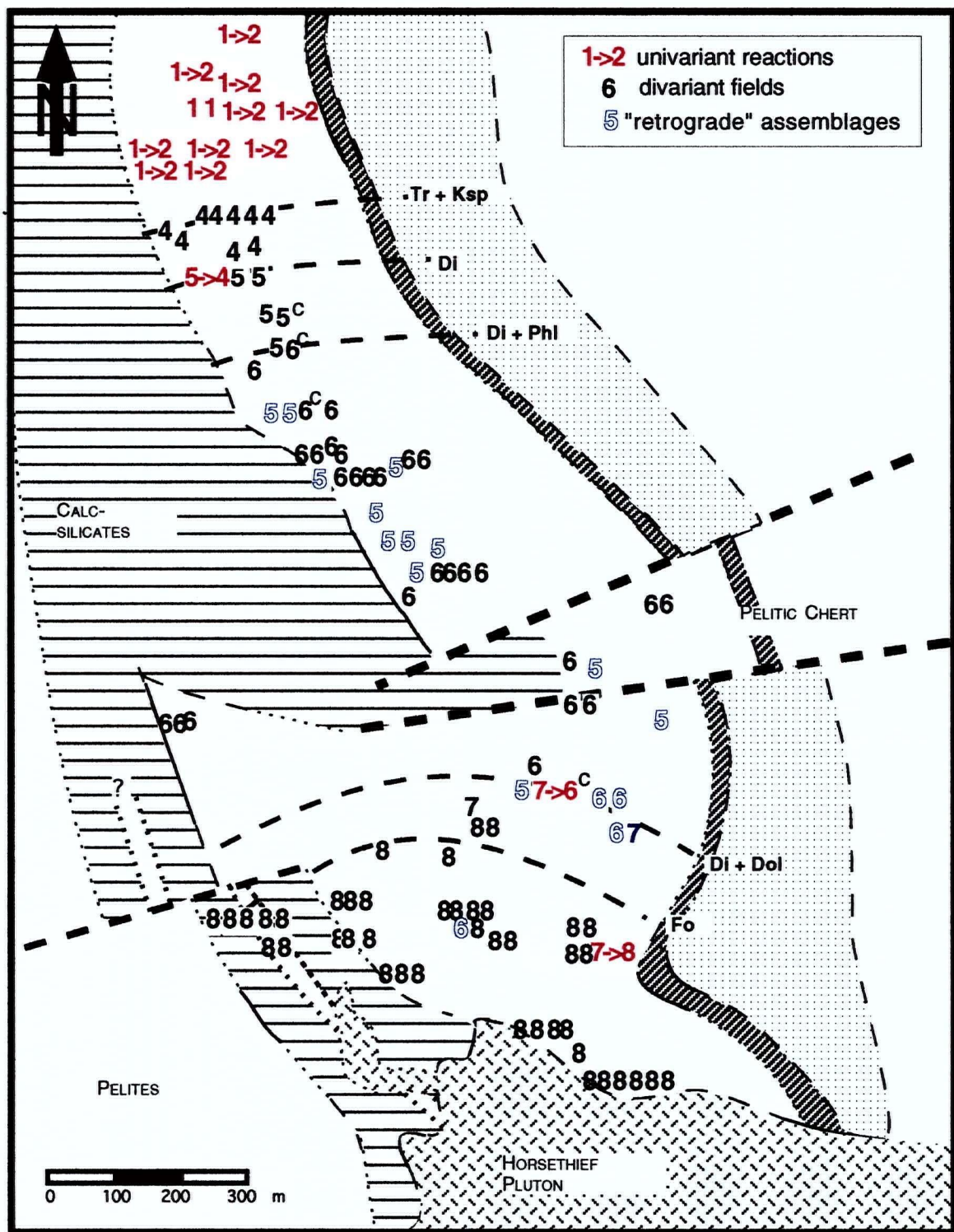


**Figure 9:** Map showing the distribution of assemblages representing the various metamorphic zones after elimination of bulk compositional effects. The zones are numbered according to the numbering of stability fields in the T-X<sub>CO2</sub> diagram in figure 8b. Assemblages refer to isobarically univariant (X->Y) or divariant (X) assemblages. "Retrograde" assemblages (X) are apparent retrograde assemblages as described in the text.

produce diopside + dolomite. In the next paragraphs it is demonstrated that this may not have been the case in the Horsethief Creek aureole and that heating alone could not have produced the mineral assemblages in the distribution observed in the Horsethief Creek aureole. Other factors also had control on the development of the peak metamorphic assemblages.

The sequence of the six identified isograds is consistent with a continuous increase in peak temperature from  $\approx 400$  to  $\approx 650$  °C at  $P \approx 2.2$  kbar and at  $X_{\text{CO}_2} \approx 0.6$  as schematically indicated in the T- $X_{\text{CO}_2}$  diagram in Figure 10.

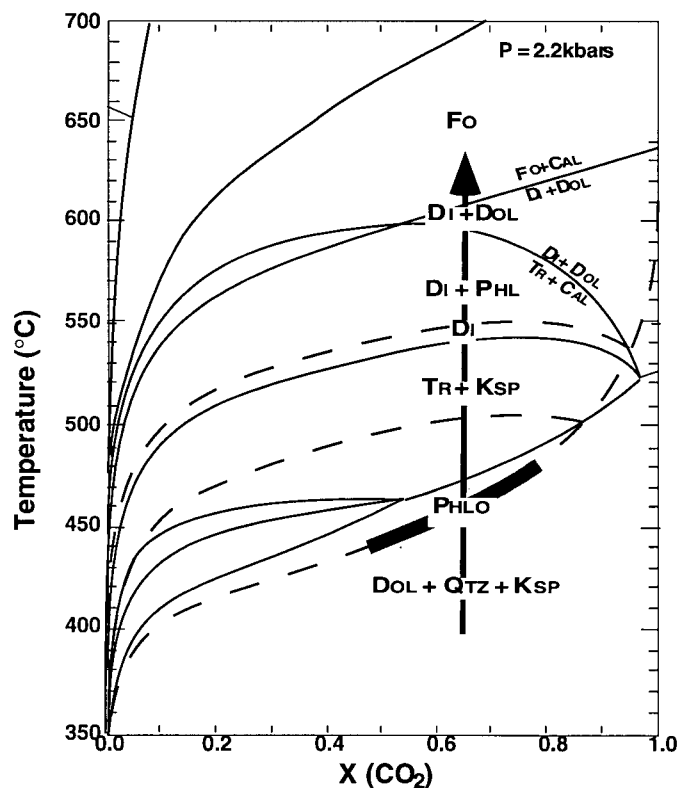


**Figure 10:** T- $X_{\text{CO}_2}$  diagram showing that the sequence of zones identified could theoretically have been produced by simple heating at  $X_{\text{CO}_2} \sim 0.6$ .

To constrain the temperatures attained in the aureole, samples with coexisting calcite and dolomite were analyzed. The  $\text{MgCO}_3$  content of calcite in equilibrium with coexisting dolomite is a function of temperature as defined by the miscibility gap between the two phases (e.g., Goldsmith and Newton (1969)). The Mg-content in calcite can easily be measured and then used to calculate the corresponding temperatures. Here, temperatures were calculated after Anovitz and

Essene (1987) with no iron-correction because of the very low iron content observed in the rocks (Table 2). Temperatures calculated using the Fe-correction yielded temperatures within 2 to 3 degrees of the values of the uncorrected calculation.

Geothermometry results are plotted in Figure 11a. Each temperature obtained is plotted as a solid circle. A total of 123 spots on 10 thin sections containing coexisting calcite - dolomite were analyzed. These are supplemented by analyses from one forsterite-bearing sample (2/5-1) that does not contain dolomite. This sample was analyzed to constrain the minimum temperature for the forsterite-in reaction assuming that the reaction was a dolomite consuming one. Only the maximum value is plotted for that sample as indicated by the solid triangle at  $\approx 25$  m from the contact. It is found to be within the temperature range observed in dolomite bearing assemblages.

The maximum value only is also plotted for the sample from the phlogopite-zone (13/1-1) where a very wide scatter, interpreted to reflect un-equilibrated grains, was observed. Multiple analyses on one grain were possible in some high-grade rocks (see Appendix A2), but in intermediate- to low-grade assemblages small grainsizes precluded multiple analyses on single crystals. In sample 2/4-1, the sample closest to the contact, some calcite grains were analyzed that appear to be inclusions within forsterite. The resulting temperatures of these grains are among - but are not exclusively - the highest recorded. The observed scatter in temperatures for each given sample can be ascribed to re-equilibration during cooling and/or exchange disequilibrium. The Mg-content in some calcite crystals varies significantly. For example, sample 2/4-1 contains calcite crystals with cores that have a higher Mg-content than the rims. In sample 8/3-2 however, calcite crystals with cores Mg-poorer relative to the rims were observed.

An additional independent temperature estimation is provided by the peak metamorphic assemblages. The vertical lines and arrows in Figure 11a represent the stability range of the mineral assemblages (as defined in Figure 8b) of each of the samples used for geothermometry. These two independent temperature determinations are in excellent agreement except for sample

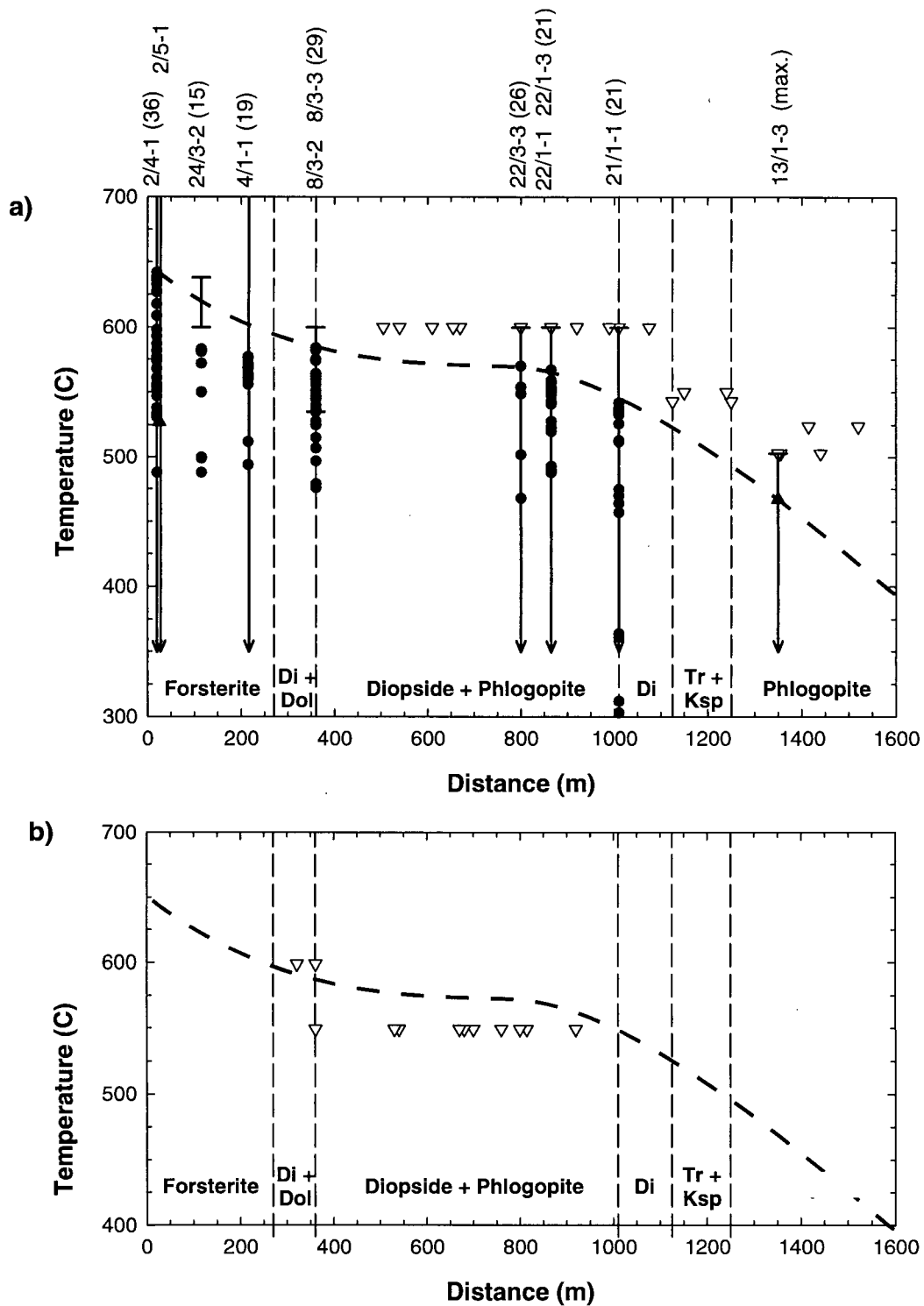


**Figure 11:** a) Plot of geothermometry data. Each solid marker represents a single analysis. The numbers at the top of the diagram refer to the sample numbers. The numbers in parentheses give the number of spots analysed at outcrop(s) at each given distance. The dashed line represents a best fit temperature profile. For description of other symbols refer to the text. b) Maximum possible temperature for the apparent retrograde assemblages compared with the best fit

24/3-2 where the highest measured temperature is slightly below what is required for the assemblage to be stable. This internal consistency of the two data sets not only confirms the good quality of the measurements but also the validity of assuming that the fluid pressure was near lithostatic at  $\approx 2.2$  kbar, in accordance with geobarometry data from the pelitic rocks (Floriet 1996). The best estimate of peak metamorphic temperatures ( $T_{\max}$ ) throughout the aureole is a smooth line drawn through the maximum calcite - dolomite - geothermometry temperatures. This best fit curve is used as the representative temperature profile below. The open triangles in Figure 11a represent the maximum temperatures at which dolomite free mineral assemblages in other samples are stable. These temperatures are all in agreement with the representative  $T_{\max}$  - profile.

In Figure 11b the  $T_{\max}$  -profile is compared to maximum temperatures recorded by apparently retrograde assemblages (r# in Table 1). These temperatures are at most only slightly ( $\leq 20^\circ$ ) below the  $T_{\max}$  -profile. Hence, nominally retrograde assemblages may have formed at or near the thermal peak and not truly retrograde after substantial cooling. Because the difference in their mineralogy could not be explained by the variable bulk composition either, other factors must have had an important influence.

The form of the  $T_{\max}$  -profile is unlike peak temperature profiles predicted by simple models of conductive cooling of igneous intrusions (e.g., Furlong *et al.* 1991). The plateau may reflect the presence of an igneous body below the middle aureole (cf. Appendix B). However, this is considered unlikely because of the small overall width (1.5 km) of the thermal aureole compared to the  $\approx 15$  km in diameter Horsethief pluton. This problem is discussed in more detail in section 4.5 below.

#### 4.4 Fluid Infiltration

Because there are several lines of evidence for syn-metamorphic fluid flow, infiltration of a H<sub>2</sub>O rich fluid must have played a significant role in the evolution of the aureole. The development of hydrous minerals like tremolite and phlogopite, often in high abundance, throughout the inner and middle aureole (Plate 7) from the anhydrous dolomite + quartz + K-feldspar ± calcite protolith requires the introduction of H<sub>2</sub>O. The prevalence of isobarically divariant mineral assemblages and the paucity of high X<sub>CO<sub>2</sub></sub> assemblages (Table 1) also require infiltration, as they are inconsistent with internal buffering of fluid composition by mineral reaction during heating (Greenwood 1975).

Infiltration of an H<sub>2</sub>O-rich fluid can trigger mineral reactions in the absence of heating or cooling as outlined in 4.4.1 below. If infiltration is heterogeneous, the development of mineral assemblages with different index minerals can result within a single outcropping. This leads to the conclusion that heterogeneities in the distribution of index minerals which cannot be explained by effects of varying bulk composition or retrograde reaction may have formed as a consequence of heterogeneous fluid infiltration. In section 4.4.2 the diopside forming reaction (5) recorded by mineral assemblages in several samples in the aureole is analyzed in light of the results from paragraph 4.4.1. Having established that fluid infiltration played an important role in the development of the aureole, oxygen and carbon stable isotope data were obtained to place further constraints on possible fluid source(s). The data and its interpretation are presented in paragraph 4.4.3. In paragraph 4.4.4 evidence for silica metasomatism in the aureole is outlined.

A comprehensive discussion about possible mechanism fluid infiltration, combining all available data, is given in the next section, section 4.5. Possible explanations for the petrographic break at the tremolite + K-feldspar isograd are also given in that section.

#### 4.4.1 Nominally Retrograde Assemblages

As outlined above, the mineral assemblages marked "r#" in Table 3 are only nominally retrograde, but their difference in mineralogy cannot be explained by the variable bulk composition. Their maximum possible temperatures are very close to the  $T_{\max}$  - profile indicating their stability at or near peak metamorphic conditions. Infiltration of a fluid with a  $X_{\text{CO}_2}$  that is in disequilibrium with the rock triggers mineral reactions as rock and fluid try to re-gain equilibrium.

The effects of infiltration of an  $\text{H}_2\text{O}$  rich fluid into rocks that were substantially heated prior to infiltration is illustrated in Figure 12. The horizontal arrows in the mid to high temperature part on the  $T$ - $X_{\text{CO}_2}$  phase diagram mark possible isothermal reaction paths that could explain the occurrences of tremolite assemblages in the diopside zone(s) and diopside occurrences in the forsterite zone. Depending on the amount of infiltration and the amount of reaction progress, assemblages with a very different mineralogy can develop. Hence, the "retrograde" assemblages in the Horsethief aureole may record near-isothermal heterogeneous fluid infiltration at the outcrop scale, not reaction during cooling.

#### 4.4.2 Reaction of Diopside to Tremolite - Textural Evidence for

##### Infiltration-triggered Reaction

A possible record of a near-isothermal reaction (as described in 4.4.1) is observed in several samples from the aureole in which cores of diopside are preserved within (up to 2 cm long) tremolite porphyroblasts (Plate 8a and b). All of these samples are marked with a "XC" or "C" in the diopside column in table 1 and with a superscript "C" in Figure 9. One of these samples (8/3-2) records the univariant assemblage diopside - dolomite - tremolite - calcite. These observations indicate that diopside reacts to tremolite by reaction (4) (i.e.,  $\text{Di} + \text{Dol} + \text{H}_2\text{O} + \text{CO}_2 = \text{Tr} + \text{Cal}$ ; cf.



Figure 4). This reaction can result from infiltration of a H<sub>2</sub>O-fluid (Figure 7). While the textural observation alone is not unequivocal evidence for prograde reaction, the relatively widespread occurrence of this texture and of other only nominally retrograde assemblages (4.4.1) support the assumption that the diopside → tremolite reaction is an essentially prograde rather than a retrograde volatilization reaction.

Interestingly, the diopside + dolomite = tremolite + calcite reaction curve is the only one with a marked negative slope in the T-X<sub>CO<sub>2</sub></sub> diagram. For this reason the isobarically univariant assemblage diopside - dolomite - tremolite - calcite can persist during down-T fluid flow of low to moderate quantities of an aqueous fluid that infiltrates diopside -dolomite bearing rocks, triggering reaction. Thus, in the case of down-T fluid flow in an aureole, the diopside - dolomite - tremolite - calcite assemblage is the only isobarically univariant assemblage predicted to be stable over a finite distance in the aureole (Ferry (1994), Dipple and Ferry (1996)).

Although this assemblage is not the only univariant assemblage in mid- to high-grade Horsethief Creek rocks it is present (sample 8/3-2). Furthermore, numerous dolomite-absent divariant diopside - tremolite - calcite (- phlogopite) samples found in the aureole show the same reaction texture as sample 8/3-2 suggesting that the same reaction proceeded, but went to completion, in these rocks. (Note that isobarically univariant assemblages are generally rare in the Horsethief Creek aureole.)

#### 4.4.3. Whole Rock Carbonate δ<sup>18</sup>O data

Isotopic ratios of light elements such as oxygen and carbon are sensitive to many physico-chemical changes in a contact-metamorphic environment. Amongst others, they can be used to determine fluid source, extent of devolatilization during reaction and the nature of fluid-rock interaction (Nabalek 1991). This is possible because "the stable isotope composition of a metamorphic rock is controlled by four factors: (1) the composition of the pre-metamorphic

protolith; (2) the effects of volatilization; (3) exchange with infiltrating fluids (with variable composition and fluid/rock ratio); (4) the temperature of the exchange." (Valley 1986, p.445).

In this section I briefly discuss the results of carbonate whole rock isotope analyses with respect to the oxygen isotopes. A description of the method, the listing of all raw and converted data and a very brief discussion of the carbon isotope data can be found in Appendix C1. An excellent overview over the use of stable isotopes in the analyses of fluid flow during contact-metamorphism is given by Nabalek (1991).

The whole rock carbonate isotope data obtained for 26 samples over the width of the aureole confirm the infiltration of isotopically distinct fluid(s) and the heterogeneous nature of infiltration. The results are ambiguous as to the source(s) of the fluid(s), but a case of combined vertical influx of pelite-derived fluids and sub-horizontal fluid flow best explains the data.

The oxygen isotope data are plotted versus distance from the contact in Figure 13a. There is a clearly discernible  $^{18}\text{O}$  depletion between carbonate samples in the phlogopite zone and those close to the pluton. Values are as high as  $\approx 23$  per mill (‰) in phlogopite zone rocks in the outermost aureole and as low as  $\approx 16$  ‰ near the contact. Although care was taken to sample unaltered parts of the rocks, the  $\delta^{18}\text{O}$  of  $\approx 13$  ‰ at  $\approx 180$  m (sample 24-1/4) may reflect influence of late low-temperature alteration. Serpentine is found in altered parts of this rock. The values of  $\approx 22 - 23$  ‰ in the outer aureole reflect values typical of unaltered dolomites (e.g., Valley 1986). The values of  $\approx 16$  ‰ in the inner aureole are significantly higher than the values expected for these rocks if they isotopically equilibrated with fluid that emanated from the adjacent granitoid (reference for 'granite'- $\delta^{18}\text{O}$  in Figure 14).

However, oxygen isotope depletion by decarbonation reactions generally accounts for a  $^{18}\text{O}$  depletion of no more than  $\approx 2$  ‰, independent on whether Rayleigh or batch decarbonation occurs (e.g., Nabalek 1991). The  $^{18}\text{O}$  depletion of  $\approx 7$  ‰ is therefore strong evidence for infiltration of an isotopically lighter fluid. The source(s) of the fluid(s) in this case is (are) not obvious. If the main source of the isotopically distinct fluid was not the pluton, the underlying metapelite is

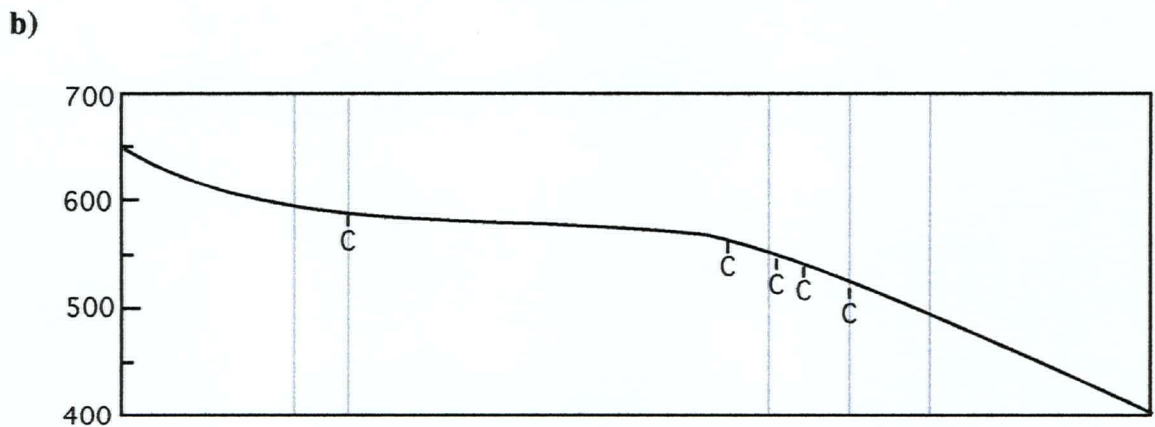
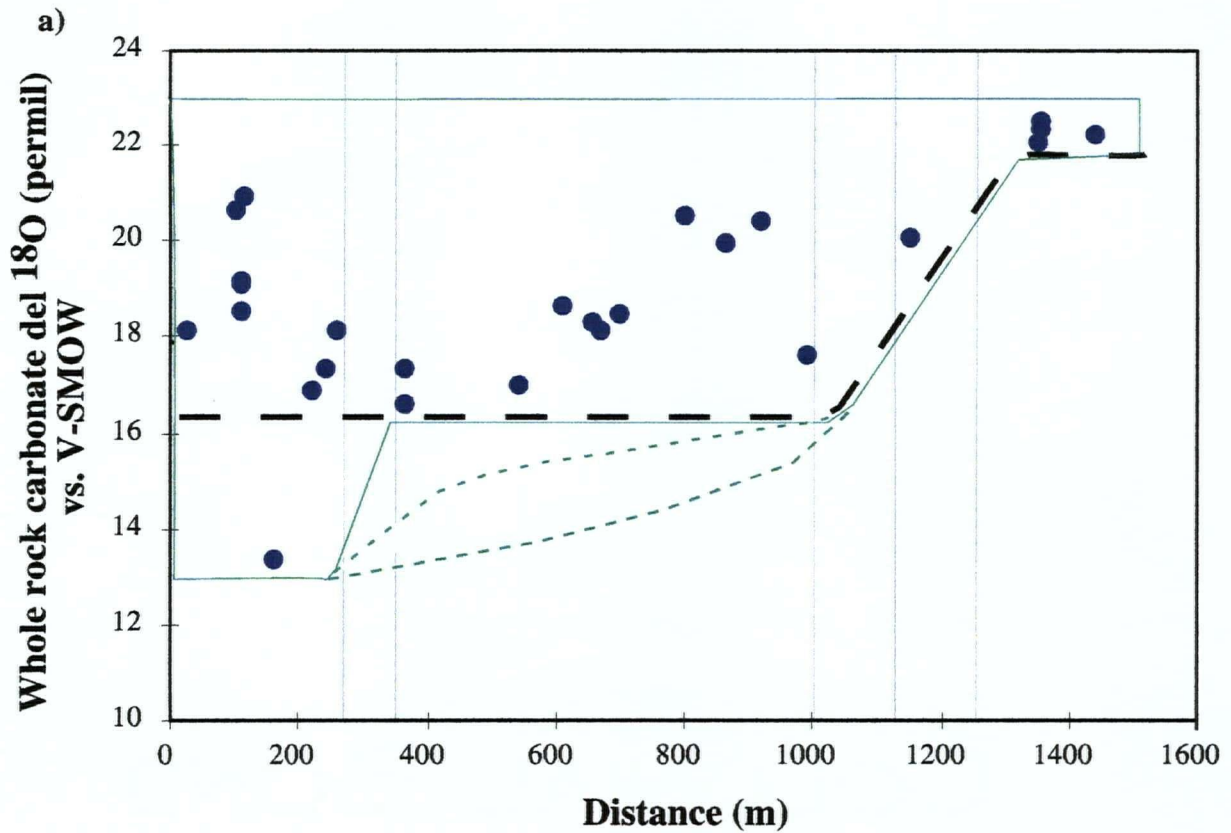


**Figure 13:** a) Whole rock carbonate oxygen isotope data. The vertical grey lines mark the locations of the isograds (Fo, Di+Dol, Di+Phl, Di, Tr with increasing distance). The thick, black dashed line outlines the oxygen isotope pattern if the sample at  $\approx 180$  m is assumed to be retrogressed. A 'front' is observed at  $\approx 1150$  m (for details see text). The thin solid green line outlines the isotope pattern if all analyses are interpreted to represent contact-metamorphic values. A "two-front" pattern emerges with the one front at  $\approx 1150$  m and the other one closeto the contact ( $\approx 200$  m). The effect that the one sample at  $\approx 180$  m has on the overall appearance can be weakened if assuming a more gradual transition as indicated by the fine dashed green lines (for possible explanations refer to text). b) "Best-fit temperature" profile and locations of samples that show the reactions texture of diopside cores within tremolites('C') (as described in paragraph 4.4.2). Note the correlation between isotope 'front', end of thermal plateau and outermost occurrence of the diopside  $\rightarrow$  tremolite reaction texture.

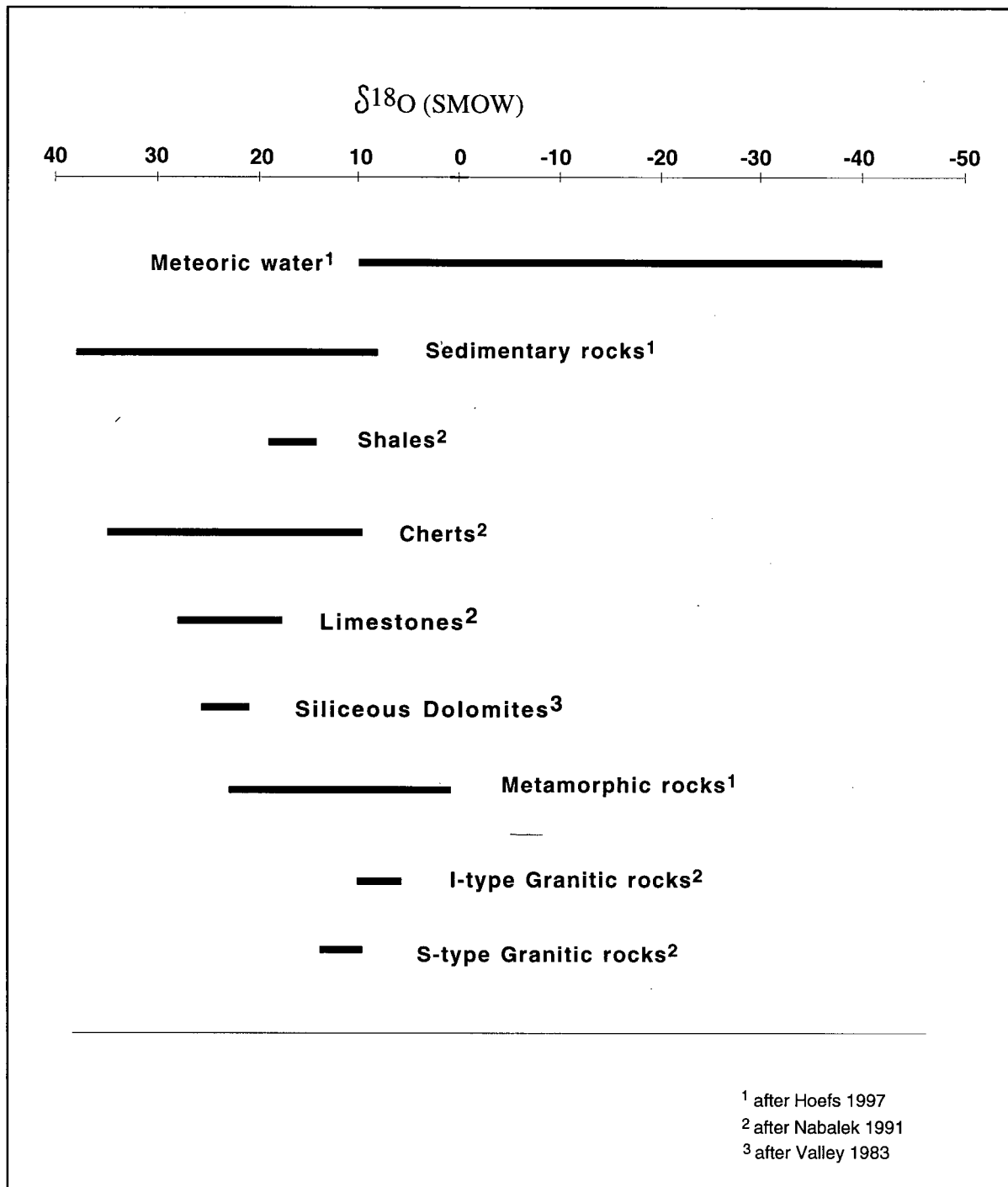


**Figure 14:** Oxygen isotope signature of various geological materials that are possible sources for the fluid(s) that infiltrated the siliceous dolomites in the Horsethief Creek aureole.

another possible source. Metapelitic rocks are presumed to have a  $\delta^{18}\text{O}$  signature of  $\approx 15 - 20 \text{‰}$  prior to contact-metamorphism (Figure 14). These values are in agreement with the  $\delta^{18}\text{O}$  observed in the Horsethief Creek aureole.

Another interesting observation is the wide scatter of  $\delta^{18}\text{O}$  at any given distance, especially in the inner aureole. Values range from as high as 21‰ to as low as 17‰ at  $\approx 100$  m distance from the contact. This points to strongly heterogeneous fluid flow in this area.

On the other hand there is no systematic change in whole rock carbonate  $\delta^{18}\text{O}$  with distance or style of infiltration. There is no correlation between the amount of veining in the rock and the carbonate whole rock  $\delta^{18}\text{O}$  values (Dipple and Niermann, 1997). Preliminary tests of 'spot-analyses' across veins by means of micro-drilling confirms this. No changes in isotope signature is found across veins into matrix material (Dipple, pers. com.). This suggests that infiltration was homogenous on the scale of individual beds and that vein and pervasive flow were well mixed. This attests to the overall strongly pervasive nature of infiltration in the Horsethief Creek aureole.

A more comprehensive discussion about possible fluid sources and fluid flow direction is possible if the isotope values are not discussed by themselves, but rather are analyzed in combination with petrographic observations and heat flow considerations. This is done in section 4.5 below.

#### 4.4.4 Silica metasomatism and intensity of infiltration

The pervasive development of high abundant tremolite in most rocks and the general absence of dolomite in the inner and middle aureole suggests that metamorphism was not isochemical and that silica was introduced into the system by the infiltrating fluid. This is also reflected by the observation of often silica richer bulk composition in and around veins, including the chaotic veining in the inner aureole (Plate 10) (cf. Figure 8c, see also Appendix C2.) Possible sources of

the silica are the interbedded chert layers, and/or the source(s) of the infiltrating fluid, namely the pelites and the pluton.

The strongly pervasive character of infiltration and silica metasomatism in all except the outermost aureole (>1250 m from contact) is unusual for contact metamorphosed siliceous dolomites. Siliceous dolomites in other contact aureoles are often reported to show more isobarically univariant assemblages and/or unreacted dolomite (Moore and Kerrick 1976; Rice 1977a b; Holness 1992). Infiltration coupled with extensive silification is, if at all, only observed to occur relatively close (<  $\approx$ 150 m) to the contact (e.g. Bucher-Nurminen, 1982).

The introduction of large amounts of silica by the fluid may have a profound influence on the permeability structure of the aureole. For example, the tremolite-in reaction (2) is coupled with a volume decrease of  $\approx$ 24 % if all  $\text{SiO}_2$  is provided by quartz. In contrast, the same reaction is coupled with a volume increase of  $\approx$ 19 vol%, if all  $\text{SiO}_2$  is provided by  $\text{SiO}_{2(\text{aq})}$ , dissolved in the infiltrating fluid. While the overall permeability is not only a function of porosity, these different volume changes of the solids can be expected to influence the infiltration geometry. In the Horsethief Creek aureole both kinds of reactions likely took place but the extent of each reaction and its influence on the permeability structure are not clear.

If one assumes that all silica was brought into the system, some first order estimates can be made about the amounts of fluids infiltrating the rocks. However, in the case of the Horsethief Creek aureole this seems futile, because of 'complications' like the interlayered chert layers. Any fluid which loses silica during reaction with the rocks would be "recharged" (become silica saturated again) when it comes in contact with one of these interlayers. As this process cannot easily be quantified, every estimate of the amount of influx would likely overestimate the amount of externally derived fluid.

## 4.5 Discussion of Possible Fluid Flow Direction(s), Fluid Source(s) and Heat Advection

In this section the possible interplay of heat and fluid flow and different scenarios of fluid infiltration, with respect to fluid flow direction and source(s), are discussed.

In paragraph 4.4.1 the atypical form of the  $T_{\max}$  profile and the possibility of heat advection are briefly discussed. In paragraphs 4.4.2 to 4.4.4 scenarios of up-Temperature, down-Temperature and vertical fluid flow in the aureole are outlined and evaluated. These models do not consider the phlogopite zone, down-grade of the petrographic break at the tremolite + K-feldspar isograd. The outermost aureole may have different reaction history. Possible explanations are outlined in paragraph 4.4.5. Two competing models are introduced to try to explain the sudden change in petrologic and infiltration character at the tremolite + K-feldspar isograd. An attempt is made to tie the implications of this observation into a model consistent with the observations in the rest of the aureole.

### 4.5.1 Heat Flow - Conductive or Advective?

Meaningful discussion of fluid flow direction and fluid sources requires the consideration of the combined petrographic, isotope and heat flow data. The former two are discussed in chapter 3 and section 4.4.3 respectively. Consideration of heat flow recorded in form of maximum temperatures reached in the rocks can support attempts to explain the overall contact-metamorphic history of an aureole. No in depth analysis is attempted here, but some aspects of possible heat flow mechanisms in the Horsethief Creek aureole are worthwhile considering. For an excellent review of thermal modelling see Furlong *et al.* (1991).

The profile of maximum temperatures ( $T_{\max}$ ) recorded in siliceous dolomitic rocks in the Horsethief Creek aureole is not in agreement with simple conduction of heat from an intrusion

with near vertical contacts to the wallrock. This form of purely conductive heat flow results in up-temperature concave  $T_{\max}$  - profiles (Jaeger 1964).

Simple models can provide valuable constraints on the thermal evolution, although in more detail it is observed that, for example, the geometry of the intrusion is a very important factor in controlling the spatial distribution of temperature in an aureole (Furlong *et al.* 1991, and citations therein). The absolute values of  $T_{\max}$  throughout an aureole are strongly influenced by the intrusive geometry (Bowers *et al.* 1990). However, Furlong *et al.* (1991, p.444) pointed out, that in "... a purely conductive regime, the average maximum width of an aureole will be approximated by ... simple models... ". For initial temperature distributions, and temperature increase (of the wallrocks) necessary for reaction similar to those assumed in the Horsethief Creek aureole [ $\Delta T$  (intrusion - wallrock) = 500 °C,  $\Delta T$  necessary for reaction 100 °C], the intrusion of a cylindrical solid igneous body would lead to the development of an aureole with a width  $\approx 1.5 a$  ( $a$  = half-width of intrusion [km]). In case of the Horsethief Creek pluton with  $a \approx 7$ , the aureole should be  $\approx 10$  km wide if heat flow was purely conductive. This is a distance much larger than that observed. Furthermore, the possibility of an intrusive body below the aureole, causing the unusual thermal plateau, may also be excluded. While such an additional heat source can lead to the development of a plateau in the temperature profile, it also is expected to result in an increase in the overall width of the aureole. Hence, the contact between the Horsethief Creek intrusion and the siliceous dolomites is assumed to be near vertical. Therefore, the significant deviations from the theoretically predicted conductive heat flow require the consideration of effects of advective heat transport (Furlong *et al.* 1991).

Systematic relatively closely spaced fractures in rocks can lead to a permeability high enough to allow for advection of heat (Furlong *et al.* 1991). Sets of narrowly spaced joints or veins are observed in all lithologies in the Horsethief Creek aureole. An additional requirement is that high permeability is maintained over (some) time to have significant effects on fluid- and heat flow. In the Horsethief Creek aureole, fluid infiltration and production can be expected to have been high.

The influx of external H<sub>2</sub>O-rich fluids into the siliceous dolomites from the large pluton and / or the underlying pelitic rocks, in which dehydration reactions proceed during contact metamorphism, can be expected to have been high. In addition, internal H<sub>2</sub>O -CO<sub>2</sub>-fluid production in the pervasively reacting siliceous dolomites themselves was also high. This results in fluid pressures likely high enough to maintain a relatively large porosity and permeability against pressure of compaction and and/or sealing processes (e.g. Fyfe *et al* 1978).

Possible implications of advective heat flow will be addressed in the discussions about fluid flow direction and sources below.

#### 4.5.2 Discussion of the possibility of horizontal fluid flow in the direction of increasing temperature

The scenario of up-Temperature (up-T) fluid flow in the siliceous dolomites in the context of a large hydrothermal convection cell is unlikely. If the convection cell operated in an open system, significant amounts of meteoric water should be involved. Meteoric waters have a very low positive to high negative  $\delta^{18}\text{O}$  signature ( $\delta^{18}\text{O}$  range in Figure 14) and therefore should lower the  $\delta^{18}\text{O}$  values below those recorded in Horsethief Creek rocks (e.g., Valley 1986 and citations therein, Holness and Fallick 1997). Small amounts of meteoric waters may have been involved, especially if their isotopic signature was altered by rocks they passed before infiltrating the siliceous dolomites.

Hydrogen isotope analyses of tremolites could possibly clarify whether meteoric waters were involved. The hydrogen isotope signature of meteoric water is very distinct from that of other geological materials and should be reflected in the minerals even if the oxygen isotope signature is ambiguous. Tremolite separation was hindered by the often very fine grained and interlocking minerals and by widespread weathering in the strongly cleaved amphiboles.

If small(er) scale convection occurred without involvement of significant amounts of meteoric waters the system was likely 'sealed' by a relatively impermeable cap above the intrusion (Etheridge *et al.* 1983, Furlong *et al.* 1991).

The recorded  $^{18}\text{O}$  depletion seems in accordance with up-T flow of fluids with an  $\delta^{18}\text{O}$  of  $\approx 18\text{‰}$  at the time of influx into the dolomites in the outer aureole. This value is in accordance with what can be expected for a fluid that equilibrated with the surrounding mainly pelitic sediments. Flow up a temperature gradient causes  $^{18}\text{O}$  depletion in the rocks because the fractionation factor ( $\alpha$ ) for fractionation of  $^{18}\text{O}$  between rock and fluid changes with temperature. In the case of carbonate,  $\alpha > 1$  at low temperatures, and approaches 1 with increasing temperatures. This leads to a  $^{18}\text{O}$  depletion of marble towards the intrusion (Dipple and Ferry, 1992). Although the temperature gradient observed in the Horsethief Creek aureole is distinct from those utilized by Dipple and Ferry, the overall depletion (including depletion by devolatilisation reactions) is comparable to that predicted for the given temperature range.

The interpretation of the  $\delta^{18}\text{O}$  isotope pattern observed in the inner aureole alone (in the scenario of up-T flow) is more uncertain. If the outlier is representative the  $^{18}\text{O}$  depletion seems to be too high to be the result of temperature induced  $^{18}\text{O}$  depletion only. If the outlier is unrepresentative, the  $\delta^{18}\text{O}$  values in the inner aureole seem to actually increase towards the pluton, or at least stay constant. This is unlikely to be the case with up-T fluid flow where the temperature gradient is expected to be steepest close to the contact. This should lead to some  $^{18}\text{O}$  depletion. Hence, up-T fluid flow in the inner aureole seems unlikely. However, as pointed out in the introduction (paragraph 1.2) the inner aureole often seems to have a special position. Fluid flow here might have been sub-vertical. The isotope values in the inner aureole are in a range expected with involvement of pelitic fluids emanating from the underlying pelites.

Whether the sequence of mineral assemblages observed in the aureole are in agreement with up-T flow is somewhat difficult to assess. If the one diopside - dolomite - tremolite - calcite assemblage observed is not representative, the assemblages could have formed with moderate

amounts of fluid infiltration (very tentative value of  $\approx 100$  moles /  $\text{cm}^2$  time integrated flux ( $q^\circ$ ) cf. Figure 2d in Dipple and Ferry 1996). Much higher amounts of fluid flux seem to result in the development of finite areas in which isobarically univariant assemblages are stable (esp. in the inner aureole) (Ferry 1994, Ferry and Dipple 1996). However, if the aforementioned isobarically univariant is representative, up-T flow is very unlikely.

The  $T_{\text{max}}$  distribution in the aureole cannot satisfactorily be explained with up-T fluid flow. As pointed out above purely conductive heat transport seems unlikely in the Horsethief Creek aureole. Heat advection by fluid in context of a convection cell can lead to a decrease in the width of an aureole in the up-T fluid flow region (decrease with respect to an aureole which experiences purely conductive heat flow) (Dipple and Ferry 1996; Furlong *et al.* 1991). However, the extent of shortening observed in the Horsethief Creek aureole seems too high to be the result of effects of up-T flowing 'cool' fluids.

Furthermore the unproportionally wide metamorphic zone(s) of mid to high grade (diopside + phlogopite plus diopside zone(s)) (Figure 13b) seem difficult to explain with this kind of model. If a decrease in the overall width of the aureole occurs, caused by heat-advective fluid flow up-T, the width of the different metamorphic zones seem to decrease proportionally and high-grade zones are in first approximation narrower than low-grade zones (Furlong *et al.* 1991). Even with a complex geometry of (steeply dipping) intrusion-wallrock contacts, where unusually wide higher-grade zones can develop in and near reentrants of the contact, these higher grade zones are not wider than the mid-to low grade metamorphic zone (Bowers *et al.*, 1990).

In summary it can be said that although up-T flow with a strong vertical component in the inner aureole cannot entirely be dismissed, it seems unlikely. Many uncertainties are connected with this hypothesis.

#### 4.5.3 Discussion of the possibility of horizontal fluid flow in the direction of decreasing temperature

Down-Temperature (down-T) flow in context of a convection cell seems unlikely in the Horsethief Creek aureole. Those parts of a convection cell in which down-T flow occurs are commonly situated above the top of the pluton (Furlong *et al.* 1991 and citations therein). Present day erosion levels in the working area show that, while it is not clear where exactly the rocks under consideration are located with respect to the original vertical extent of the intrusive body, they were not above the pluton. Elevations in the intrusive rocks reach higher than those in the working area.

In the case of likely lithologically controlled down-T fluid flow the crystallizing pluton can be expected and is often observed to be the main source of infiltrating fluid (e.g., Valley 1983), and in theory, a sharp front is expected to develop in the infiltrated rocks. Upstream from such a front the rocks should be fully equilibrated with the infiltrating igneous fluid while downstream from it the isotopic composition of the carbonate rocks are unchanged. No igneous values with  $\delta^{18}\text{O}$  as low as  $\approx 10\text{‰}$  are observed in Horsethief Creek carbonates. One explanation could be disequilibrium in isotope exchange between the magma derived fluid and the infiltrated rocks. But the high temperatures recorded in contact aureoles are generally considered to be sufficiently high for a fast equilibration, and in many other aureoles, where the fluid is considered to be of igneous origin, values of  $\delta^{18}\text{O} \approx 10\text{‰}$  are recorded (e.g. Nabalek *et al.* 1984, Cook *et al.* 1997, and examples in Valley 1986).

Furthermore, the amount of fluid emanating from an intrusion and the distance of  $^{18}\text{O}$  depletion in an aureole with down-T flow can be approximated by some simple calculations (Dipple and Ferry, 1992). Fluid emanating horizontally from a crystallizing magma with 10 wt%  $\text{H}_2\text{O}$  is expected to drive isotopic depletion to a distance of around  $0.087 r$  (with  $r$  = radius of a (cylindrical) pluton [km], 0.08 mole oxygen/cm<sup>3</sup> rock, density of intrusion = 2.5 g / cm<sup>3</sup> and

complete exsolution and expulsion of the H<sub>2</sub>O). In the Horsethief Creek case  $r \approx 7$ , and <sup>18</sup>O depletion should reach no further than 600 m. This distance can be expected to be even smaller with a higher mole oxygen per cm<sup>3</sup> rock value of the originally very dolomite rich lithology (0.125 mole oxygen / cm<sup>3</sup> rock). This distance of <sup>18</sup>O depletion is significantly smaller than observed. If the pluton was the main source of the fluids these must have been channeled into the siliceous dolomites to provide the required larger amounts of fluids. Such a channeling was proposed for the siliceous dolomites in the Alta aureole (Cook *et al.*, 1997) where the Grizzly thrust just above the pluton is considered to be the low permeability 'cap'. This likely caused layer parallel fluid flow at its bottom. In case of the Horsethief Creek rocks no likely candidate for such a barrier is known.

However, if significant amounts of igneous fluids infiltrated the aureole their isotopic signature must have been altered immediately after, or before, flowing across the pluton - wallrock contact to produce the relatively high  $\delta^{18}\text{O}$  values in the inner aureole. This could result from mixing with another fluid. A possible source for additional fluid are the underlying pelites. At the time of intrusion, low-grade meta-pelite are presumed to have a  $\delta^{18}\text{O}$  signature of  $\approx 15 - 20$  ‰ (Figure 14). In the case of (sub-)vertical flow isotopic exchange across the pluton-wallrock contact may have changed the isotopic values of fluid on either side of that contact.

The mineral assemblages in the siliceous dolomites are generally in agreement with down-T flow of moderate to high total fluid fluxes, depending on whether the diopside - dolomite - tremolite - calcite sample is representative or not (Dipple and Ferry, 1996). The isobarically univariant assemblages in the phlogopite zone may be an exception. This is further discussed below in section 4.6.

The  $T_{\text{max}}$  profile is likely not in agreement with down-T flow in all of the aureole (if the unusual  $T_{\text{max}}$  profile is the result of heat advection). With heat advection by down-T fluid flow the width of the aureole is not expected to decrease.

In summary, lithologically controlled horizontal fluid flow in the direction of decreasing temperature throughout all of the Horsethief Creek aureole is unlikely. The isotopic signature in the inner aureole is too high, and  $^{18}\text{O}$  depletion is observed at greater distances than can likely be expected in the case of horizontal flow of plutonic fluid only. Some combination of down-T flow in the middle and outer aureole and some other process in the inner aureole seems possible.

Hence, although both up- and especially down-temperature fluid flow scenarios cannot strictly be excluded, uncertainties are linked with both scenarios.

Additional uncertainty in the determination of fluid flow direction and fluid source(s) is introduced by the fact that the above used models are fairly simple. Many of the complex and interacting processes in aureoles, like for example changes in permeability and flow pattern with reaction, are not considered and could potentially alter the model results significantly (e.g., Furlong *et al.* 1991, Cartwright and Buick 1996). However, interpretation of Horsethief Creek data with the methods currently available suggests that the pelitic rocks underlying the siliceous dolomites may have played a significant role in the infiltration history of the aureole.

#### 4.5.4 Discussion of the possibility of vertical fluid flow

Further evidence that vertical fluid flow of fluids liberated by dehydration reactions in the pelites may have played a significant role in the infiltration history of siliceous dolomites comes from a more detailed comparison of petrographic observations and geothermometry results with the isotope data.

If one had to point out an 'isotopic front' in the system it could be placed at  $\approx 1150$  m as indicated by the dashed line in Figure 13. Interestingly, the thermal plateau at temperatures of  $\approx 560$  °C as shown in Figure 13b ends at  $\approx 950$  m, and the temperature of  $\approx 525$  °C necessary for the diopside-forming reaction under internally buffered conditions (reaction (5)) is reached at

≈1180 m. The outermost sample showing the diopside to tremolite reaction texture analyzed in section 4.4.2 was found at ≈1050 m. This indicates that infiltration up to that distance from the pluton occurred in rocks that were significantly pre-heated. Diachronous heat- and fluid flow is thought to be not uncommon in contact metamorphic environments. A model of rapid heating of the inner aureole followed by infiltration of an aqueous fluid was invoked to explain the mineral assemblages observed in argillitic rocks in the Notch Peak aureole (Nabalek *et al.* 1984). The formation of forsterite, in rocks of the rapidly heated rocks of the inner aureole, directly from the protolith (and possibly with silica in the fluid) was proposed for other aureoles (Bucher-Nurminen 1981, Holness 1992). What is remarkable in case of the Horsethief Creek aureole is, that this process of heating preceding infiltration is not restricted to the inner aureole but seems to have been operative to distances >1 km.

#### 4.5.4.1 Metamorphism of the pelite and its implications for the siliceous dolomite

In the pelites, fluids are expected to be liberated at temperatures of ≈520 - 540 °C by means of the reaction



(Bucher and Frey 1994, Pattison and Tracy 1991, Fig. 47), a reaction observed in the contact-metamorphic pelitic rocks by Floriet (1996). This match of data supports the hypothesis that the pelitic rocks were an important source of fluid(s) that infiltrated the siliceous dolomites in the Horsethief Creek aureole.

The fluids evolving from the pelites would be buoyant and have the tendency to escape upwards. Relatively pure massive carbonate rocks are considered to be comparably impermeable and were found to be barriers for uprising fluids, leading to layer-parallel flow along lithologic boundaries (Hay and Evans 1988, Holness and Graham 1995, Nabalek *et al.* 1984, Ferry 1989,

Cook 1997). However, in case of the Horsethief Creek aureole sub-vertical, pre-contact-metamorphic joints which developed in all lithologies and trend across bedding could have played a major role in facilitating infiltration across layering.

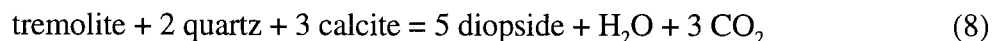
#### 4.5.4.2 *Metamorphism of the siliceous dolomite in the middle aureole*

At temperatures  $\geq 525$  °C, similar to those necessary to drive reaction in the metapelites, the thermally driven diopside producing reaction (5) proceeds in the siliceous dolomites. This reaction is coupled with a negative reaction volume of the solids of 39 %, which is large, especially when compared with the volume reduction of 'only' 23 % during the tremolite-in (2) and of 13 % during the phlogopite-in (1) reactions (for molar volumes see Appendix D). Hence, this diopside forming reaction (5) leads to a local reaction-enhanced porosity and possibly permeability. It is likely restricted to areas where both reactants are readily available namely the contact between chert and siliceous dolomites, as transport of material has to occur by diffusion. This is a relatively sluggish and small scale process (e.g. Bickle and McKenzie 1983). A possible example of a rock that may have experienced such a reaction is shown in plate 9.

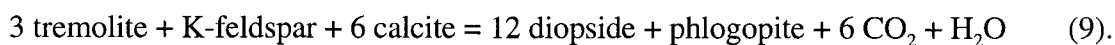
Once fluid is released by the underlying pelites, it rises and infiltrates into the siliceous dolomites predominately by means of the pre-contact metamorphic joints, and possibly along the chert - carbonate contact (Heinrich 1993, Nabalek *et. al.* 1992, Jamtveit *et al.* 1992, Plate 7 ). This leads to a combined upward and sub-horizontal fluid flow. The fluid channeling along fractures is reflected by the abundant systematic veins in the siliceous dolomite. The veins are now observed to be filled with tremolite or to have been nucleation 'points' for tremolite sprays. Signs for sub-horizontal flow are less obvious. Observations of textures like that shown in Plate 7 are rare. Possible further evidence for sub-horizontal fluid flow may come from the overall development of the aureole outbound the diopside isograd. This is discussed in detail below.

In parts of the rocks in the middle aureole, where diopside was formed prior to infiltration, subsequent infiltration would trigger tremolite formation by reaction (4). In the parts of the rocks where no diopside was formed prior to infiltration tremolite may have formed directly from the protolith by reaction (2) at temperatures of infiltration and reaction  $\geq 520$  °C, which are the temperatures necessary to liberate the fluid in the metapelites. This hypothesis is supported by the fact that (a) although the diopside  $\rightarrow$  tremolite reaction texture is found throughout most of the aureole it is not very common; (b) one of the most widespread assemblages in the aureole is tremolite - calcite - K-feldspar which can form by reaction (2) in the presence of abundant silica, likely brought into the system by SiO<sub>2</sub>-bearing fluids (4.4.5). With massive infiltration but no silica metasomatism the tremolite + K-feldspar + calcite assemblage could only have formed in quartz rich areas (i.e., near the chert layers by the combined or successive reactions (1) (2) and (4) (cf. Figure 4, esp. reaction stoichiometry of reaction (4)). In areas with less silica available some dolomite and/or phlogopite should remain preserved in the rocks. Such assemblages are present, but especially dolomite-bearing ones are rare.

If temperatures continued to rise after the onset of infiltration, and if infiltration of an aqueous- (SiO<sub>2aq</sub>) -fluid persisted, diopside could form from tremolite during peak thermal conditions by reactions:



or



The different reaction paths for the formation of tremolite and diopside may have led to the development of different textures. Diopside that is interpreted to have formed from the protolith is found to be large and bladed. Other diopside, which may have formed from tremolite along reaction (8) or (9), occurs in relatively small (mm) roundish crystals rather than in long blades, while the tremolite occurs in smaller needles. No reaction texture (tremolite  $\rightarrow$  diopside) was found that could support this assumption.

#### 4.5.4.3 Metamorphism of the siliceous dolomite in the tremolite + K-feldspar zone

In the aureole outbound of the diopside isograd, i.e., in the tremolite + K-feldspar zone, tremolite had to form from the protolith because maximum temperatures reached in this zone are too low for the diopside producing reaction (5). These temperatures also are below the  $\approx 520 - 540$  °C at which the pelitic rocks dehydrate. Hence, the influx of fluid into the tremolite zone rocks was likely from higher grade, sub-horizontally channeled along the chert - carbonate contacts.

#### 4.5.4.4 The $T_{max}$ -profile

Possible further support of the hypothesis of vertical fluid flow comes from the analysis of the  $T_{max}$ -profile in light of possibly vertical fluid flow. As pointed out above (4.5.1) the overall width of the aureole is relatively small. Aureoles of around the same width (1 - 2 km) are observed to have developed around plutons that are considerably smaller (2 - 5 km) than the  $\approx 15$  km in diameter Horsethief Creek pluton (e.g., Bowman 1994; Rice 1977a). In contrast to these examples, isograds in the Elkhorn aureole, where the existence of strongly vertical flow during contact metamorphism is well established (Bowman and Essene 1982, Bowman *et al.* 1985), are found to be telescoped to  $\approx 100$  m only. The (highest grade) periclase (brucite after periclase) zone is observed to be up to 20 m wide. The Black Butte stock around which this aureole developed is about 1 km wide and an aureole of several hundred meters in width could be expected if heat flow was purely conductive. The mineral assemblages in the Horsethief Creek aureole are different so that the interpretations from Elkhorn are not directly transferable. It is interesting to note however, that in the Horsethief Creek aureole, not only the overall width of the aureole is relatively small, but also that a very wide ( $\approx 640$  m) relatively high-grade diopside + phlogopite

zone developed, which is succeeded down-grade, i.e. outside the zone of proposed vertical flow, by a narrow ~125 m wide tremolite + K-feldspar zone. With strong vertical fluid flow the conductive heat profile might become significantly distorted by vertical heat advection. 'Heat' is taken out of the system before it can reach the outer parts of the aureole, so that the zone of heating is considerably shortened, similar to what is observed in the Horsethief Creek aureole. No attempt to quantify the effects of heat advection by vertical fluid flow was made.

#### *4.5.4.5 The inner aureole - a special case*

Despite strong evidence for possible involvement of large amounts of pelitic fluid, some involvement of plutonic fluid is likely, especially in the inner aureole where chaotic veining was observed. This kind of fracturing is commonly developed in host rocks near intrusions and is interpreted to be the result of overpressuring of fluids expelled from the cooling pluton.

The wide scatter of  $\delta^{18}\text{O}$  values at any given distance in the aureole can be interpreted to reflect interaction of the rocks with different amounts of the fluids caused by heterogeneities in infiltration pattern. However, the scatter is especially well marked in the stoped and chaotically fractured rocks close to the contact where differences in permeability are expected to be large. In addition, the involvement of igneous fluid was likely largest in the zone near the pluton wallrock contact. Hence, the variability in  $\delta^{18}\text{O}$  values may not (only) reflect differences in the total amount of fluids the rocks interacted with but (also) different proportions of igneous and metamorphic fluid that equilibrated with the rock. In the latter case the sample at  $\approx 180$  m in figure 13a which was originally assumed to be retrograded may represent a rock that equilibrated with a relatively large proportion of igneous fluid instead.

As of the timing of peak metamorphism in the aureole in the case of predominantly vertical fluid influx, it can be said that reaction / metamorphism likely progressed continuously with the

thermal peak 'wandering out' from pluton. Details of the relative timing of metamorphism in various parts of the aureole are not clear.

In summary it can be said that a likely model of fluid infiltration into siliceous dolomites in the Horsethief Creek aureole is one of strong vertical flow of fluid, which was released from the underlying pelites with the onset of contact metamorphism, probably mixed with sub-horizontal down-T fluid flow and some involvement of plutonic fluid.

However, so far all attempts to decipher the contact-metamorphic evolution of the rocks ignored the phlogopite zone. This zone seems to be distinct from the rest of the aureole. A sharp transition from isobarically divariant assemblages in most of the aureole to isobarically univariant assemblages in the phlogopite zone occurs. Implications of this observation are discussed below.

Furthermore, the nature of metamorphism affecting the calc-silicate layer that lies between the pelite and the siliceous dolomite is not known. Outcrop is sparse as the unit lies in the topographic lows. The rocks are made up of mm - cm wide biotite - diopside - quartz rich layers. Joints were observed but veins were rarely found.

#### **4.6 The Petrologic Break - A Change in Infiltration Character**

Another striking feature of the aureole is the significant break in the petrologic character at the tremolite + K-feldspar isograd, at an inferred peak temperature of  $\approx 500$  °C. Up-grade of the tremolite + K-feldspar isograd the aureole is dominated by isobarically divariant mineral assemblages while the phlogopite zone down-grade of the tremolite + K-feldspar isograd is characterized by the isobarically univariant assemblage dolomite - K-feldspar + minor phlogopite  $\pm$  calcite (Table 3, Figure 9).

A talc zone is predicted by the models of Ferry (1994), except for very low fluid flow (time integrated flux  $< 100$  mole /  $\text{cm}^2$ ) during down-T flow. No talc zone is observed in the Horsethief

Creek aureole. This could result if the infiltrating fluid had a  $X_{\text{CO}_2} > \approx 0.54$  because infiltration of  $\text{CO}_2$ -rich fluids would not trigger any talc producing reaction (Figure 4).

The absence of a *conspicuous* phlogopite zone in the outer aureole however is unlikely to be the consequence of a fluid- $X_{\text{CO}_2}$  too high to trigger reaction. This would require the infiltrating fluids to have a  $X_{\text{CO}_2} > \approx 0.82$ . The possibility of such high  $X_{\text{CO}_2}$  values to develop is remote when significant amounts of  $\text{H}_2\text{O}$ -bearing fluid infiltrate a rock.

A change in infiltration regime at the tremolite + K-feldspar isograd is likely required. While the inner and middle aureole has to have experienced substantial and pervasive infiltration of an externally derived  $\text{H}_2\text{O}$ -bearing fluid at or near the peak of metamorphism, the mineral assemblages in the phlogopite zone must have been heated in the absence of significant infiltration. Reaction here was governed by internally buffered fluid composition.

This apparent lack of large amounts of fluid infiltration into phlogopite zone rocks can be explained as either reflecting a) a real lack of significant amounts of infiltration, b) conditions that did not allow for reaction despite infiltration, or c) both. In the first case, if the main fluid source were the underlying pelites, vertical influx would cease approximately at the diopside isograd and the horizontal flow component might not have been strong enough to transport fluids out into the phlogopite zone rocks. This, however, is not very likely because layers with abundant Fe-amphibole were found in the (Mg-) phlogopite zone. This requires that significant amounts of fluid were present at a time where temperatures were high enough to drive reactions. Hence, cases a) and c) can basically be excluded.

Hence, fluid infiltration likely occurred but for some reason no reaction was triggered in the phlogopite zone (Mg-) rocks. In this case fluid infiltration could have been restricted to a time in the thermal development of the aureole when the outer aureole had not been heated up enough to allow for reaction with the infiltrating  $\text{H}_2\text{O}$ - $\text{CO}_2$  fluid. The thermal peak in the outermost aureole would only be reached after infiltration ceased. This idea of diachronous heat and fluid flow is similar to that proposed for the argillitic rocks in the Notch Peak aureole by Nabalek *et al.* (1984).

Alternatively, if fluid infiltration and heating were coexisting, some other process must have hindered reaction.

#### 4.6.1. A Model of diachronous heat and fluid flow

The first model evoked to explain the petrologic break at the tremolite + K-feldspar isograd presumes diachronous heat- and fluid flow, whereby the intrusive body is assumed to be the heat source as well as a main source for the fluid(s) that infiltrated the siliceous dolomites. This model is built on results of computer simulations by Dipple and Ferry (1996). They simulated the contact-metamorphic development of a simple model aureole (initial rock composition 10 mol% quartz and 90 mol% dolomite) by coupling mineral reaction, heat- and fluid flow. The results showed that rocks in the middle to outer aureole can experience early infiltration and reaction at temperatures below peak metamorphic ones, leading to the development of low-grade mineral assemblages. With continued heating after the cessation of infiltration the low-grade assemblages react to higher grade isobarically divariant assemblages along shallow reaction curves with thermal maxima (Figure 15 a). Traces of a possible early talc zone in the outer aureole are erased during this "annealing" process (Figure 15 b). Rocks even further away from the pluton (in the outermost aureole) do not reach sufficiently high temperatures during infiltration to drive any mineral reaction. Only during the continued, post-infiltration heating internally buffered isobarically univariant assemblages are produced (Figure 15b). In the Horsethief Creek aureole the missing talc zone and the observation of generally only small amounts of phlogopite in isobarically univariant assemblages can be interpreted to reflect such an annealing process where fluid flow ceased early in the thermal evolution of the outer aureole.

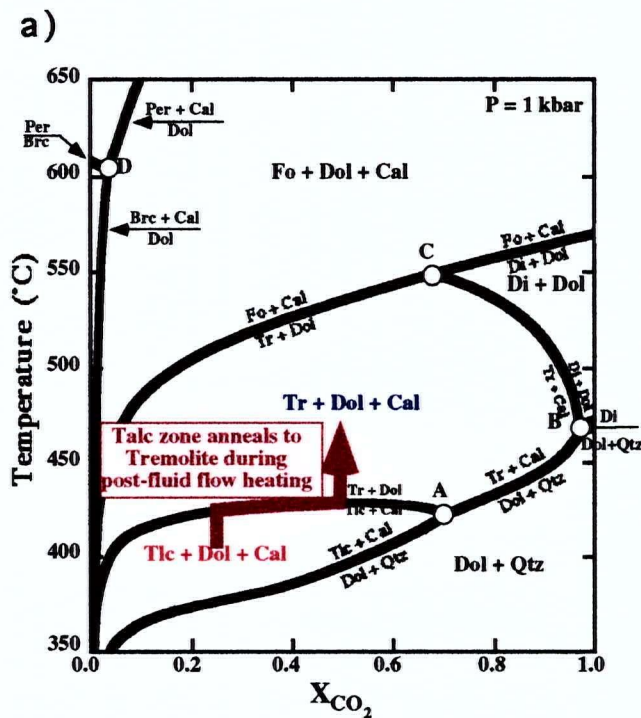
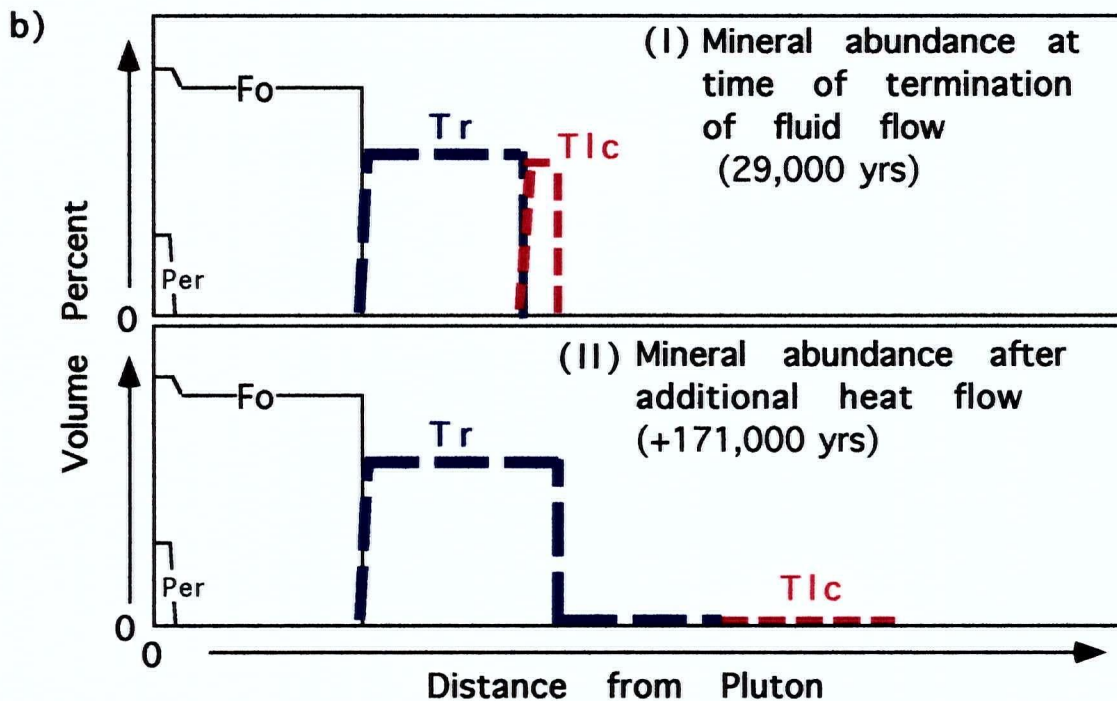
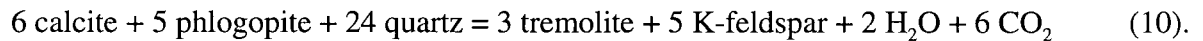


**Figure 15: a)** T- $X_{CO_2}$  diagram for pure siliceous dolomites (CMS-HC) at  $P=1\text{ kb}$  (after Dipple and Ferry 1996). The thick red arrow indicates the reaction path for rocks that developed talc assemblages during infiltration early on in the thermal development of the aureole and 'anneal' during heating after the termination of infiltration (for more details refer to text). **b) (I):** Mineral abundances over the width of the aureole resulting from a simulation of contact metamorphism with diachronous heat- and fluid flow in pure siliceous dolomites. A total of 400 moles  $H_2O/cm^2$  flowed down-temperature with a Darcy flux of  $1 \times 10^{-8} \text{ cm/s}$  for 29,000 years. **(II)** Modes after an additional 171,000 years of heat flow without infiltration. The two figures show the effect of 'annealing': low-grade divariant assemblages (high percentage Tlc area) react to divariant mid-grade assemblages (high percentage Tr area) and rocks in a greater distance from the contact only develop univariant assemblages (low percentage [ $\approx 0\%$ ]) assemblages (after Dipple and Ferry 1996 - their Figures 3 a-b).



There are however some problems connected with this model of diachronous heat and fluid flow. First, if an early (during infiltration) developed phlogopite zone annealed to a divariant tremolite bearing assemblage it could only be by reaction



This reaction requires a very large amount of  $\text{SiO}_2$ . Although it can be argued that silica is highly abundant in form of chert layers and nodules it is questionable whether that silica was available for reaction in all parts of the rock. With no infiltration of an external fluid, diffusion alone might not be sufficient to transport for reaction necessary components through all of the rocks (e.g., Bickle and McKenzie, 1987). Annealing of rocks during infiltration developed phlogopite and tremolite + phlogopite zones would not occur in areas that were outside the regions reached by diffusive silica. The assemblages tremolite - phlogopite - calcite and possibly also phlogopite - dolomite - calcite in the rocks that did not experience reaction (2) during infiltration would be preserved because both of the reactions that could possibly proceed at higher temperatures, i.e. reactions (2) and (3), require (the not available)  $\text{SiO}_2$  as a reactant.

In the Horsethief Creek aureole none of the rocks in the lower tremolite + K-feldspar zone exhibit an isobarically divariant phlogopite - dolomite - calcite assemblage, and no dolomite was found preserved in rocks of this grade. The assemblage tremolite - calcite - phlogopite which is expected to be widespread in the upper tremolite + K-feldspar zone, is observed, but only in rocks in the lower tremolite + K-feldspar zone and not as widespread as would be expected.

A second line of evidence that refutes the hypothesis of annealing of the outer Horsethief Creek aureole is that a very steep and hence unlikely temperature gradient of  $\approx 480^\circ/\text{km}$  would have been required during the time of infiltration. High-grade rocks down to the diopside isograd at  $\approx 1125$  m are interpreted to have experienced infiltration only after reaching temperatures of  $>520^\circ\text{C}$  (paragraph 4.4.2). In the annealing scenario the tremolite + K-feldspar-bearing assemblages in rocks in the current (lower) tremolite + K-feldspar zone are presumed to have formed by annealing (i.e., heating to  $T \geq 500^\circ\text{C}$  after the cessation of fluid infiltration) of

phlogopite-assemblages which had formed during the earlier fluid infiltration event. The current phlogopite zone in >1250 m is presumed to have formed at about the same time at which the 'old' phlogopite zone annealed, i.e., only after cessation of fluid infiltration. The 'old' phlogopite isograd is presumed to have been approximately where now the tremolite + K-feldspar isograd is positioned (i.e., 1250 m). Hence, with a presumed intermediate  $X_{\text{CO}_2}$  of the infiltrating fluid (e.g., no talc zone) temperatures must have been around 460 °C at 1250 m. Only if rocks in >1250 m had temperatures <460 °C infiltration of that fluid would not have triggered reaction (1). Hence, there must have been a temperature difference of about 60 degrees over 125 m. This very steep temperature gradient seems not very likely.

Third, a possible contradiction are the occasionally found higher abundance of phlogopite (up to 8 vol%) in samples where the minerals formed in a preferred orientation (Plates 4a and b) or in veins (Plate 5). This requires that locally fluid was available at temperatures necessary for reaction but that it generally did not infiltrate (most of) the rocks, leading to the widespread development of internally buffered isobarically univariant phlogopite assemblages. If the fluid is not the same as that of the main infiltration event it has to be linked to some late but not retrograde ( $T > 450$  °C required, cf. Fig 13b) minor infiltration event(s). This is possible but at this point it seems philosophical to speculate about the likelihood of the coincidence between late infiltration and existence of temperatures necessary for reaction.

In summary it can be said that although the process of diachronous heat- and fluid flow is capable of producing a break in petrologic character, with divariant assemblages up-temperature and isobarically univariant assemblages down-temperature from it, this is not likely to be the case in the Horsethief Creek aureole.

#### 4.6.2 A model of vertical fluid flow

The second model evoked to explain the petrologic break at the tremolite + K-feldspar isograd in the Horsethief Creek aureole implies that the underlying pelites are the main source for the fluids that infiltrated the siliceous dolomites, and that the temperature for the critical dehydration reaction (7) is  $\approx 525 - 540$  °C. Heating to critical temperature(s) and infiltration are basically concurrent events. These 'critical' temperatures are recorded only in the rocks inbound the diopside isograd in  $\approx 1125$  m. Hence, all rocks down-grade from the diopside isograd would not experience vertical infiltration of pelitic fluid. However, there are layers with tremolite in high abundance in  $>1125$  m. Hence, some fluid infiltration must have occurred in these rocks and was likely subhorizontal in nature. As pointed out earlier permeability is likely higher at the lithologic contact between the carbonate and chert layers and fluids in all parts of the aureole may have had a subhorizontal component in fluid flow direction. If fluids enter rocks in the tremolite + K-feldspar zone mostly channeled along these contacts (possibly spreading out along veins), reaction (2) can take place at and near these contacts and around the veins, as far as  $\text{SiO}_{2\text{aq}}$  is advective-diffusively transported into the dolostones. This observation is in accordance with field observations. The width of tremolite bearing layers generally decreases towards the lower tremolite + K-feldspar zone (less reactive fluid available), but the abundance of tremolite in these layers is usually high.

Further down-temperature, in the phlogopite zone, reaction (1) would not take place if no K-feldspar was available near the fluid conduits, i.e. near the chert layers and/or veins. Relatively pure dolomite is considered relatively impermeable to grain-edge flow (Holness and Graham 1995, Hay and Evans 1988). The feldspar is usually relatively low in abundance and evenly distributed throughout the rock and therefore not readily available for reaction with fluid. Hence, with no pervasive infiltration no pervasive reaction (1) can occur in the phlogopite zone, and

without pervasive reaction no pervasive infiltration can occur. This is in agreement with observations in these rocks where mostly isobarically univariant assemblages developed.

The hypothesis of initial channeling of fluids and development of pervasive infiltration only by means of reaction-enhanced permeability is further supported by the occurrence of the thick actinolite layers with highly abundant amphibole in the (Mg-) phlogopite zone. Iron endmembers of solid solution phases react at lower temperatures than Mg-endmembers (e.g., Philpotts, Chap.17, 1990). This explains the possibility of the Fe-amphibole forming reaction to occur in a zone where temperatures for Mg-amphibole reactions are already too low. (No quantification of temperature lowering as a function of iron content was done for this case.) Unlike the phlogopite reaction, where K-feldspar, or, the components potassium and aluminum, are needed, actinolite formation (analogous to the tremolite forming reaction (2)) only requires the addition of silica (and H<sub>2</sub>O) to the Fe-dolomites. Fluids that infiltrate along the chert - carbonate contacts are likely silica saturated. Reaction is not only possible at the chert - carbonate contact but also along the veins and as far as silica - bearing fluid can infiltrate the rock. Potassium and aluminum necessary for reaction (1) in the phlogopite zone in contrast had to be brought into solution in the pelites. It is unlikely that any significant amount of these component escaped filtering-out by reaction in the higher-grade rocks they were in contact with before entering the phlogopite zone. Furthermore unlike the silica content, no "recharge" can occur once the fluid left the 'source-rock'.

In summary it can be said that this model of fluids which were predominantly liberated by dehydration reaction in the metapelite and infiltrated the overlying siliceous dolomites, presents a possible explanation for the observations made in siliceous dolomites of the Horsethief Creek aureole. Some plutonic fluid likely was involved especially in the inner aureole. Fluid flow direction had a strong vertical but also some sub-horizontal component; the latter likely the result of changes in lithology. Thin chert layers interlayered with the carbonate rock may have caused preferred flow along their contacts with the carbonate while also keeping fluid silica saturated.

However, the model is based on numerous assumptions that were not quantified. More detailed work would be needed to further constrain the hypotheses that are presented here.

Furthermore, the situation in detail can be expected to have been even more complex. This is indicated for examples by the occurrence of talc cores within tremolite and tremolite - talc veins in rocks in the middle aureole. This attests to localized infiltration early and late in the thermal evolution of this part of the aureole.

## CHAPTER 5

### SUMMARY AND CONCLUSION

Complex interactions between a protolith of variable composition, and heat- and fluid flow led to the development of a  $\approx 1.5$  km wide distinct aureole in potassic siliceous dolomites. Peak metamorphic conditions of  $\approx 2.2$  kb and 650 - 450 °C for the inner and outer aureole respectively are recorded in the rocks. The prograde isograds recorded are: Phl, Tr+Ksp, Di, Di+Phl, Di+Dol and Fo with increasing proximity to the contact. 'Irregularities' in the distribution of these index minerals can be explained in part by varying bulk composition and in part by spatial and temporal heterogeneity in fluid infiltration. Infiltration of a significant amount of a H<sub>2</sub>O-bearing fluid is recorded by the widespread occurrence of hydrous minerals often in high abundance (tremolite up to 65 vol%) and the prevalence of isobarically divariant mineral assemblages throughout nearly all of the aureole ( $\leq 1250$  m). The almost complete disappearance of dolomite in the inner and middle aureole attests to the widespread availability of silica for reaction. This requires at least local metasomatism. The interbedded chert layers and nodules may have been a main source for that silica. In addition, the chert - carbonate contacts likely acted as fluid channels along strike. Abundant methodical sets of subvertical veins filled with metamorphic minerals a record of significant sub-vertical fluid flow and attest to the importance of structural controls in facilitating infiltration.

The siliceous dolomites in the Horsethief Creek aureole are interpreted to have experienced fluid infiltration with mixed vertical and down-T fluid flow components. The distribution and variance of the mineral assemblages suggest down-T fluid flow, but the isotope signature excludes the idea of the pluton being the (only) source of the infiltrating fluid. The involvement of

significant amounts of (isotopically unaltered) meteoric fluids can also be excluded. Other additional sources are necessary to explain the unusually high  $\delta^{18}\text{O}$  values in the inner aureole. The underlying pelitic rocks which dehydrate with the onset of contact metamorphism are the most likely source. The evolving fluid would be buoyant and rise and have an isotope signature that can explain the relatively high  $\delta^{18}\text{O}$  values in the inner aureole. Fluid flow across lithological boundaries was facilitated by a pre-contact metamorphic subvertical joint system. Once silica-saturated aqueous fluid has entered the dolostone, reactions will be triggered that further enhance permeability leading to pervasive infiltration and reaction. Furthermore the overall small width of the aureole and the wide plateau in the maximum temperatures recorded in the aureole hint at possible advective heat flow out of the (siliceous dolomite) system - possible with strong vertical fluid flow.

A different fluid regime governed the outermost aureole (phlogopite zone) where only isobarically univariant phlogopite-bearing metamorphic assemblages are observed. Temperatures in this zone were below that necessary to trigger the critical dehydration reaction in the pelites. This resulted in less fluid being available. Fluid that did find its way into the phlogopite zone was presumably brought into the siliceous dolomites by way of sub-horizontal channeling along the chert - carbonate contacts. Unlike the tremolite (+ K-feldspar) - zone rocks in which the addition of only silica and  $\text{H}_2\text{O}$  to the dolostones is required for reaction (both of which are available in the fluid), dolostones in the phlogopite zone require the presence (or addition) of potassium and aluminum rather than silica for reaction. These components were not in the fluid (not in significant amounts) and the matrix - K-feldspar is present only in variable and relatively small amounts and relatively evenly distributed in the matrix. Hence, in most rocks it was not available in large quantity for reaction near the fluid channels. Without reaction - enhancement of permeability the bulk of the dolostone was relatively impermeable. This led to the development of internally buffered isobarically univariant assemblages.

The complex heating-, infiltration- and reaction history recorded in the rocks rules out the possibility of progressive metamorphism in the siliceous dolomites of the Horsethief Creek aureole.

## References:

- Abercrombie, H. J., Skippen, G. B. and Marshall, D. D. (1987): F-OH substitution in natural tremolite, talc and phlogopite. *Contrib. Mineral. Petrol.* 97, 305-312.
- Anovitz, L. M. and Essene, E. J. (1987): Phase equilibria in the system  $\text{CaCO}_3\text{-MgCO}_3\text{-FeCO}_3$ ; *J. Petrol.* 28 (2), 389-414.
- Archibald, D.A. et al. (1983): Geochronology and tectonic implications of magmatism and metamorphism, southern Kootenay Arc and neighboring regions, southeastern British Columbia. Part I: Jurassic to mid-Cretaceous; *Can. J. Earth Sci.* 20, 1891-1913.
- Archibald, D.A. et al. (1984): Geochronology and tectonic implications of magmatism and metamorphism, southern Kootenay Arc and neighbouring regions, southeastern British Columbia. Part II: Mid-Cretaceous to Eocene; *Can. J. Earth Sci.* 21, 567-583.
- Berman, R.G. (1988): Internally-Consistent Thermodynamic Data for Minerals in the System  $\text{Na}_2\text{O-K}_2\text{O-CaO-MgO-FeO-Fe}_2\text{O}_3\text{-Al}_2\text{O}_3\text{-SiO}_2\text{-TiO}_2\text{-H}_2\text{O-CO}_2$ ; *J. Petrol.* 29-2, 445-522.
- Bickle, M. and Baker, J. (1990): Migration of reaction and isotopic fronts in infiltration zones: assessments of fluid flux in metamorphic terrains; *Earth Planet. Sc. Ltrs* 98, 1-13.
- Bickle, M. J. and McKenzie (1987): The transport of heat and matter by fluids during metamorphism; *Contrib. Mineral. Petrol.* 95, 384-392.
- Bowers, J. R., *et al.* (1990): Conduction model for the thermal evolution of the Cupsuptic aureole, Maine; *Am. J. Sci.* 290, 644-665.
- Bowman, J. R. and Essene, E. J. (1982): P-T- $X_{\text{CO}_2}$  conditions of contact metamorphism in the Black Butte aureole, Elkhorn, Montana; *Am. J. Sci.* 282, 311-340.
- Bowman, J. R., O'Neil, J. R. and Essene, E. J. (1985): Contact skarn formation at Elkhorn, Montana. II: Origin and evolution of C-O-H skarn fluids; *Am. J. Sci.* 285, 621-660.
- Bowman, J. R., Willett, S. D. and Cook, S. J. (1994): Oxygen isotopic transport and exchange during fluid flow: one-dimensional models and applications; *Am. J. Sci.* 294, 1-55.
- Brandon A.D. and Lambert R. S. (1993): Geochemical characterization of mid-Cretaceous granitoids of the Kootenay Arc in the southern Canadian Cordillera; *Can. J. Earth Sci.* 30, 1076-1090.
- Bucher-Nurminen, K. (1982): On the mechanism of contact aureole formation in dolomitic country rock by the Adamello intrusion (northern Italy); *Am. Min.* 67, 1101-1177.

- Cartwright, I and Buick I. S. (1996): Determining the direction of contact metamorphic fluid flow: an assessment of mineral and stable isotope criteria; *J. Met. Geol.* 14, 289-305.
- Cartwright, I. and Weaver, T. R. (1997): Two-dimensional patterns of metamorphic fluid flow and isotopic resetting in layered and fractured rocks; *J. metamorphic Geol.* 15, 497-512.
- Cook, F. A. and Van der Velden, A.J. (1995): Three-dimensional crustal structure of the Purcell anticlinorium in the Cordillera of southwestern Canada; *GSA Bulletin*, 107-6, 642-664.
- Cook, S.J. *et al.* (1997): Contact Metamorphism Surrounding the Alta Stock: Finite Element Model Simulation of Heat- and  $^{18}\text{O}/^{16}\text{O}$  mass-Transport During Prograde Metamorphism; *Am. J. Sc.* 297, 1-55.
- Coplan, T. B. (1994): Reporting of stable hydrogen, carbon, and oxygen isotopic abundances (Technical Report); *Pure appl. chem.*, 66, 273-276.
- Criss, R. E. and Taylor, H. P. Jr. (1986): Meteoric-Hydrothermal Systems; In: Valley, J. W., Taylor, H. P., Jr. and O'Neil J. R. (eds.): *Stable Isotopes in High Temperature Geological Processes*; *MSA Rev.Min.* Vol 16, 373-444.
- Dipple, G. M. and Ferry J. M. (1992): Fluid flow and stable isotopic alteration in rocks at elevated temperatures with applications to metamorphism; *Geoch. Cosmo. Acta* 56, 3539-3550.
- \_\_\_\_\_ (1996): The effect of thermal history on the development of mineral assemblages during infiltration-driven contact metamorphism; *Contrib. Mineral. Petrol.* 124, 334-345.
- Dipple, G. M. and Niermann, M. C. (1997): Permeability structure of the contact metamorphic-hydrothermal system at Horsethief Creek, British Columbia, Canada; ext. abstract, *Geofluids* 2, Belfast.
- Etheridge, M. A., Wall, V. J. and Vernon, R. H. (1983): The role of the fluid phase during regional metamorphism and deformation; *J. metamorphic Geol.* 1, 205-226.
- Ferry, J. M. (1989): Contact metamorphism of the roof pendants at Hope Valley, Alpine County, California, USA - A record of the hydrothermal system of the Sierra Nevada batholith-; *Contrib. Mineral. Petrol.* 101, 402-417.
- \_\_\_\_\_ (1991): Dehydration and decarbonation reactions as a record of fluid infiltration; in: Kerrick, D. M. (ed.), *Contact Metamorphism*, *MSA Rev.Min.* 26, 351-393.
- \_\_\_\_\_ (1994a): Role of fluid flow in the contact metamorphism of siliceous dolomitic limestones; *Am. Min.* 79, 719-736.

- \_\_\_\_\_ (1994b): A historical review of metamorphic fluid flow; *J. Geophys. Res.* 99 B8, 15,487-15,498.
- Floriet, C. (1996): Characterization of the Horsethief Creek metamorphic aureole at Taurus Notch, southeastern British Columbia; Map 82K/10; B.Sc. thesis, University of British Columbia.
- Furlong, K. P., Hanson, R. B. and Bower, J. R. (1991): Modeling thermal regimes; in: Kerrick, D. M. (ed.), *Contact Metamorphism*, *MSA Rev.Min.*26, 437-505.
- Fyfe, W. S. Price, N. J. and Thompson, A. B. (1978): *Fluids in the Earth's crust*; Elsevier, Amsterdam, 383pp.
- Gerdes, M. L., Baumgartner, L. P. and Person, M. (1995): Stochastic permeability models of fluid flow during contact metamorphism; *Geology* 23/10, 945-948.
- Goldsmith, J. R. and Newton, R. C. (1969): P-T-X relations in the system  $\text{CaCO}_3\text{-MgCO}_3$  at high temperatures and pressures; *Am. J. Sci.* 267A, 160-190.
- Greenwood, H. J. (1975): Buffering of pore fluids by metamorphic reactions; *Am. J. Sci.* 275, 573-93.
- Hay, R. S. and Evans, B. (1988): Intergranular distribution of pore fluid and the nature of high-angle grain boundaries in limestone and marble; *J. Geophys. Res.* 93 B8, 8959-8974.
- Heinrich, W. (1993): Fluid infiltration through metachert layers at the contact aureole of the Bufa del Diente intrusion, northeast Mexico: Implications for wollastonite formation and fluid immiscibility; *Am. Min.*78, 804-818.
- Holness, M. B. (1992): Metamorphism and fluid infiltration of the calc-silicate aureole of the Beinn an Dubhaich Granite, Skye; *J. Petrol.* 33-6, 1261-1293.
- \_\_\_\_\_ (1993): Temperature and pressure dependence of quartz-aqueous fluid dihedral angles: the control of adsorbed  $\text{H}_2\text{O}$  on the permeability of quartzites; *Earth Planet. Sci. Lett.* 117, 363-377.
- \_\_\_\_\_ (1997): Fluid flow paths and mechanisms of fluid infiltration in carbonates during contact metamorphism: the Beinn an Dubhaich aureole, Skye; *J. metamorphic. Geol.* 15, 59-70.
- Holness, M. B. and Fallick, A.E. (1997): Palaeohydrology of the calcsilicate aureole of the Beinn an Dubhaich granite, Skye, Scotland: a stable isotopic study; *J. metamorphic. Geol.* 15, 71-83.

- Holness, M. B. and Graham, C.M. (1991): Equilibrium dihedral angles in the system H<sub>2</sub>O-CO<sub>2</sub>-NaCl-Calcite and implications for fluid flow during metamorphism; *Contrib. Mineral. Petrol.* 108, 368-383.
- \_\_\_\_\_ (1995): P-T-X effects on equilibrium carbonate-H<sub>2</sub>O-CO<sub>2</sub>-NaCl dihedral angles: constraints on carbonate permeability and the role of deformation during fluid infiltration; *Contrib. Mineral. Petrol.* 119, 301-313.
- Hover Granath, V. C., Papike J. J., Labotka, T. C. (1983): The Notch Peak contact metamorphic aureole, Utah: Petrology of the Big Horse Limestone Member of the Orr formation; *GSA bulletin* 94, 889-906.
- Hutchison, C. S. (1974): *Laboratory Handbook of Petrographic Techniques*; Wiley and Sons, New York; p25.
- Jaeger, J. C. (1964): Thermal effects of intrusions; *Rev. Geophys.*,2, 443-466.
- Jamtveit, B., Grorud, H. F. and Bucher-Nurminen, K. (1992): Contact metamorphism of layered carbonate-shale sequences in the Oslo Rift II: Migration of isotopic and reaction fronts around cooling plutons; *Earth Planet. Sci. Lett.* 114, 131-148.
- Kretz, R. (1983): Symbols for rock-forming minerals; *Am. Min.* 68, 277-279.
- Labotka, Th. C., Nabalek, P. I., Papike, J. J. (1988): Fluid infiltration through the Big Horse Limestone Member in the Notch Peak contact-metamorphic aureole, Utah; *Am. Min.* 73, 1302-1324.
- Marchildon, N. and Dipple, G. M. (1998): Irregular isograds, reaction instabilities, and the evolution of permeability during metamorphism; *Geology*, 26/1, 15-18.
- Moore, J. N. and Kerrick, D.M. (1976): Equilibria in siliceous dolomites of the Alta aureole, Utah; *Am. J. Sc.* 276, 502-524.
- Nabalek, P.I. (1991): Stable Isotope Monitors; in: Kerrick, D. M. (ed.), *Contact Metamorphism*, *MSA Rev.Min.*26, 395-435.
- Nabalek, P, I., Labotka, T. C. and Russ-Nabalek, C. (1992): Stable isotope evidence for the role of diffusion, infiltration, and local structure on the contact metamorphism of calc-silicate rocks at Notch Peak, Utah; *J. Petrol.* 33/ 3, 557-583.
- Nabelek, P.I. *et al.* (1984): Contrasting fluid/rock interaction between the Notch Peak granitic intrusion and argillites and limestones in western Utah: evidence from stable isotopes and phase assemblages; *Contrib. Mineral. Petrol.* 86, 25-34.

- Ortoleva, P., *et al.* (1987): Geochemical self-organization II: The reactive-infiltration instability; *Am. J. Sci.* 287, 1008-1040.
- Pattison, D. R. M. and Tracy, R. J. (1991): Phase equilibria and thermobarometry of metapelites; in: Kerrick, D. M. (ed.), *Contact Metamorphism*, MSA Rev.Min.26, 105-206.
- Perkins, E. H., Brown, T. H. and Berman, R. G. (1980): PT-System, TX-System, PX-System: three programs for calculation of pressure - temperature - composition phase diagrams. *Comp. Geosci.* 12, 749-755.
- Philpotts, A. R. (1990): Mineral reactions among solid solutions; in: *Principles of Igneous and Metamorphic Petrology*; Prentice Hall, N. J., 345-367.
- Pouchou, J. L. and Pichoir, F. (1985): PAP  $\phi(\sigma Z)$  procedure for improved quantitative microanalysis; *Microbeam Analysis*, 1985, 104-106.
- Reesor, J. E. (1973): *Geology of the Lardeau map-area, East-half, British Columbia*; GSC Memoir 369.
- Rice, J. M. (1977a): Progressive metamorphism of impure dolomitic limestone in the Marysville aureole, Montana; *Am. J. Sc.* 277, 1-24.
- \_\_\_\_\_ (1977b): Contact Metamorphism of Impure Dolomitic Limestone in the Boulder Aureole, Montana; *Contrib. Mineral. Petrol.* 59, 237-259.
- Schliestedt, M. and Matthews, A. (1987): Transformation of blueschist to greenschist facies rocks as a consequence of fluid infiltration, Sifnos (Cyclades), Greece; *Contrib. Mineral. Petrol.* 97, 237-250.
- Suzuki, K. (1977): Local equilibrium during the contact metamorphism of siliceous dolomites in Kasuga-mura, Japan; *Contrib. Mineral. Petrol.* 61, 79-89.
- Twiss, R. J. and Moores, E. M. (1992): *Structural Geology*; New York, Freeman, 532p.
- Valley, J. W. (1986): Stable Isotope Geochemistry of Metamorphic Rocks; in: Valley, J. W., Taylor, H. P. and O'Neil, J. R. (eds.) *Stable Isotopes in High Temperature Geological Processes*, MSA Rev. Min. 16, 445-489.
- Walther J.V. (1996): Fluid production and isograd reactions at contacts of carbonate-rich and carbonate-poor layers during progressive metamorphism; *J. Metam. Geol.* 14, 351-360.
- Warren M. J. and Price R. A. (1992): Tectonic significance of stratigraphic and structural contrasts between the Purcell Anticlinorium and the Kootenay Arc, East of Duncan Lake (82K); BCGS, *Geol. Fieldwork* 1992, paper 1993-1.

Zhu, C. and Sverjensky, D. A. (1992): F-Cl-OH partitioning between biotite and apatite;  
*Geochim. Cosmochim. Acta* 56, 3425-3467.

**APPENDIX A**

**ELECTRONMICROPROBE DATA  
AND GEOTHERMOMETRY RESULTS**

All results are reported as oxides weight percent and number of cations

Phlogopite (some of the minerals analysed are talc (t) - some of the bad totals reflect chloritization)

Label	Ox%(F)	Ox%(Na)	Ox%(Mg)	Ox%(Al)	Ox%(Si)	Ox%(Cl)	Ox%(K)	Ox%(Ca)	Ox%(Ti)	Ox%(Cr)	Ox%(Mn)	Ox%(Fe)	Ox%(Ni)	Oxide sums
241-1	0.006	0.006	54.575	0.003	42.598	0.027	0.001	0.030	0.002	0.032	0.149	3.999	0.033	101.46
241-2	0.264	0.298	25.661	17.708	38.920	0.081	9.993	0.039	0.387	0.002	0.028	1.388	0.002	94.77
241-3	0.283	0.343	25.057	18.004	38.724	0.115	10.222	0.197	0.430	0.002	0.026	1.524	0.035	94.96
241-4	0.307	0.314	25.272	17.742	38.822	0.082	10.316	0.155	0.430	0.002	0.009	1.614	0.002	95.16
241-5	0.265	0.506	25.160	17.728	39.282	0.081	10.120	0.055	0.747	0.037	0.002	1.426	0.002	95.45
241-6	0.341	0.474	25.925	16.026	39.898	0.002	10.058	0.268	0.472	0.002	0.002	1.462	0.002	94.87
241-7	0.255	0.519	25.252	17.951	39.003	0.069	10.010	0.068	0.735	0.035	0.047	1.492	0.002	95.44
241-8	0.216	0.482	26.517	15.645	39.722	0.020	9.515	0.101	0.704	0.026	0.051	1.470	0.002	94.47
241-9	0.216	0.576	25.748	16.713	39.470	0.047	9.595	0.184	0.787	0.052	0.002	1.476	0.002	94.87
241-10	1.024	0.156	27.885	11.995	43.154	0.190	9.942	0.203	0.513	0.002	0.002	0.726	0.009	95.80
241-11	1.047	0.122	27.874	12.117	42.668	0.084	10.042	0.211	0.457	0.028	0.014	0.766	0.002	95.43
241-12	1.193	0.183	27.760	12.116	43.111	0.056	10.208	0.253	0.474	0.039	0.002	0.694	0.029	96.12
241-13	1.075	0.175	27.690	12.009	43.087	0.003	10.105	0.729	0.450	0.020	0.002	0.652	0.005	96.00
241-14	1.019	0.165	27.918	12.604	42.714	0.110	10.409	0.083	0.462	0.002	0.002	0.753	0.002	96.29
241-15	1.110	0.104	28.186	11.192	44.407	0.072	9.684	0.062	0.330	0.002	0.002	0.582	0.036	95.77
241-16	1.053	0.147	27.600	12.286	42.784	0.161	10.312	0.176	0.478	0.037	0.005	0.747	0.005	95.79
241-17	1.155	0.202	27.500	12.470	42.298	0.215	10.463	0.146	0.480	0.002	0.035	0.652	0.016	95.63
811-1	1.970	0.189	28.351	12.306	43.072	0.035	10.705	0.160	0.391	0.002	0.004	0.819	0.002	98.00
811-2	1.913	0.180	28.292	12.650	42.432	0.045	10.472	0.167	0.543	0.022	0.012	0.794	0.002	97.52
811-3	1.984	0.174	27.871	12.202	43.181	0.035	10.193	0.144	0.702	0.026	0.031	0.814	0.002	97.36
811-4	2.322	0.119	28.446	12.472	42.593	0.036	10.504	0.089	0.473	0.026	0.033	0.971	0.038	98.12
811-5	1.726	0.220	28.353	12.189	43.301	0.021	10.224	0.050	0.428	0.002	0.030	0.711	0.002	97.26
811-6	1.623	0.153	27.504	13.595	41.841	0.085	10.758	0.125	0.399	0.039	0.002	0.949	0.002	97.71
811-7	1.960	0.077	28.784	11.609	43.519	0.048	9.952	0.084	0.119	0.002	0.026	0.697	0.002	96.88
2523-1	1.289	0.330	27.678	12.855	42.648	0.086	10.238	0.190	0.392	0.028	0.045	1.026	0.002	96.81
2523-2	1.365	0.344	27.840	12.888	42.113	0.207	9.550	0.158	0.373	0.002	0.002	1.081	0.002	95.92
1932-1	0.839	0.096	26.920	13.090	42.443	0.252	10.588	0.083	0.561	0.011	0.028	1.300	0.002	96.21
1932-2	0.732	0.121	27.462	12.585	43.067	0.400	10.475	0.073	0.312	0.007	0.033	1.219	0.002	96.47
1932-3	0.948	0.075	27.509	12.512	42.642	0.320	10.568	0.080	0.205	0.011	0.005	1.210	0.002	96.09
1932-4	0.868	0.089	27.099	12.793	43.091	0.215	10.409	0.129	0.492	0.015	0.066	1.302	0.024	96.59
1932-5	0.175	0.141	24.003	1.068	58.524	0.127	0.163	13.523	0.045	0.002	0.028	0.569	0.002	98.37
1932-6	0.170	0.147	24.135	1.068	58.359	0.068	0.188	13.465	0.050	0.007	0.054	0.674	0.010	98.32
1932-7	0.879	0.112	27.501	12.693	43.055	0.224	10.358	0.056	0.491	0.058	0.031	1.022	0.007	96.49
1932-8	0.217	0.076	24.446	0.621	59.098	0.066	0.180	13.520	0.022	0.002	0.018	0.591	0.002	98.86
1932-9	0.802	0.128	27.008	13.875	42.448	0.183	10.466	0.052	0.501	0.067	0.005	0.991	0.010	96.54
1932-10	0.788	0.101	27.625	12.461	43.042	0.196	10.575	0.064	0.466	0.002	0.047	0.887	0.002	96.26
1932-11	0.832	0.101	27.696	12.281	43.467	0.240	10.597	0.056	0.452	0.052	0.005	0.926	0.002	96.71
2221-talc1	0.140	0.060	31.047	0.171	63.674	0.015	0.084	0.090	0.030	0.035	0.016	0.854	0.002	96.20
2221-12	0.212	0.109	30.675	0.264	64.145	0.002	0.032	0.053	0.013	0.002	0.012	0.726	0.028	96.29
2221-13	0.255	0.088	31.067	0.362	63.878	0.002	0.170	0.104	0.002	0.002	0.002	0.802	0.025	96.76
2221-14	0.178	0.055	31.049	0.294	63.701	0.059	0.100	0.101	0.012	0.002	0.002	0.740	0.002	96.29
2221-15	0.241	0.002	35.211	15.074	35.007	0.038	0.013	0.120	0.034	0.024	0.004	1.515	0.002	87.29
2221-16	0.260	0.014	35.471	14.519	35.642	0.015	0.005	0.209	0.028	0.007	0.002	1.314	0.052	87.54
2221-17	0.225	0.030	28.893	5.687	44.681	0.008	0.001	7.392	0.002	0.002	0.002	0.881	0.014	87.88
1313-1	2.226	0.116	25.167	15.926	42.035	0.294	10.543	0.214	0.660	0.067	0.069	1.240	0.014	98.56
1313-2	2.466	0.062	25.281	13.757	44.785	0.233	9.922	0.166	0.520	0.013	0.039	1.189	0.009	98.44
1313-3	2.626	0.059	25.474	14.316	43.354	0.355	10.285	0.114	0.572	0.002	0.016	1.386	0.016	98.57
1313-4	2.644	0.114	25.291	15.098	42.913	0.176	10.404	0.117	0.348	0.046	0.002	0.987	0.055	98.19
1313-5	2.556	0.086	25.352	14.346	43.641	0.135	10.165	0.127	0.386	0.002	0.002	1.158	0.002	97.96
1313-6	2.559	0.099	24.877	12.556	38.721	0.284	8.867	4.089	0.600	0.022	0.002	1.101	0.002	93.78
1313-7	2.920	0.077	25.809	13.167	44.415	0.341	9.862	0.246	0.638	0.050	0.035	1.375	0.002	98.94

Label	Ox%(F)	Ox%(Na)	Ox%(Mg)	Ox%(Al)	Ox%(Si)	Ox%(C)	Ox%(K)	Ox%(Ca)	Ox%(Ti)	Ox%(Cr)	Ox%(Mn)	Ox%(Fe)	Ox%(Ni)	Oxide sums
1313-8	2.641	0.090	25.360	10.613	40.685	0.382	8.226	4.165	0.680	0.002	0.009	1.520	0.017	94.39
2213-1	0.707	0.130	19.976	6.976	31.753	0.086	5.578	19.246	0.224	0.002	0.044	0.475	0.010	85.21
2213-2	1.308	0.095	27.161	11.757	44.371	0.133	10.270	0.294	0.037	0.004	0.037	0.772	0.002	96.58
2213-11	0.603	0.145	28.840	0.168	61.912	0.181	0.036	0.932	0.020	0.002	0.002	0.600	0.061	93.50
2213-12	0.337	0.126	30.008	0.114	63.131	0.080	0.015	0.301	0.002	0.002	0.002	0.644	0.024	94.84
2213-13	0.376	0.141	30.252	0.108	62.462	0.158	0.039	0.331	0.002	0.002	0.002	0.414	0.002	94.29
2213-3	1.286	0.110	27.836	10.815	44.815	0.233	9.125	0.728	0.278	0.002	0.002	0.790	0.002	96.04
2213-14	0.269	0.065	30.767	0.114	63.291	0.007	0.010	0.197	0.004	0.002	0.002	0.569	0.002	95.30
2213-15	0.521	0.124	28.414	0.141	58.938	0.098	0.049	0.794	0.013	0.011	0.002	0.434	0.002	89.54
2213-16	0.304	0.112	28.910	0.107	58.758	0.074	0.035	0.747	0.010	0.002	0.019	0.468	0.028	89.57
2213-17	0.221	0.079	30.703	0.173	62.712	0.010	0.088	0.235	0.002	0.002	0.048	0.498	0.009	94.76
2213-18	0.371	0.065	30.470	0.146	63.112	0.034	0.053	0.288	0.002	0.018	0.005	0.500	0.002	95.06
2213-4	0.964	0.066	27.170	12.484	43.172	0.080	10.474	0.261	0.782	0.002	0.051	0.730	0.002	96.24
2213-5	1.086	0.106	27.403	11.522	44.287	0.063	10.021	0.206	0.403	0.002	0.004	0.706	0.002	95.81
2213-6	1.066	0.122	27.729	11.864	43.700	0.093	10.342	0.225	0.442	0.002	0.018	0.722	0.002	96.33
2213-7	1.155	0.074	27.206	11.974	43.529	0.134	10.310	0.495	0.418	0.002	0.002	0.686	0.002	95.99
2213-8	1.124	0.024	27.708	11.827	43.719	0.101	10.090	0.227	0.413	0.002	0.035	0.736	0.010	96.02
2213-19	0.065	0.041	26.989	0.130	48.297	0.069	0.080	9.642	0.004	0.013	0.053	0.418	0.002	85.80
2821-1	0.755	0.096	24.799	16.077	41.340	0.338	10.307	0.168	0.780	0.032	0.021	0.920	0.003	95.64
2821-2	0.745	0.090	24.559	16.120	40.945	0.199	10.370	0.195	1.034	0.050	0.002	1.370	0.002	95.86
2821-3	0.838	0.089	24.741	16.470	41.387	0.297	10.349	0.241	0.642	0.024	0.012	0.790	0.002	95.88
2821-4	0.569	0.111	23.499	15.818	40.184	0.406	10.061	1.401	0.968	0.002	0.002	1.429	0.002	94.45
2821-5	0.752	0.090	24.736	16.529	41.192	0.282	10.383	0.196	0.600	0.002	0.002	0.620	0.002	95.39
2821-6	0.635	0.092	24.624	16.284	40.984	0.436	10.359	0.247	1.021	0.011	0.042	1.093	0.026	95.85
2821-7	0.621	0.102	25.032	15.772	41.326	0.268	10.168	0.113	0.785	0.002	0.016	0.648	0.002	94.85
2821-8	0.712	0.105	24.641	16.582	41.092	0.342	10.486	0.145	0.865	0.002	0.021	0.937	0.002	95.93
2213-9	1.066	0.038	27.824	11.666	43.845	0.098	10.192	0.272	0.437	0.002	0.002	0.802	0.002	96.24
2811-1	1.642	0.097	24.888	15.742	42.047	0.189	10.510	0.159	0.401	0.035	0.021	0.618	0.002	96.35
2811-2	1.936	0.073	24.638	13.567	41.793	0.434	10.127	0.189	1.067	0.011	0.023	2.223	0.002	96.08
2811-3	1.770	0.098	24.402	15.247	40.938	0.427	10.180	0.266	0.908	0.039	0.007	1.135	0.002	95.42
2811-4	1.651	0.080	16.676	14.798	48.548	0.254	11.691	0.167	0.481	0.048	0.002	1.088	0.002	95.48
2811-5	1.808	0.070	20.622	12.351	51.734	0.291	8.683	0.208	0.409	0.063	0.024	1.321	0.002	97.59
2811-6	1.326	0.076	24.550	15.559	39.102	0.177	6.541	0.587	0.539	0.017	0.023	4.023	0.002	92.52
2811-7	0.812	0.007	18.041	8.438	20.112	0.314	3.318	14.675	0.372	0.004	0.009	1.937	0.004	68.04
2811-8	1.518	0.068	23.587	12.897	37.041	0.280	5.996	1.670	0.610	0.039	0.042	3.092	0.002	86.84
1311-1	2.589	0.088	21.588	11.612	52.338	0.229	9.320	0.133	0.399	0.048	0.002	0.927	0.002	99.27
1311-2	2.390	0.095	24.229	10.887	34.050	0.274	8.137	6.920	0.533	0.004	0.031	1.084	0.004	88.63
1311-3	2.503	0.102	24.441	14.940	41.747	0.171	9.993	0.115	1.533	0.028	0.050	0.948	0.002	96.57
1311-4	2.053	0.039	22.942	9.844	30.109	0.194	7.469	9.875	0.567	0.002	0.002	1.142	0.002	84.24
1311-5	1.865	0.095	24.594	11.154	31.144	0.145	5.593	8.321	0.300	0.002	0.092	1.450	0.002	84.69
1311-6	1.706	0.011	23.759	9.075	25.466	0.141	5.633	12.111	0.460	0.022	0.023	1.244	0.002	79.65
1311-7	2.511	0.078	24.891	13.059	37.834	0.224	9.153	3.579	0.664	0.028	0.002	1.285	0.002	93.31
1311-8	3.238	0.045	25.038	12.146	45.487	0.233	9.823	0.555	0.578	0.002	0.002	1.449	0.002	98.59
1311-9	2.153	0.057	15.513	6.856	65.301	0.085	6.310	0.164	0.142	0.009	0.012	0.540	0.002	97.13
1311-10	3.017	0.108	25.234	12.079	39.285	0.329	9.245	3.536	0.581	0.030	0.038	1.377	0.002	94.86
1311-11	3.087	0.057	25.762	13.150	43.307	0.310	10.204	0.478	0.592	0.009	0.002	1.294	0.002	98.25
1311-12	3.365	0.066	26.520	12.042	45.172	0.174	9.612	0.112	0.175	0.002	0.009	0.712	0.002	97.96
1311-13	1.928	0.111	23.760	16.248	41.600	0.335	10.150	0.052	1.287	0.002	0.002	0.769	0.002	96.35
1311-14	2.424	0.101	24.729	15.352	41.943	0.222	9.856	0.122	1.095	0.011	0.002	0.692	0.002	96.55
1311-15	2.837	0.104	24.960	14.082	42.797	0.269	10.051	0.137	0.806	0.004	0.002	1.328	0.004	97.38
1311-16	1.018	0.038	22.754	4.409	14.222	0.095	3.232	21.737	0.167	0.002	0.052	0.907	0.002	68.63
1311-17	0.677	0.023	19.240	2.255	19.514	0.113	1.853	21.648	0.073	0.002	0.040	0.579	0.002	66.02
1311-18	2.722	0.101	25.879	12.430	38.509	0.311	9.435	3.194	0.429	0.011	0.002	1.116	0.002	94.14

Label	NbCat(F)	NbCat(Na)	NbCat(Mg)	NbCat(Al)	NbCat(Si)	NbCat(Ci)	NbCat(K)	NbCat(Ca)	NbCat(Ti)	NbCat(Cr)	NbCat(Mn)	NbCat(Fe)	NbCat(Ni)	Oxide Sums
241-1	0.002	0.001	10.518	0.001	5.508	0.005	0.000	0.004	0.000	0.003	0.016	0.432	0.003	101.46
241-2	0.083	0.081	5.387	2.939	5.481	0.016	1.795	0.006	0.041	0.000	0.003	0.164	0.000	94.77
241-3	0.089	0.094	5.265	2.991	5.459	0.023	1.838	0.030	0.046	0.000	0.003	0.180	0.004	94.96
241-4	0.096	0.086	5.303	2.944	5.465	0.016	1.853	0.023	0.055	0.000	0.001	0.190	0.000	95.16
241-5	0.083	0.137	5.250	2.925	5.499	0.016	1.807	0.008	0.079	0.004	0.005	0.167	0.000	95.45
241-6	0.107	0.130	5.445	2.662	5.614	0.000	1.808	0.041	0.050	0.000	0.000	0.172	0.000	94.87
241-7	0.079	0.141	5.271	2.963	5.462	0.013	1.788	0.010	0.077	0.004	0.006	0.175	0.000	95.44
241-8	0.068	0.132	5.578	2.602	5.606	0.004	1.713	0.015	0.075	0.003	0.006	0.174	0.000	94.47
241-9	0.068	0.157	5.395	2.769	5.595	0.009	1.721	0.028	0.083	0.006	0.000	0.174	0.000	94.87
2511-10	0.316	0.042	5.771	1.983	5.992	0.037	1.761	0.030	0.054	0.000	0.000	0.084	0.001	95.80
2511-11	0.325	0.033	5.798	1.993	5.954	0.016	1.788	0.032	0.048	0.003	0.002	0.089	0.000	95.43
2511-12	0.368	0.049	5.736	1.980	5.976	0.011	1.805	0.038	0.049	0.004	0.000	0.080	0.003	96.12
2511-13	0.332	0.047	5.728	1.964	5.980	0.001	1.789	0.108	0.047	0.002	0.000	0.076	0.001	96.00
2511-14	0.314	0.044	5.765	2.058	5.918	0.021	1.840	0.012	0.048	0.000	0.006	0.087	0.000	96.29
2511-15	0.341	0.028	5.804	1.822	6.134	0.014	1.707	0.009	0.034	0.000	0.000	0.067	0.004	95.77
2511-16	0.326	0.040	5.728	2.016	5.957	0.031	1.832	0.026	0.050	0.000	0.001	0.087	0.001	95.79
2511-17	0.359	0.055	5.729	2.054	5.912	0.042	1.866	0.022	0.051	0.000	0.004	0.076	0.002	95.63
811-1	0.600	0.050	5.780	1.984	5.892	0.007	1.868	0.024	0.040	0.000	0.000	0.094	0.000	98.00
811-2	0.585	0.048	5.794	2.049	5.831	0.009	1.836	0.025	0.056	0.002	0.001	0.091	0.000	97.52
811-3	0.605	0.046	5.701	1.973	5.925	0.007	1.784	0.021	0.072	0.003	0.004	0.093	0.000	97.36
811-4	0.707	0.032	5.802	2.012	5.829	0.007	1.834	0.013	0.049	0.003	0.004	0.111	0.004	98.12
811-5	0.527	0.059	5.796	1.970	5.939	0.004	1.789	0.007	0.044	0.000	0.003	0.082	0.000	97.26
811-6	0.496	0.041	5.633	2.201	5.749	0.016	1.886	0.018	0.107	0.004	0.000	0.109	0.000	97.71
811-7	0.600	0.021	5.900	1.882	5.985	0.009	1.746	0.012	0.012	0.000	0.003	0.080	0.000	96.88
2523-1	0.396	0.088	5.696	2.092	5.888	0.017	1.803	0.028	0.041	0.003	0.005	0.119	0.000	96.81
2523-2	0.422	0.093	5.769	2.112	5.855	0.040	1.694	0.024	0.039	0.000	0.000	0.126	0.000	95.92
1932-1	0.260	0.026	5.581	2.146	5.904	0.048	1.879	0.012	0.059	0.001	0.003	0.151	0.000	96.21
1932-2	0.226	0.033	5.672	2.052	5.968	0.077	1.852	0.011	0.033	0.001	0.004	0.141	0.000	96.47
1932-3	0.294	0.020	5.712	2.054	5.941	0.062	1.878	0.012	0.022	0.001	0.001	0.141	0.000	96.09
1932-4	0.267	0.024	5.586	2.085	5.959	0.041	1.836	0.019	0.051	0.002	0.008	0.151	0.003	96.59
1932-5	0.050	0.035	4.622	0.163	7.561	0.023	0.027	1.872	0.004	0.000	0.003	0.062	0.000	98.37
1932-6	0.049	0.037	4.654	0.151	7.550	0.012	0.031	1.866	0.005	0.001	0.006	0.073	0.001	98.32
1932-7	0.270	0.030	5.667	2.068	5.952	0.043	1.827	0.008	0.051	0.006	0.004	0.118	0.001	96.49
1932-8	0.062	0.019	4.681	0.094	7.593	0.012	0.029	1.861	0.002	0.000	0.002	0.064	0.000	98.86
1932-9	0.247	0.034	5.562	2.259	5.865	0.035	1.845	0.008	0.052	0.007	0.001	0.115	0.001	96.54
1932-10	0.243	0.027	5.708	2.036	5.967	0.038	1.870	0.010	0.049	0.000	0.006	0.103	0.000	96.26
1932-11	0.255	0.027	5.696	1.997	5.997	0.046	1.865	0.008	0.047	0.006	0.001	0.107	0.000	96.71
1313-1	0.674	0.031	5.105	2.584	5.721	0.055	1.830	0.031	0.068	0.007	0.007	0.141	0.002	98.56
1313-2	0.741	0.016	5.090	2.190	6.049	0.044	1.710	0.024	0.053	0.001	0.004	0.134	0.001	98.44
1313-3	0.794	0.016	5.158	2.292	5.890	0.067	1.782	0.017	0.058	0.000	0.002	0.158	0.002	98.57
1313-4	0.801	0.030	5.132	2.423	5.842	0.033	1.807	0.017	0.036	0.005	0.000	0.112	0.006	98.19
1313-5	0.774	0.023	5.144	2.301	5.940	0.025	1.765	0.019	0.040	0.000	0.000	0.132	0.000	97.96
1313-6	0.826	0.028	5.376	2.145	5.614	0.057	1.640	0.635	0.065	0.003	0.000	0.134	0.000	93.78
1313-7	0.878	0.020	5.196	2.086	5.999	0.064	1.699	0.036	0.065	0.005	0.004	0.155	0.000	98.94

Label	NbCat(F)	NbCat(Na)	NbCat(Mg)	NbCat(Al)	NbCat(Si)	NbCat(C)	NbCat(K)	NbCat(Ca)	NbCat(Ti)	NbCat(Cr)	NbCat(Mn)	NbCat(Fe)	NbCat(Ni)	Oxide sum
1313-8	0.844	0.025	5.427	1.796	5.841	0.076	1.506	0.841	0.073	0.000	0.001	0.183	0.002	94.39
2213-1	0.263	0.042	4.980	1.375	5.311	0.020	1.190	3.449	0.028	0.000	0.006	0.066	0.001	85.21
2213-2	0.401	0.025	5.575	1.908	6.110	0.025	1.804	0.043	0.039	0.001	0.004	0.089	0.000	96.58
2213-3	0.394	0.029	5.717	1.757	6.176	0.029	1.604	0.108	0.044	0.003	0.000	0.091	0.000	96.04
2213-4	0.297	0.018	5.607	2.037	5.978	0.015	1.850	0.039	0.081	0.000	0.006	0.085	0.000	96.24
2213-5	0.335	0.028	5.653	1.880	6.129	0.012	1.769	0.031	0.042	0.000	0.000	0.082	0.000	95.81
2213-6	0.328	0.033	5.712	1.932	6.039	0.018	1.823	0.046	0.046	0.000	0.002	0.083	0.000	96.33
2213-7	0.357	0.020	5.627	1.958	6.040	0.026	1.825	0.074	0.044	0.000	0.000	0.080	0.000	95.99
2213-8	0.346	0.007	5.716	1.929	6.051	0.019	1.781	0.034	0.046	0.000	0.004	0.085	0.001	96.02
2213-9	0.328	0.010	5.731	1.900	6.059	0.019	1.797	0.040	0.043	0.000	0.000	0.093	0.000	96.24
2821-1	0.234	0.026	5.147	2.639	5.757	0.065	1.831	0.025	0.082	0.004	0.003	0.107	0.000	95.64
2821-2	0.231	0.025	5.105	2.650	5.744	0.077	1.841	0.029	0.108	0.006	0.000	0.160	0.000	95.86
2821-3	0.259	0.024	5.118	2.694	5.744	0.057	1.832	0.036	0.067	0.003	0.001	0.092	0.000	95.88
2821-4	0.180	0.031	4.973	2.647	5.705	0.080	1.822	0.213	0.103	0.000	0.000	0.170	0.000	94.45
2821-5	0.233	0.024	5.138	2.715	5.741	0.054	1.846	0.029	0.063	0.001	0.000	0.072	0.000	95.39
2821-6	0.197	0.025	5.112	2.673	5.709	0.084	1.841	0.037	0.107	0.001	0.005	0.127	0.003	95.85
2821-7	0.194	0.028	5.223	2.602	5.785	0.052	1.816	0.017	0.083	0.000	0.002	0.076	0.000	94.85
2821-8	0.220	0.028	5.104	2.716	5.711	0.066	1.859	0.022	0.090	0.000	0.000	0.109	0.000	95.93
2811-1	0.505	0.026	5.129	2.565	5.813	0.036	1.854	0.024	0.042	0.004	0.002	0.071	0.000	96.35
2811-2	0.604	0.020	5.147	2.241	5.857	0.084	1.811	0.028	0.112	0.001	0.003	0.261	0.001	96.08
2811-3	0.553	0.027	5.106	2.523	5.747	0.083	1.823	0.040	0.096	0.004	0.001	0.133	0.000	95.42
2811-4	0.507	0.022	3.428	2.405	6.695	0.049	2.057	0.025	0.050	0.005	0.000	0.126	0.000	95.48
2811-5	0.534	0.018	4.076	1.930	6.861	0.053	1.469	0.030	0.041	0.007	0.003	0.147	0.000	97.59
2811-6	0.424	0.021	5.262	2.637	5.623	0.035	1.200	0.091	0.058	0.002	0.003	0.484	0.000	92.52
2811-7	0.385	0.003	5.733	2.120	4.288	0.093	0.902	3.352	0.060	0.001	0.002	0.345	0.000	68.04
2811-8	0.519	0.020	5.402	2.336	5.691	0.059	1.175	0.275	0.071	0.005	0.005	0.397	0.000	86.54
1311-1	0.754	0.022	4.213	1.792	6.853	0.042	1.557	0.019	0.039	0.005	0.000	0.102	0.000	99.27
1311-2	0.832	0.029	5.645	2.006	5.323	0.059	1.623	1.159	0.063	0.001	0.004	0.142	0.000	88.63
1311-3	0.771	0.027	5.040	2.436	5.776	0.033	1.764	0.017	0.160	0.003	0.006	0.110	0.000	96.37
1311-4	0.765	0.013	5.724	1.942	5.040	0.045	1.595	1.771	0.071	0.000	0.000	0.160	0.000	84.24
1311-5	0.676	0.011	5.970	2.141	5.072	0.033	1.162	1.452	0.037	0.000	0.013	0.197	0.000	84.69
1311-6	0.681	0.004	6.347	1.917	4.565	0.035	1.288	2.326	0.062	0.003	0.003	0.186	0.000	79.65
1311-7	0.816	0.022	5.418	2.247	5.525	0.045	1.705	0.560	0.073	0.003	0.000	0.157	0.000	93.31
1311-8	0.975	0.010	5.052	1.938	6.158	0.044	1.696	0.080	0.059	0.000	0.000	0.164	0.000	98.59
1311-9	0.609	0.011	2.936	1.026	8.293	0.015	1.022	0.022	0.014	0.001	0.001	0.057	0.000	97.13
1311-10	0.966	0.030	5.408	2.047	5.649	0.066	1.696	0.545	0.063	0.004	0.005	0.166	0.000	94.86
1311-11	0.939	0.015	5.248	2.118	5.919	0.059	1.779	0.070	0.061	0.001	0.000	0.148	0.000	98.25
1311-12	1.016	0.017	5.361	1.925	6.127	0.033	1.663	0.016	0.018	0.000	0.001	0.081	0.000	97.96
1311-13	0.593	0.030	4.898	2.649	5.754	0.064	1.791	0.017	0.134	0.006	0.000	0.089	0.000	96.35
1311-14	0.744	0.027	5.084	2.496	5.786	0.042	1.734	0.018	0.114	0.001	0.000	0.080	0.000	96.55
1311-15	0.868	0.028	5.115	2.282	5.884	0.051	1.763	0.020	0.083	0.001	0.000	0.153	0.000	97.38
1311-16	0.510	0.016	7.630	1.169	3.199	0.029	0.928	5.239	0.028	0.000	0.010	0.171	0.000	68.63
1311-17	0.340	0.010	6.467	0.599	4.401	0.035	0.533	5.231	0.012	0.000	0.008	0.109	0.000	66.02
1311-18	0.877	0.028	5.585	2.121	5.576	0.062	1.743	0.496	0.047	0.001	0.000	0.135	0.000	94.14

Tremolite

Label	Ox*(F)	Ox*(Na)	Ox*(Mg)	Ox*(Al)	Ox*(Si)	Ox*(Cl)	Ox*(K)	Ox*(Ca)	Ox*(Ti)	Ox*(Cr)	Ox*(Mn)	Ox*(Fe)	Oxide sum
1932-1	0.051	0.233	23.703	1.899	57.332	0.246	0.186	13.447	0.038	0.020	0.060	0.930	98.14
1932-2	0.093	0.139	24.063	0.984	57.537	0.088	0.183	13.584	0.076	0.002	0.046	0.706	97.48
1932-3	0.093	0.123	23.988	0.773	57.840	0.102	0.138	13.666	0.045	0.041	0.002	0.750	97.56
1932-4	0.278	0.122	23.992	0.888	58.029	0.131	0.125	13.352	0.029	0.033	0.016	0.734	97.73
1932-5	0.206	0.124	23.978	0.932	57.931	0.070	0.143	13.470	0.065	0.013	0.040	0.677	97.65
1932-6	0.144	0.163	23.967	0.998	58.010	0.126	0.123	13.349	0.061	0.002	0.032	0.794	97.77
1932-7	0.175	0.281	23.762	1.778	57.535	0.190	0.208	13.409	0.030	0.002	0.007	0.729	98.11
1214-1	0.154	0.273	23.651	1.687	57.342	0.035	0.136	13.478	0.043	0.002	0.018	1.016	98.03
1214-2	0.062	0.284	23.819	1.804	57.307	0.120	0.148	13.571	0.032	0.044	0.035	1.011	98.24
1214-3	0.021	0.204	23.429	1.433	56.926	0.088	0.128	13.845	0.048	0.004	0.065	1.001	97.19
1214-4	0.348	0.321	23.534	2.198	56.895	0.112	0.165	13.379	0.102	0.002	0.054	1.135	98.24
1214-5	0.236	0.346	23.262	2.279	56.952	0.040	0.137	13.275	0.090	0.002	0.049	1.109	97.78
1214-6	0.144	0.344	23.387	2.303	56.814	0.082	0.138	13.564	0.068	0.017	0.025	1.206	97.87
2221-1	0.465	0.088	23.305	0.210	59.589	0.022	0.058	13.479	0.023	0.009	0.051	0.668	97.96
2221-2	0.258	0.117	24.446	0.263	58.753	0.038	0.065	13.489	0.061	0.002	0.019	0.576	98.09
2221-3	0.279	0.064	23.897	0.218	58.055	0.002	0.042	13.982	0.012	0.002	0.053	0.614	97.22
2221-4	0.237	0.064	24.288	0.228	58.410	0.040	0.054	13.639	0.020	0.002	0.044	0.635	97.66
2221-5	0.194	0.310	23.532	1.751	57.420	0.164	0.177	13.426	0.090	0.002	0.048	0.753	97.80
2221-6	0.197	0.174	22.099	0.933	59.330	0.086	0.093	13.494	0.054	0.002	0.023	0.493	96.98
2221-7	0.006	0.123	24.014	0.686	58.336	0.107	0.061	13.566	0.018	0.002	0.023	0.595	97.54
2213-1	0.231	0.365	24.164	0.811	57.858	0.096	0.143	13.128	0.018	0.002	0.023	0.486	97.32
2213-2	0.226	0.408	24.349	0.992	57.606	0.078	0.170	13.353	0.049	0.050	0.002	0.589	97.87
2213-3	0.318	0.279	24.217	0.549	57.125	0.046	0.124	13.428	0.039	0.050	0.012	0.421	96.41
2213-4	0.138	0.351	24.210	0.758	57.122	0.102	0.164	13.334	0.045	0.002	0.002	0.488	96.89
2213-5	0.329	0.461	24.166	1.193	53.932	0.088	0.128	13.964	0.028	0.002	0.009	0.397	94.70
2213-6	0.397	0.553	24.471	1.864	56.316	0.046	0.634	12.037	0.078	0.022	0.046	0.498	96.96

Tremolite cations per 23 oxygens

Label	NbCat(F)	NbCat(Na)	NbCat(Mg)	NbCat(Al)	NbCat(Si)	NbCat(Cl)	NbCat(K)	NbCat(Ca)	NbCat(Ti)	NbCat(Cr)	NbCat(Mn)	NbCat(Fe)	Oxide sum
1932-1	0.016	0.061	4.801	0.304	7.792	0.046	0.032	1.958	0.004	0.002	0.007	0.106	98.14
1932-2	0.028	0.037	4.900	0.155	7.860	0.017	0.032	1.988	0.008	0.000	0.005	0.081	97.48
1932-3	0.028	0.033	4.878	0.124	7.892	0.019	0.024	1.998	0.005	0.005	0.000	0.086	97.56
1932-4	0.084	0.032	4.867	0.142	7.898	0.025	0.022	1.947	0.003	0.004	0.002	0.084	97.73
1932-5	0.063	0.033	4.867	0.150	7.890	0.013	0.025	1.965	0.007	0.001	0.005	0.077	97.65
1932-6	0.044	0.043	4.860	0.160	7.891	0.024	0.021	1.945	0.006	0.000	0.004	0.090	97.77
1932-7	0.053	0.074	4.809	0.285	7.812	0.036	0.036	1.951	0.003	0.000	0.001	0.083	98.11
1214-1	0.047	0.072	4.834	0.270	7.798	0.007	0.024	1.964	0.004	0.000	0.002	0.116	98.03
1214-2	0.019	0.075	4.822	0.289	7.783	0.023	0.026	1.975	0.003	0.005	0.004	0.115	98.24
1214-3	0.006	0.054	4.796	0.232	7.818	0.017	0.022	2.037	0.005	0.001	0.008	0.115	97.19
1214-4	0.105	0.085	4.771	0.352	7.738	0.021	0.029	1.949	0.011	0.000	0.006	0.129	98.24
1214-5	0.072	0.092	4.729	0.366	7.767	0.008	0.024	1.940	0.009	0.000	0.006	0.127	97.78
1214-6	0.044	0.091	4.754	0.370	7.748	0.012	0.024	1.953	0.007	0.002	0.003	0.138	97.87
2221-1	0.140	0.023	4.699	0.033	8.061	0.004	0.010	1.954	0.002	0.001	0.006	0.076	97.96
2221-2	0.078	0.031	4.932	0.042	7.953	0.007	0.011	1.956	0.006	0.000	0.002	0.065	98.09
2221-3	0.085	0.017	4.874	0.035	7.945	0.000	0.007	2.050	0.001	0.000	0.002	0.070	97.22
2221-4	0.072	0.017	4.926	0.037	7.948	0.008	0.009	1.989	0.002	0.000	0.005	0.072	97.66
2221-5	0.041	0.082	4.777	0.281	7.820	0.031	0.031	1.959	0.009	0.000	0.006	0.086	97.80
2221-6	0.060	0.046	4.490	0.150	8.088	0.016	0.016	1.971	0.006	0.000	0.003	0.056	96.98
2221-7	0.002	0.033	4.871	0.110	7.939	0.020	0.011	1.978	0.002	0.000	0.003	0.068	97.54
2213-1	0.070	0.097	4.918	0.131	7.900	0.018	0.025	1.920	0.002	0.000	0.003	0.056	97.32
2213-2	0.068	0.108	4.939	0.159	7.840	0.015	0.030	1.947	0.005	0.005	0.000	0.067	97.87
2213-3	0.068	0.075	4.980	0.089	7.882	0.009	0.022	1.985	0.004	0.006	0.001	0.049	96.41
2213-4	0.097	0.094	4.961	0.123	7.853	0.019	0.029	1.964	0.005	0.000	0.005	0.056	96.89
2213-5	0.104	0.127	5.105	0.199	7.643	0.017	0.023	2.120	0.003	0.000	0.001	0.047	94.70
2213-6	0.122	0.147	5.014	0.302	7.742	0.009	0.111	1.773	0.008	0.002	0.005	0.057	96.96

**Diopside**

Label	Ox%(Na)	Ox%(Mg)	Ox%(Al)	Ox%(Si)	Ox%(Ca)	Ox%(Ti)	Ox%(Cr)	Ox%(Mn)	Ox%(Fe)	Oxide Sum
811-1	0.227	18.439	0.758	55.124	25.026	0.055	0.024	0.084	0.506	100.2421
811-2	0.111	18.515	0.279	55.486	25.279	0.016	0.015	0.019	0.578	100.2975
811-3	0.045	18.524	0.274	54.972	25.610	0.055	0.002	0.075	0.345	99.9015
811-4	0.276	18.012	1.322	54.824	25.027	0.102	0.002	0.018	0.278	99.8603
2523-1	0.003	18.538	0.093	54.581	25.443	0.042	0.002	0.075	0.513	99.2908
2523-2	0.047	18.537	0.213	55.105	25.295	0.033	0.002	0.061	0.560	99.8535
2523-3	0.022	18.417	0.107	54.638	25.302	0.043	0.002	0.051	0.563	99.1454
2523-4	0.030	18.263	0.233	54.878	25.182	0.002	0.002	0.046	0.677	99.3123
2523-5	0.020	18.416	0.194	54.466	25.491	0.017	0.026	0.002	0.639	99.2699

**Diopside** (cations per 6 oxygens)

Label	NbCat(Na)	NbCat(Mg)	NbCat(Al)	NbCat(Si)	NbCat(Ca)	NbCat(Ti)	NbCat(Cr)	NbCat(Mn)	NbCat(Fe)	Oxide Sum
811-1	0.016	0.989	0.032	1.984	0.965	0.002	0.001	0.003	0.015	100.24
811-2	0.008	0.993	0.012	1.996	0.974	0.000	0.000	0.001	0.017	100.30
811-3	0.003	0.998	0.012	1.987	0.992	0.002	0.000	0.002	0.010	99.90
811-4	0.019	0.969	0.056	1.978	0.967	0.003	0.000	0.001	0.008	99.86
2523-1	0.000	1.006	0.004	1.987	0.993	0.001	0.000	0.002	0.016	99.29
2523-2	0.003	0.999	0.009	1.993	0.980	0.001	0.000	0.002	0.017	99.85
2523-3	0.002	1.000	0.005	1.991	0.988	0.001	0.000	0.002	0.017	99.15
2523-4	0.002	0.990	0.010	1.996	0.981	0.000	0.000	0.001	0.021	99.31
2523-5	0.001	1.000	0.008	1.985	0.995	0.001	0.001	0.000	0.020	99.27

**Forsterite**

Label	Ox%(Na)	Ox%(Mg)	Ox%(Al)	Ox%(Si)	Ox%(Ca)	Ox%(Ti)	Ox%(Cr)	Ox%(Mn)	Ox%(Fe)	Ox%(Ni)	Oxide sum
241-1	0.002	54.414	0.003	42.204	0.108	0.020	0.002	0.184	4.010	0.044	100.99
241-2	0.002	54.615	0.003	42.264	0.039	0.002	0.002	0.182	3.842	0.028	100.98
241-3	0.005	54.229	0.004	42.228	0.062	0.014	0.002	0.205	3.862	0.002	100.61
241-4	0.009	54.445	0.003	42.339	0.044	0.002	0.002	0.126	3.864	0.002	100.84
241-5	0.002	54.276	0.010	42.255	0.032	0.011	0.047	0.232	4.037	0.002	100.91
241-6	0.014	54.069	0.003	42.012	0.065	0.002	0.002	0.184	3.790	0.002	100.14
241-7	0.002	54.310	0.003	42.307	0.146	0.002	0.002	0.233	4.060	0.017	101.08
241-8	0.002	54.377	0.003	41.924	0.039	0.005	0.002	0.166	3.977	0.028	100.52
241-9	0.005	54.159	0.008	42.031	0.054	0.004	0.002	0.205	3.943	0.012	100.42
241-10	0.012	54.187	0.005	42.367	0.078	0.011	0.002	0.220	4.193	0.002	101.08
241-11	0.010	53.633	0.007	42.037	0.063	0.015	0.002	0.201	4.630	0.051	100.65
241-12	0.002	53.384	0.003	42.220	0.036	0.002	0.002	0.209	5.126	0.010	100.99
2511-13	0.002	54.428	0.003	41.829	0.040	0.006	0.002	0.179	3.179	0.012	99.68
2511-14	0.002	54.017	0.003	41.915	0.045	0.002	0.013	0.158	3.049	0.005	99.21
2511-15	0.002	54.435	0.016	41.787	0.018	0.002	0.037	0.158	3.143	0.005	99.60
2511-16	0.009	54.649	0.004	41.999	0.041	0.002	0.019	0.172	2.607	0.017	99.52
2511-17	0.009	54.942	0.003	41.934	0.014	0.011	0.052	0.147	2.559	0.009	99.68
2511-18	0.002	54.693	0.003	42.183	0.039	0.002	0.019	0.156	2.877	0.002	99.98
241-19	0.003	54.549	0.009	42.018	0.025	0.019	0.002	0.140	2.743	0.002	99.51
811-1	0.022	55.736	0.003	42.168	0.014	0.002	0.039	0.121	2.626	0.002	100.73
811-2	0.002	54.270	0.003	39.443	0.034	0.002	0.002	0.149	2.438	0.007	96.35
811-3	0.002	54.241	0.005	41.486	0.097	0.013	0.011	0.140	2.554	0.002	98.55
811-4	0.002	54.641	0.003	41.787	0.067	0.002	0.002	0.122	2.595	0.002	99.22
2523-1	0.002	52.097	0.007	39.375	0.073	0.003	0.002	0.176	3.619	0.010	95.36
2523-2	0.006	51.882	0.005	39.919	0.051	0.028	0.034	0.161	3.718	0.037	95.84
2523-3	0.009	42.080	0.004	30.102	0.018	0.054	0.002	0.157	3.324	0.042	75.79
2523-4	0.002	53.637	0.014	41.750	0.044	0.031	0.002	0.187	4.528	0.019	100.21
2523-5	0.002	53.153	0.003	41.743	0.042	0.005	0.013	0.172	4.767	0.002	99.90
2523-6	0.002	53.049	0.009	41.919	0.002	0.002	0.004	0.190	4.656	0.002	99.84
2523-7	0.002	54.920	0.003	41.921	0.058	0.015	0.002	0.156	2.895	0.002	99.97
2523-8	0.002	53.491	0.093	42.153	0.075	0.031	0.002	0.133	3.904	0.024	99.91
2523-9	0.007	53.841	0.009	42.030	0.049	0.004	0.002	0.148	3.711	0.002	99.80

**Forsterite (cations per 4 oxygens)**

Label	NbCat(Na)	NbCat(Mg)	NbCat(Al)	NbCat(Si)	NbCat(Ca)	NbCat(Ti)	NbCat(Cr)	NbCat(Mn)	NbCat(Fe)	NbCat(Ni)	Oxide sum
241-1	0.000	1.917	0.000	0.998	0.003	0.000	0.000	0.004	0.079	0.001	100.99
241-2	0.000	1.922	0.000	0.998	0.001	0.000	0.000	0.004	0.076	0.001	100.98
241-3	0.000	1.916	0.000	1.001	0.002	0.000	0.000	0.004	0.077	0.000	100.61
241-4	0.000	1.918	0.000	1.001	0.001	0.000	0.000	0.003	0.076	0.000	100.84
241-5	0.000	1.914	0.000	1.000	0.001	0.000	0.001	0.005	0.080	0.000	100.91
241-6	0.001	1.918	0.000	1.000	0.002	0.000	0.000	0.004	0.076	0.000	100.14
241-7	0.000	1.912	0.000	0.999	0.004	0.000	0.000	0.005	0.080	0.000	101.08
241-8	0.000	1.925	0.000	0.996	0.001	0.000	0.000	0.003	0.079	0.001	100.52
241-9	0.000	1.918	0.000	0.999	0.001	0.000	0.000	0.004	0.078	0.000	100.42
241-10	0.001	1.908	0.000	1.001	0.002	0.000	0.000	0.004	0.083	0.000	101.08
241-11	0.000	1.901	0.000	1.000	0.002	0.000	0.000	0.004	0.092	0.001	100.65
241-12	0.000	1.889	0.000	1.002	0.001	0.000	0.000	0.004	0.102	0.000	100.99
2511-13	0.000	1.935	0.000	0.998	0.001	0.000	0.000	0.004	0.063	0.000	99.68
2511-14	0.000	1.927	0.000	1.003	0.001	0.000	0.000	0.003	0.061	0.000	99.21
2511-15	0.000	1.937	0.001	0.998	0.001	0.000	0.001	0.003	0.063	0.000	99.60
2511-16	0.000	1.941	0.000	1.001	0.001	0.000	0.000	0.004	0.052	0.000	99.52
2511-17	0.000	1.948	0.000	0.998	0.000	0.000	0.001	0.003	0.051	0.000	99.68
2511-18	0.000	1.935	0.000	1.001	0.001	0.000	0.000	0.003	0.057	0.000	99.98
2511-19	0.000	1.938	0.000	1.001	0.001	0.000	0.000	0.003	0.055	0.000	99.51
811-2	0.000	1.997	0.000	0.974	0.001	0.000	0.000	0.003	0.050	0.000	96.35
811-3	0.000	1.946	0.000	0.998	0.003	0.000	0.000	0.003	0.051	0.000	98.55
811-4	0.000	1.946	0.000	0.999	0.002	0.000	0.000	0.003	0.052	0.000	99.22
2523-1	0.000	1.945	0.000	0.986	0.002	0.000	0.000	0.004	0.076	0.000	95.36
2523-2	0.000	1.926	0.000	0.994	0.001	0.001	0.001	0.003	0.077	0.001	95.84
2523-3	0.001	1.991	0.000	0.956	0.001	0.001	0.000	0.004	0.088	0.001	75.79
2523-4	0.000	1.909	0.000	0.997	0.001	0.001	0.000	0.004	0.090	0.000	100.21
2523-5	0.000	1.899	0.000	1.000	0.001	0.000	0.000	0.004	0.096	0.000	99.90
2523-6	0.000	1.894	0.000	1.004	0.000	0.000	0.000	0.004	0.093	0.000	99.84
2523-7	0.000	1.945	0.000	0.996	0.002	0.000	0.000	0.003	0.058	0.000	99.97
2523-8	0.000	1.901	0.003	1.005	0.002	0.001	0.000	0.003	0.078	0.001	99.91
2523-9	0.000	1.915	0.000	1.003	0.001	0.000	0.000	0.003	0.074	0.000	99.80

Carbonates Mg, Ca, Mn, Fe, C by stoichiometry O by stoichiometry dolomites labeled (#-Dx) standards labeled s#

Label	Ox%(C)	Ox%(Mg)	Ox%(Ca)	Ox%(Mn)	Ox%(Fe)	oxsum	NbCat(C)	NbCat(O)	NbCat(Mg)	NbCat(Ca)	NbCat(Mn)	NbCat(Fe)	Label
s078-1	44.488	0.132	56.503	0.002	0.002	101.13	2	0	0.007	1.993	0.000	0.000	s078-1
s271-1	48.276	22.071	30.747	0.002	0.080	101.18	2	0	0.998	1.000	0.000	0.002	s271-1
s078-2	45.237	0.168	57.406	0.002	0.002	102.81	2	0	0.008	1.992	0.000	0.000	s078-2
832-1	44.469	2.690	52.754	0.083	0.135	100.13	2	0	0.132	1.862	0.002	0.004	832-1
832-2	44.485	2.410	53.092	0.141	0.168	100.30	2	0	0.118	1.873	0.004	0.005	832-2
832-3	44.605	2.453	53.289	0.002	0.174	100.52	2	0	0.120	1.875	0.000	0.005	832-3
832-4	44.655	2.587	53.131	0.058	0.161	100.59	2	0	0.127	1.868	0.002	0.004	832-4
832-D1	46.903	19.034	30.289	0.045	3.796	100.07	2	0	0.091	1.014	0.001	0.099	832-D1
832-D2	47.520	21.086	30.467	0.062	0.900	100.04	2	0	0.969	1.006	0.002	0.023	832-D2
832-D3	47.095	19.680	30.207	0.021	3.089	100.09	2	0	0.002	1.007	0.001	0.080	832-D3
832-D4	47.481	20.971	30.210	0.072	1.361	100.09	2	0	0.964	0.999	0.002	0.035	832-D4
832-5	44.783	2.689	53.228	0.002	0.120	100.82	2	0	0.131	1.866	0.000	0.003	832-5
832-6	44.523	2.392	53.351	0.031	0.217	100.41	2	0	0.112	1.881	0.001	0.006	832-6
832-7	44.788	1.866	54.310	0.058	0.154	101.18	2	0	0.091	1.903	0.002	0.004	832-7
832-8	45.047	1.302	55.371	0.124	0.156	102.00	2	0	0.063	1.929	0.003	0.004	832-8
832-9	45.132	2.486	53.860	0.072	0.172	101.72	2	0	0.120	1.873	0.002	0.005	832-9
832-10	44.731	1.613	54.678	0.096	0.002	101.12	2	0	0.079	1.919	0.003	0.000	832-10
832-11	44.600	1.913	54.003	0.052	0.164	100.73	2	0	0.094	1.900	0.001	0.005	832-11
832-12	44.380	1.829	53.859	0.024	0.165	100.26	2	0	0.090	1.905	0.001	0.005	832-12
832-13	45.074	2.808	53.198	0.079	0.345	101.50	2	0	0.136	1.852	0.002	0.009	832-13
832-D5	46.742	20.399	30.040	0.097	1.366	98.64	2	0	0.953	1.009	0.003	0.036	832-D5
832-D6	46.953	20.870	29.997	0.059	0.967	98.84	2	0	0.971	1.003	0.002	0.025	832-D6
832-D7	47.051	20.675	30.542	0.041	0.793	99.10	2	0	0.960	1.019	0.001	0.021	832-D7
832-14	44.381	2.554	52.775	0.155	0.184	100.00	2	0	0.126	1.866	0.004	0.004	832-14
832-15	40.488	2.340	48.122	0.089	0.184	100.00	2	0	0.126	1.866	0.004	0.006	832-15
832-16	44.501	1.598	54.400	0.120	0.002	100.61	2	0	0.078	1.919	0.003	0.000	832-16
832-17	43.852	1.713	53.284	0.089	0.182	99.12	2	0	0.085	1.907	0.003	0.005	832-17
832-18	44.858	1.473	54.979	0.021	0.149	101.48	2	0	0.072	1.924	0.001	0.004	832-18
832-D8	47.567	20.941	30.810	0.055	0.803	100.18	2	0	0.961	1.017	0.001	0.021	832-D8
832-D9	47.154	20.839	30.502	0.062	0.698	99.26	2	0	0.965	1.015	0.002	0.018	832-D9
2211-1	44.222	2.362	52.981	0.031	0.076	99.67	2	0	0.117	1.880	0.001	0.002	2211-1
2211-2	44.437	2.376	53.299	0.024	0.002	100.14	2	0	0.117	1.883	0.001	0.000	2211-2
2211-3	43.994	2.253	52.792	0.083	0.089	99.21	2	0	0.108	1.883	0.002	0.003	2211-3
2211-4	44.441	2.203	53.410	0.034	0.164	100.25	2	0	0.108	1.886	0.001	0.005	2211-4
2211-5	44.513	2.384	53.297	0.089	0.047	100.33	2	0	0.117	1.879	0.003	0.001	2211-5
2211-D1	47.102	20.793	30.370	0.052	1.256	99.81	2	0	0.980	1.007	0.001	0.033	2211-D1
2211-D2	44.226	2.172	53.274	0.045	0.031	99.75	2	0	0.107	1.891	0.001	0.001	2211-D2
2211-6	44.251	2.251	53.191	0.055	0.077	99.85	2	0	0.111	1.885	0.001	0.002	2211-6
2211-7	44.131	1.353	54.298	0.017	0.052	99.85	2	0	0.067	1.931	0.001	0.001	2211-7
2211-8	44.195	1.405	54.238	0.069	0.088	99.99	2	0	0.069	1.926	0.002	0.001	2211-8
2211-9	44.364	2.350	53.172	0.041	0.074	100.00	2	0	0.116	1.881	0.001	0.002	2211-9
2211-D3	47.506	21.319	30.026	0.031	1.058	99.94	2	0	0.980	0.992	0.001	0.027	2211-D3
2211-D4	46.751	20.359	30.127	0.002	1.438	98.68	2	0	0.951	1.011	0.000	0.038	2211-D4
2211-11	44.405	2.475	53.017	0.086	0.070	100.05	2	0	0.122	1.874	0.002	0.002	2211-11
2211-12	44.573	2.334	53.488	0.041	0.039	100.48	2	0	0.114	1.864	0.001	0.001	2211-12
2211-13	44.168	2.346	52.916	0.028	0.104	99.56	2	0	0.116	1.880	0.001	0.003	2211-13
2211-14	44.767	2.336	53.653	0.055	0.127	100.94	2	0	0.114	1.881	0.002	0.004	2211-14
2211-D5	47.352	20.872	30.917	0.107	0.386	99.63	2	0	0.962	1.025	0.003	0.010	2211-D5
2211-D6	47.276	20.965	30.324	0.097	0.866	99.53	2	0	0.968	1.007	0.003	0.022	2211-D6
s078	44.324	0.158	56.258	0.002	0.002	100.74	2	0	0.008	1.992	0.000	0.000	s078
S078	0.000	0.000	0.000	0.000	0.000	0.00	0	0	0.000	0.000	0.000	0.000	S078
S271	47.869	21.670	30.809	0.002	0.054	100.40	2	0	0.988	1.010	0.000	0.001	S271
S078	43.664	0.115	55.433	0.031	0.030	99.27	2	0	0.006	1.993	0.001	0.001	S078
S271	47.853	21.665	30.757	0.035	0.068	100.38	2	0	0.989	1.009	0.001	0.002	S271
833-1	44.654	2.016	53.899	0.062	0.190	100.82	2	0	0.099	1.895	0.002	0.005	833-1
833-2	44.181	2.228	52.987	0.052	0.218	99.67	2	0	0.110	1.882	0.001	0.006	833-2

Label	Ox(C )	Ox%(Mg)	Ox%(Ca)	Ox%(Mn)	Ox%(Fe)	oxsum	NbCat(C )	NbCat(O )	NbCat(Mg)	NbCat(Ca)	NbCat(Mn)	NbCat(Fe)	Label
833-3	44.377	2.133	53.392	0.103	0.138	100.14	2	0	0.105	1.888	0.003	0.004	833-3
833-4	44.062	2.191	52.820	0.124	0.231	99.43	2	0	0.109	1.882	0.004	0.006	833-4
833-5	44.601	2.169	53.657	0.110	0.093	100.63	2	0	0.106	1.888	0.003	0.006	833-5
833-6	44.887	2.054	54.178	0.093	0.115	101.33	2	0	0.100	1.894	0.003	0.003	833-6
833-7	44.315	2.029	53.461	0.079	0.158	100.04	2	0	0.100	1.894	0.002	0.004	833-7
833-D1	47.470	20.788	30.965	0.093	0.681	100.00	2	0	0.956	1.024	0.002	0.018	833-D1
833-D2	47.598	21.042	30.746	0.090	0.721	100.20	2	0	0.985	1.024	0.002	0.019	833-D2
833-D3	47.447	20.786	30.957	0.121	0.630	99.94	2	0	0.957	1.024	0.003	0.016	833-D3
833-D4	47.134	20.548	30.637	0.121	0.952	99.39	2	0	0.952	1.026	0.003	0.016	833-D4
833-8	44.139	2.391	52.742	0.048	0.176	99.50	2	0	0.118	1.870	0.001	0.005	833-8
833-10	44.417	2.216	53.356	0.045	0.161	100.19	2	0	0.109	1.908	0.001	0.004	833-10
833-11	43.931	1.716	53.399	0.106	0.140	99.29	2	0	0.085	1.908	0.003	0.004	833-11
833-12	44.132	1.549	53.960	0.076	0.079	99.80	2	0	0.077	1.919	0.002	0.002	833-12
833-13	44.437	2.114	53.542	0.052	0.129	100.27	2	0	0.104	1.891	0.001	0.004	833-13
833-14	44.654	2.347	53.415	0.145	0.138	100.70	2	0	0.115	1.877	0.004	0.004	833-14
833-15	44.431	2.393	53.120	0.041	0.174	100.16	2	0	0.118	1.877	0.001	0.005	833-15
833-D5	47.169	20.610	30.753	0.111	0.761	99.40	2	0	0.954	1.023	0.003	0.020	833-D5
833-D6	47.229	20.747	30.769	0.076	0.629	99.45	2	0	0.959	1.023	0.002	0.016	833-D6
411-1	44.379	2.594	52.806	0.055	0.099	99.95	2	0	0.125	1.868	0.002	0.003	411-1
411-2	44.186	2.520	52.764	0.007	0.037	99.51	2	0	0.125	1.874	0.000	0.001	411-2
411-3	44.396	2.392	53.094	0.065	0.128	100.07	2	0	0.118	1.877	0.002	0.004	411-3
411-4	44.670	1.540	54.607	0.052	0.168	101.04	2	0	0.075	1.919	0.001	0.005	411-4
411-5	44.523	2.532	53.100	0.031	0.111	100.30	2	0	0.124	1.872	0.001	0.003	411-5
411-D1	47.521	20.943	31.216	0.042	0.219	99.94	2	0	0.962	1.031	0.001	0.006	411-D1
411-D2	47.834	21.088	31.308	0.052	0.343	100.62	2	0	0.963	1.027	0.001	0.009	411-D2
411-D3	47.769	21.024	31.361	0.002	0.333	100.49	2	0	0.961	1.030	0.000	0.009	411-D3
411-D4	47.617	20.854	31.367	0.052	0.330	100.22	2	0	0.956	1.034	0.001	0.009	411-D4
411-6	44.083	1.869	53.518	0.065	0.004	99.54	2	0	0.093	1.906	0.002	0.000	411-6
411-7	44.329	2.395	53.120	0.034	0.009	99.89	2	0	0.118	1.881	0.001	0.000	411-7
411-8	44.705	2.450	53.497	0.069	0.008	100.73	2	0	0.120	1.878	0.002	0.002	411-8
411-9	44.619	2.454	53.375	0.007	0.078	100.53	2	0	0.120	1.878	0.000	0.002	411-9
411-D5	47.572	21.067	30.829	0.062	0.555	100.08	2	0	0.967	1.017	0.002	0.014	411-D5
411-D6	47.056	21.089	30.269	0.121	0.334	98.87	2	0	0.979	1.010	0.003	0.009	411-D6
411-10	44.419	2.347	53.291	0.003	0.055	100.11	2	0	0.115	1.883	0.000	0.002	411-10
411-11	44.348	1.714	54.060	0.002	0.083	100.21	2	0	0.084	1.913	0.000	0.002	411-11
411-12	44.091	2.469	52.685	0.014	0.067	99.33	2	0	0.122	1.876	0.000	0.002	411-12
411-13	44.356	2.518	52.914	0.055	0.078	99.92	2	0	0.124	1.872	0.002	0.002	411-13
411-14	44.518	2.508	53.169	0.083	0.007	100.28	2	0	0.123	1.875	0.002	0.002	411-14
411-15	44.349	2.402	53.048	0.045	0.112	99.96	2	0	0.118	1.877	0.001	0.003	411-15
411-16	44.181	2.414	52.854	0.052	0.057	99.56	2	0	0.119	1.878	0.001	0.002	411-16
411-17	44.279	2.577	52.780	0.038	0.038	99.71	2	0	0.127	1.871	0.001	0.001	411-17
411-18	44.216	2.473	52.548	0.041	0.085	99.16	2	0	0.123	1.874	0.001	0.002	411-18
411-19	44.426	2.596	52.955	0.055	0.002	100.03	2	0	0.128	1.871	0.002	0.000	411-19
411-D7	47.235	20.984	30.667	0.073	0.350	99.31	2	0	0.970	1.019	0.002	0.009	411-D7
411-D8	47.794	20.992	31.410	0.024	0.347	100.57	2	0	0.959	1.032	0.001	0.009	411-D8
411-D9	47.824	21.042	31.360	0.052	0.342	100.62	2	0	0.961	1.029	0.001	0.009	411-D9
411-D10	47.417	20.974	30.899	0.097	0.344	99.73	2	0	0.966	1.023	0.003	0.009	411-D10
241-1	44.487	2.104	53.641	0.056	0.057	100.39	2	0	0.103	1.893	0.003	0.002	241-1
241-2	44.453	2.246	53.325	0.086	0.162	100.27	2	0	0.110	1.883	0.002	0.005	241-2
241-3	44.396	2.655	52.770	0.048	0.091	99.96	2	0	0.131	1.866	0.001	0.003	241-3
241-4	44.574	2.413	53.238	0.107	0.153	100.49	2	0	0.118	1.875	0.003	0.004	241-4
241-5	44.567	2.149	53.711	0.093	0.021	100.54	2	0	0.105	1.892	0.001	0.001	241-5
241-6	44.451	2.325	53.230	0.120	0.107	100.23	2	0	0.114	1.880	0.003	0.003	241-6
241-D1	47.686	20.978	31.234	0.035	0.409	100.34	2	0	0.961	1.028	0.001	0.011	241-D1
241-D2	47.638	20.914	31.160	0.155	0.418	100.28	2	0	0.959	1.027	0.004	0.011	241-D2
241-7	44.797	1.941	54.206	0.070	0.070	101.17	2	0	0.095	1.899	0.004	0.002	241-7
241-8	44.663	2.080	53.941	0.096	0.002	100.78	2	0	0.102	1.896	0.003	0.003	241-8
241-9	44.411	2.556	52.910	0.052	0.109	100.04	2	0	0.126	1.870	0.001	0.003	241-9
241-10	44.450	2.568	52.826	0.114	0.195	100.15	2	0	0.126	1.865	0.003	0.005	241-10
241-11	44.445	2.347	53.151	0.134	0.145	100.22	2	0	0.115	1.877	0.004	0.004	241-11
241-12	44.721	1.898	54.187	0.083	0.120	101.01	2	0	0.093	1.902	0.002	0.003	241-12
241-13	44.409	2.284	53.272	0.124	0.052	100.14	2	0	0.112	1.883	0.004	0.001	241-13
241-14	44.559	1.668	54.369	0.089	0.024	100.71	2	0	0.082	1.915	0.003	0.001	241-14

Label	Ox%(C )	Ox%(Mg)	Ox%(Ca)	Ox%(Mn)	Ox%(Fe)	oxsum	NbCat(C )	NbCat(O )	NbCat(Mg)	NbCat(Ca)	NbCat(Mn)	NbCat(Fe)	Label
241-D3	47.747	20.327	31.248	0.155	0.459	100.54	2	0	0.957	1.027	0.004	0.012	241-D3
241-D4	47.859	21.116	31.205	0.117	0.400	100.70	2	0	0.963	1.023	0.003	0.010	241-D4
241-D5	47.998	20.938	31.148	0.090	0.391	100.16	2	0	0.961	1.027	0.002	0.010	241-D5
241-D6	47.617	20.862	31.206	0.190	0.382	100.26	2	0	0.957	1.029	0.005	0.015	241-D6
241-D7	47.720	20.881	31.187	0.138	0.594	100.52	2	0	0.955	1.026	0.004	0.015	241-D7
241-15	43.903	3.033	51.522	0.113	0.146	98.72	2	0	0.151	1.842	0.003	0.004	241-15
241-16	44.308	3.507	51.357	0.021	0.227	99.45	2	0	0.173	1.820	0.001	0.006	241-16
241-17	44.023	3.341	51.419	0.003	0.035	98.82	2	0	0.166	1.853	0.000	0.001	241-17
241-18	44.017	2.983	51.693	0.124	0.190	99.01	2	0	0.148	1.843	0.004	0.005	241-18
241-19	44.550	2.730	52.861	0.031	0.110	100.28	2	0	0.134	1.862	0.001	0.003	241-19
241-20	44.491	2.086	53.614	0.141	0.083	100.41	2	0	0.102	1.891	0.004	0.002	241-20
241-21	44.270	2.136	53.302	0.055	0.121	99.88	2	0	0.105	1.890	0.002	0.003	241-21
241-22	44.751	3.166	52.408	0.103	0.167	100.59	2	0	0.155	1.838	0.003	0.005	241-22
241-23	44.677	3.459	51.918	0.110	0.145	100.31	2	0	0.169	1.824	0.003	0.004	241-23
241-D8	47.284	20.886	30.815	0.052	0.437	99.47	2	0	0.965	1.023	0.001	0.011	241-D8
241-D9	47.586	20.876	31.064	0.124	0.555	100.20	2	0	0.958	1.025	0.003	0.014	241-D9
241-24	44.534	2.876	52.462	0.110	0.255	100.24	2	0	0.141	1.849	0.003	0.007	241-24
241-25	44.083	2.785	52.138	0.072	0.134	99.21	2	0	0.138	1.856	0.002	0.004	241-25
241-26	44.560	2.596	52.960	0.151	0.190	99.21	2	0	0.127	1.865	0.004	0.003	241-26
241-27	43.916	2.515	52.344	0.041	0.110	98.93	2	0	0.125	1.871	0.001	0.003	241-27
241-28	44.455	2.487	53.056	0.100	0.069	100.17	2	0	0.122	1.873	0.003	0.002	241-28
241-29	44.502	3.472	51.750	0.058	0.105	99.89	2	0	0.170	1.825	0.002	0.003	241-29
241-30	44.115	3.275	51.499	0.090	0.113	99.09	2	0	0.162	1.832	0.003	0.003	241-30
241-D10	47.087	20.489	30.925	0.100	0.632	99.23	2	0	0.950	1.031	0.003	0.016	241-D10
241-D11	47.360	20.842	30.859	0.076	0.559	99.70	2	0	0.961	1.023	0.002	0.014	241-D11
241-31	43.788	3.280	51.053	0.124	0.108	98.35	2	0	0.164	1.830	0.004	0.003	241-31
241-32	43.903	3.382	51.052	0.117	0.120	98.57	2	0	0.168	1.825	0.003	0.003	241-32
241-33	44.235	3.397	51.421	0.120	0.160	99.33	2	0	0.168	1.825	0.003	0.004	241-33
241-34	44.278	3.413	51.434	0.093	0.212	99.43	2	0	0.168	1.823	0.003	0.006	241-34
241-35	44.224	3.352	51.427	0.145	0.190	99.34	2	0	0.166	1.825	0.004	0.005	241-35
241-36	44.595	3.286	52.001	0.107	0.216	99.34	2	0	0.161	1.830	0.003	0.006	241-36
2213-37	43.715	2.119	52.673	0.069	0.036	100.21	2	0	0.106	1.891	0.002	0.001	2213-37
2213-38	44.050	2.293	52.996	0.090	0.065	98.61	2	0	0.113	1.882	0.003	0.002	2213-38
2213-39	43.858	1.931	53.435	0.048	0.042	99.43	2	0	0.098	1.899	0.002	0.001	2213-39
2213-40	43.964	0.396	53.095	0.065	0.068	99.02	2	0	0.096	1.900	0.002	0.002	2213-40
2213-41	44.054	2.019	53.149	0.002	0.198	99.88	2	0	0.020	1.975	0.000	0.006	2213-41
2213-D12	47.372	21.046	30.772	0.002	0.400	99.45	2	0	0.970	1.894	0.002	0.004	2213-D12
2213-42	44.189	2.293	52.996	0.065	0.042	99.59	2	0	0.096	1.882	0.000	0.010	2213-42
2213-43	44.050	1.968	53.309	0.065	0.042	99.63	2	0	0.098	1.882	0.003	0.002	2213-43
2213-44	43.856	1.654	53.486	0.072	0.051	99.12	2	0	0.082	1.914	0.002	0.001	2213-44
2213-45	44.283	1.658	54.006	0.031	0.117	100.10	2	0	0.082	1.914	0.001	0.082	2213-45
2213-46	44.264	1.693	53.844	0.124	0.136	100.06	2	0	0.084	1.909	0.004	0.004	2213-46
2213-D13	47.431	21.214	30.567	0.104	0.357	99.67	2	0	0.977	1.012	0.003	0.009	2213-D13
2432-1	44.216	2.524	52.621	0.103	0.165	99.63	2	0	0.125	1.868	0.003	0.005	2432-1
2432-2	44.354	2.656	52.721	0.021	0.110	99.86	2	0	0.131	1.866	0.001	0.003	2432-2
2432-3	44.391	1.661	54.130	0.028	0.132	100.34	2	0	0.082	1.914	0.001	0.004	2432-3
2432-D1	47.618	20.961	31.172	0.090	0.352	100.19	2	0	0.961	1.027	0.002	0.009	2432-D1
2432-D2	47.376	20.912	30.906	0.093	0.382	99.67	2	0	0.964	1.024	0.002	0.010	2432-D2
2432-D3	47.247	20.792	30.892	0.052	0.445	99.43	2	0	0.961	1.026	0.001	0.012	2432-D3
2432-4	43.679	1.505	53.494	0.017	0.074	98.77	2	0	0.075	1.922	0.001	0.002	2432-4
2432-5	44.046	2.650	52.336	0.052	0.080	99.16	2	0	0.131	1.865	0.002	0.002	2432-5
2432-6	43.895	2.646	52.103	0.079	0.112	98.83	2	0	0.132	1.863	0.002	0.003	2432-6
2432-7	43.113	4.433	48.611	0.017	0.107	96.36	2	0	0.235	1.770	0.001	0.005	2432-7
2432-8	43.328	5.213	47.733	0.048	0.242	96.56	2	0	0.253	1.729	0.001	0.007	2432-8
2432-9	43.424	2.559	51.674	0.083	0.043	97.78	2	0	0.129	1.868	0.002	0.001	2432-9
2432-10	43.722	2.195	52.568	0.079	0.036	98.60	2	0	0.110	1.887	0.002	0.001	2432-10
2432-11	43.721	1.891	53.061	0.027	0.002	98.70	2	0	0.094	1.905	0.001	0.000	2432-11
2432-12	43.736	1.816	53.167	0.041	0.041	98.77	2	0	0.091	1.908	0.000	0.001	2432-12
2432-13	44.159	1.752	53.716	0.002	0.149	99.78	2	0	0.087	1.909	0.000	0.004	2432-13
2432-DGL1	47.810	20.812	31.628	0.073	0.364	100.69	2	0	0.951	1.038	0.002	0.006	2432-DGL1
2432-14	44.819	4.076	44.339	0.048	0.211	100.39	2	0	0.199	1.794	0.001	0.009	2432-14
2432-15	43.882	1.540	53.654	0.089	0.064	99.23	2	0	0.077	1.919	0.003	0.002	2432-15
2432-16	44.194	2.638	52.538	0.017	0.120	99.51	2	0	0.130	1.866	0.001	0.003	2432-16

Label	Ox%(C )	Ox%(Mg)	Ox%(Ca)	Ox%(Mn)	Ox%(Fe)	oxsum	NbCat(C )	NbCat(O )	NbCat(Mg)	NbCat(Ca)	NbCat(Mn)	NbCat(Fe)	Label
2432-17	44.012	2.262	52.877	0.021	0.055	99.23	2	0	0.112	1.886	0.001	0.002	2432-17
2432-18	43.917	1.740	53.461	0.096	0.006	99.22	2	0	0.087	1.911	0.003	0.000	2432-18
2432-D6	47.355	20.874	30.889	0.100	0.430	99.65	2	0	0.963	1.024	0.003	0.011	2432-D6
2432-D7	47.234	20.710	31.067	0.086	0.310	99.41	2	0	0.957	1.032	0.002	0.008	2432-D7
2233-1	44.058	2.297	52.834	0.024	0.118	99.33	2	0	0.114	1.882	0.001	0.003	2233-1
2233-2	43.888	2.345	52.599	0.021	0.062	98.91	2	0	0.117	1.881	0.001	0.002	2233-2
2233-3	44.005	2.245	52.791	0.062	0.141	99.24	2	0	0.111	1.883	0.002	0.004	2233-3
2233-4	43.908	1.762	53.314	0.041	0.195	99.22	2	0	0.088	1.906	0.001	0.006	2233-4
2233-5	43.698	2.342	52.263	0.072	0.134	98.51	2	0	0.117	1.877	0.002	0.004	2233-5
2233-6	44.018	1.483	53.911	0.052	0.097	99.56	2	0	0.074	1.922	0.002	0.003	2233-6
2233-D1	47.127	20.846	30.654	0.035	0.438	99.14	2	0	0.966	1.021	0.001	0.011	2233-D1
2233-D2	47.215	20.877	30.720	0.035	0.479	99.33	2	0	0.966	1.021	0.001	0.012	2233-D2
2233-7	43.825	2.412	52.334	0.052	0.147	98.77	2	0	0.120	1.874	0.002	0.004	2233-7
2233-8	43.684	1.246	53.794	0.041	0.102	98.85	2	0	0.062	1.934	0.001	0.003	2233-8
2233-9	43.402	1.530	53.088	0.048	0.066	98.13	2	0	0.077	1.920	0.001	0.002	2233-9
2233-10	43.971	2.482	52.442	0.045	0.128	99.07	2	0	0.123	1.872	0.001	0.004	2233-10
2233-D3	46.733	20.883	29.926	0.038	0.694	98.27	2	0	0.976	1.005	0.001	0.018	2233-D3
2233-D4	46.881	20.827	30.390	0.062	0.417	98.58	2	0	0.970	1.017	0.002	0.011	2233-D4
2233-11	44.181	2.370	52.850	0.069	0.124	98.59	2	0	0.117	1.878	0.002	0.003	2233-11
2233-12	43.505	2.292	52.124	0.052	0.107	98.08	2	0	0.115	1.881	0.002	0.003	2233-12
2233-13	43.794	2.312	52.462	0.083	0.077	98.73	2	0	0.110	1.886	0.002	0.002	2233-13
2233-14	43.194	2.166	51.897	0.065	0.101	97.42	2	0	0.110	1.886	0.002	0.003	2233-14
2233-15	43.933	2.061	53.016	0.041	0.086	99.14	2	0	0.102	1.894	0.001	0.002	2233-15
2233-D5	46.824	20.762	30.349	0.045	0.511	98.49	2	0	0.968	1.017	0.001	0.013	2233-D5
2233-D6	47.215	21.073	30.606	0.007	0.303	99.20	2	0	0.975	1.017	0.000	0.008	2233-D6
2233-D7	47.381	21.238	30.501	0.007	0.416	99.54	2	0	0.979	1.010	0.000	0.011	2233-D7
2233-16	43.560	2.304	52.292	0.002	0.111	98.17	2	0	0.116	1.884	0.000	0.000	2233-16
2233-17	43.711	2.310	52.371	0.103	0.042	98.54	2	0	0.115	1.881	0.003	0.001	2233-17
2233-18	43.436	1.234	53.536	0.072	0.051	98.33	2	0	0.062	1.935	0.002	0.001	2233-18
2233-19	43.768	1.591	53.378	0.152	0.078	98.97	2	0	0.079	1.914	0.004	0.002	2233-19
2233-20	43.921	1.450	53.807	0.096	0.085	99.36	2	0	0.092	1.923	0.002	0.002	2233-20
2233-21	43.974	1.859	53.288	0.045	0.160	99.33	2	0	0.092	1.902	0.001	0.005	2233-21
2233-D8	46.970	21.029	30.221	0.107	0.350	98.99	2	0	0.978	1.010	0.001	0.002	2233-D8
2233-D9	46.745	21.024	29.957	0.052	0.408	98.70	2	0	0.982	1.006	0.001	0.009	2233-D9
2233-D10	46.884	20.925	30.218	0.124	0.405	98.19	2	0	0.975	1.012	0.003	0.011	2233-D10
2233-22	43.773	2.378	52.397	0.101	0.083	98.64	2	0	0.119	1.879	0.000	0.002	2233-22
2233-23	43.741	2.094	52.653	0.093	0.126	98.71	2	0	0.105	1.889	0.003	0.004	2233-23
2233-24	43.671	0.894	54.320	0.031	0.077	98.99	2	0	0.045	1.952	0.001	0.002	2233-24
2233-25	43.850	2.203	52.664	0.107	0.082	98.91	2	0	0.110	1.885	0.003	0.002	2233-25
2233-26	43.625	2.242	52.345	0.028	0.134	98.37	2	0	0.112	1.883	0.001	0.004	2233-26
2233-27	43.812	2.132	52.727	0.041	0.130	98.84	2	0	0.106	1.889	0.001	0.004	2233-27
2233-D11	46.561	20.595	30.197	0.002	0.617	97.97	2	0	0.966	1.018	0.000	0.016	2233-D11
2233-D12	47.417	21.125	30.652	0.104	0.384	99.68	2	0	0.973	1.015	0.003	0.010	2233-D12
2233-D13	47.173	20.938	30.613	0.002	0.471	99.20	2	0	0.969	1.019	0.000	0.012	2233-D13
2233-28	43.673	1.361	53.612	0.086	0.099	98.83	2	0	0.068	1.927	0.002	0.003	2233-28
2233-29	43.662	1.382	53.569	0.127	0.057	98.80	2	0	0.069	1.926	0.004	0.002	2233-29
2233-30	43.403	1.295	53.391	0.107	0.129	98.24	2	0	0.065	1.931	0.001	0.004	2233-30
2233-31	43.683	1.999	52.710	0.100	0.120	98.61	2	0	0.100	1.894	0.003	0.003	2233-31
2233-32	43.652	2.049	52.645	0.065	0.098	98.51	2	0	0.103	1.893	0.002	0.003	2233-32
2233-D14	47.444	20.927	30.864	0.107	0.506	99.85	2	0	0.963	1.021	0.003	0.013	2233-D14
2233-D15	47.167	21.169	30.273	0.004	0.485	99.10	2	0	0.980	1.007	0.000	0.013	2233-D15
1313-1	44.849	1.151	55.475	0.002	0.091	101.57	2	0	0.056	1.941	0.000	0.003	1313-1
1313-2	44.650	0.431	56.189	0.066	0.071	101.41	2	0	0.021	1.975	0.002	0.002	1313-2
1313-3	44.767	0.306	56.554	0.014	0.070	101.71	2	0	0.015	1.983	0.000	0.002	1313-3
1313-4	44.866	0.244	56.817	0.002	0.114	101.95	2	0	0.012	1.988	0.000	0.001	1313-4
1313-D1	47.128	20.888	30.245	0.045	0.914	99.22	2	0	0.968	1.007	0.001	0.024	1313-D1
1313-D2	47.395	21.001	30.399	0.069	0.927	99.79	2	0	0.968	1.007	0.002	0.024	1313-D2
1313-5	44.151	0.263	55.807	0.045	0.065	100.33	2	0	0.013	1.984	0.001	0.002	1313-5
1313-6	44.239	0.488	55.618	0.031	0.065	100.44	2	0	0.024	1.973	0.001	0.002	1313-6
1313-D3	48.053	21.467	30.793	0.045	0.690	101.05	2	0	0.975	1.006	0.001	0.018	1313-D3
1313-D4	47.827	21.273	30.759	0.021	0.736	100.62	2	0	0.971	1.009	0.001	0.019	1313-D4
1313-7	44.496	0.416	56.100	0.024	0.002	101.04	2	0	0.020	1.979	0.001	0.000	1313-7
1313-8	44.338	0.371	55.952	0.031	0.008	100.70	2	0	0.018	1.981	0.001	0.000	1313-8

Label	Ox%(C )	Ox%(Mg)	Ox%(Ca)	Ox%(Mn)	Ox%(Fe)	oxsum	NbCat(C )	NbCat(O )	NbCat(Mg)	NbCat(Ca)	NbCat(Mn)	NbCat(Fe)	Label
1313-9	45.008	1.012	55.703	0.014	0.295	102.03	2	0	0.049	1.943	0.000	0.008	1313-9
1313-10	44.359	1.487	54.298	0.038	0.164	100.35	2	0	0.073	1.921	0.001	0.005	1313-10
1313-11	45.058	1.590	55.001	0.042	0.217	101.91	2	0	0.077	1.916	0.001	0.006	1313-11
1313-12	44.781	0.256	56.613	0.021	0.100	101.77	2	0	0.103	1.984	0.001	0.003	1313-12
1313-13	44.625	0.235	56.516	0.002	0.100	101.40	2	0	0.012	1.988	0.000	0.001	1313-13
1313-14	44.612	0.319	56.401	0.002	0.002	101.33	2	0	0.016	1.984	0.000	0.001	1313-14
1313-D5	47.701	21.309	30.666	0.056	0.552	100.28	2	0	0.975	1.009	0.001	0.014	1313-D5
1313-15	45.140	0.518	56.727	0.038	0.034	102.48	2	0	0.025	1.972	0.001	0.002	1313-15
1313-D6	47.250	21.028	30.413	0.028	0.666	99.39	2	0	0.972	1.010	0.001	0.017	1313-D6
1313-16	45.036	0.589	56.480	0.017	0.096	102.22	2	0	0.029	1.968	0.001	0.003	1313-16
1313-17	44.626	0.335	56.297	0.002	0.130	101.39	2	0	0.016	1.980	0.000	0.004	1313-17
1313-18	44.635	0.375	56.242	0.052	0.092	101.40	2	0	0.018	1.978	0.001	0.003	1313-18
2111-1	43.967	0.675	55.003	0.100	0.006	99.75	2	0	0.034	1.964	0.003	0.000	2111-1
2111-2	44.121	1.541	53.931	0.073	0.114	99.78	2	0	0.076	1.919	0.002	0.003	2111-2
2111-3	43.967	0.848	54.773	0.002	0.092	99.68	2	0	0.042	1.955	0.000	0.003	2111-3
2111-4	44.289	1.880	53.706	0.114	0.031	100.02	2	0	0.093	1.903	0.003	0.001	2111-4
2111-D1	47.049	20.984	30.203	0.101	0.613	98.95	2	0	0.974	1.008	0.003	0.016	2111-D1
2111-5	44.246	1.506	54.182	0.007	0.125	100.07	2	0	0.074	1.922	0.000	0.004	2111-5
2111-6	44.349	2.105	53.461	0.052	0.104	100.07	2	0	0.104	1.892	0.002	0.003	2111-6
2111-7	44.641	2.142	53.755	0.055	0.137	100.73	2	0	0.105	1.890	0.002	0.004	2111-7
2111-8	44.574	0.587	55.914	0.021	0.067	101.16	2	0	0.029	1.969	0.001	0.002	2111-8
2111-9	44.178	1.367	54.320	0.024	0.069	99.96	2	0	0.068	1.930	0.001	0.002	2111-9
2111-10	44.653	0.575	56.017	0.048	0.057	101.35	2	0	0.028	1.969	0.001	0.002	2111-10
2111-11	44.628	2.025	53.947	0.076	0.057	100.73	2	0	0.099	1.897	0.002	0.002	2111-11
2111-12	44.227	0.653	55.344	0.080	0.053	100.36	2	0	0.032	1.964	0.002	0.002	2111-12
2111-13	44.531	0.870	55.399	0.104	0.068	100.97	2	0	0.043	1.953	0.003	0.002	2111-13
2111-D2	47.143	20.954	30.255	0.070	0.784	99.21	2	0	0.971	1.007	0.002	0.020	2111-D2
2111-D3	47.551	21.080	30.695	0.122	0.610	100.06	2	0	0.972	1.013	0.003	0.016	2111-D3
2111-14	44.440	2.188	53.480	0.080	0.053	100.24	2	0	0.108	1.889	0.002	0.002	2111-14
2111-15	44.598	2.099	53.702	0.138	0.127	100.66	2	0	0.103	1.890	0.004	0.004	2111-15
2111-16	44.582	2.146	53.685	0.125	0.068	100.61	2	0	0.105	1.890	0.004	0.002	2111-16
2111-17	44.517	2.193	53.591	0.038	0.070	100.41	2	0	0.108	1.889	0.001	0.002	2111-17
2111-18	44.360	1.408	54.476	0.055	0.061	100.36	2	0	0.069	1.928	0.002	0.002	2111-18
2111-19	44.113	1.453	54.092	0.035	0.091	99.78	2	0	0.072	1.925	0.001	0.003	2111-19
2111-20	44.544	1.877	53.920	0.111	0.181	100.63	2	0	0.092	1.900	0.003	0.003	2111-20
2111-21	44.230	2.123	53.285	0.062	0.094	99.79	2	0	0.105	1.891	0.002	0.003	2111-21
2111-D4	47.347	20.892	30.767	0.045	0.598	99.65	2	0	0.964	1.020	0.001	0.016	2111-D4
S271	48.124	21.702	31.026	0.035	0.100	100.99	2	0	0.985	1.012	0.001	0.003	S271
251-1	44.497	1.992	53.799	0.024	0.143	100.45	2	0	0.098	1.898	0.001	0.004	251-1
251-2	44.790	2.080	53.995	0.066	0.170	101.10	2	0	0.101	1.892	0.002	0.005	251-2
251-3	44.920	1.946	54.430	0.045	0.085	101.43	2	0	0.095	1.902	0.001	0.002	251-3
251-4	44.429	1.922	53.748	0.045	0.201	100.35	2	0	0.095	1.899	0.001	0.006	251-4
251-5	44.705	1.832	54.325	0.038	0.080	100.98	2	0	0.090	1.907	0.001	0.002	251-5
251-6	44.503	2.028	53.809	0.035	0.065	100.44	2	0	0.100	1.898	0.001	0.002	251-6
251-7	44.864	1.939	54.341	0.100	0.064	101.31	2	0	0.094	1.901	0.003	0.002	251-7
251-8	45.455	1.965	55.017	0.079	0.137	102.65	2	0	0.094	1.900	0.002	0.004	251-8
251-9	44.629	1.874	54.098	0.052	0.158	100.81	2	0	0.092	1.903	0.001	0.002	251-9
251-10	44.856	1.848	54.371	0.059	0.217	101.35	2	0	0.090	1.903	0.002	0.006	251-10
251-11	44.717	1.832	54.270	0.048	0.159	101.03	2	0	0.090	1.905	0.001	0.004	251-11
251-12	44.781	1.974	54.172	0.104	0.082	101.11	2	0	0.096	1.899	0.003	0.002	251-12
251-13	44.764	1.989	54.253	0.024	0.002	101.03	2	0	0.097	1.899	0.001	0.000	251-13
251-14	44.473	1.883	54.005	0.052	0.007	100.42	2	0	0.092	1.906	0.001	0.000	251-14
251-15	44.836	2.047	54.153	0.079	0.089	100.42	2	0	0.100	1.896	0.002	0.002	251-15
251-16	44.649	1.870	54.192	0.024	0.105	100.84	2	0	0.092	1.905	0.001	0.003	251-16
251-17	45.031	1.845	54.654	0.090	0.142	101.73	2	0	0.090	1.905	0.003	0.003	251-17
251-18	44.865	1.904	54.373	0.048	0.115	101.33	2	0	0.093	1.902	0.001	0.004	251-18
251-19	44.735	1.836	54.407	0.035	0.020	101.03	2	0	0.090	1.909	0.001	0.001	251-19

### Geothermometry calculations

Mg+Ca are restandardised to 1

Label	rim (r); core (c) midway (m) inclusion (incl)	oxide sum	restandardised Mg+Ca=1 NbCat st Mg	restandardised Mg+Ca=1 NbCat st Ca	T calc: Anovitz & Essene T/K	T/C
241-1		100.39	0.052	0.948	807.00	533.85
241-2		100.27	0.055	0.945	820.55	547.40
241-3		99.96	0.065	0.935	854.75	581.60
241-4		100.49	0.059	0.941	834.58	561.43
241-5		100.54	0.053	0.947	810.89	537.74
241-6		100.23	0.057	0.943	827.50	554.35
241-7	r	101.17				
241-8	c	100.78	0.051	0.949	803.94	530.79
241-9	(c)	100.04	0.063	0.937	846.90	573.75
241-10	r	100.15	0.063	0.937	847.99	574.84
241-11	r	100.22	0.058	0.942	829.58	556.43
241-12		101.01				
241-13		100.14	0.056	0.944	823.97	550.82
241-14		100.71	0.041	0.959	761.55	488.40
241-15	r	98.72				
241-16	(c)	99.45	0.087	0.913	915.21	642.06
241-17	(r)	98.82				
241-18		99.01	0.074	0.926	881.65	608.50
241-19		100.28	0.067	0.933	859.80	586.65
241-20	(r)	100.41	0.051	0.949	805.64	532.49
241-21	c	99.88	0.053	0.947	811.07	537.92
241-22		100.59	0.078	0.922	890.74	617.59
241-23		100.31	0.085	0.915	910.31	637.16
241-24	incl?	100.24	0.071	0.929	871.48	598.33
241-25		99.21	0.069	0.931	866.33	593.18
241-26	c	100.38	0.064	0.936	849.66	576.51
241-27	m	98.93				
241-28	r	100.17	0.061	0.939	840.95	567.80
241-29		99.89	0.085	0.915	911.71	638.56
241-30		99.09	0.081	0.919	900.98	627.83
241-31	"incl" with dol	98.35				
241-32		98.57				
241-33		99.33	0.084	0.916	908.68	635.53
241-34	"incl"	99.43	0.085	0.915	909.54	636.39
241-35		99.34	0.083	0.917	905.94	632.79
241-36		100.21	0.081	0.919	899.72	626.57
2432-1		99.63	0.063	0.937	845.40	572.25
2432-2		99.86	0.065	0.935	854.90	581.75
2432-3		100.34	0.041	0.959	761.44	488.29
2432-4		98.77				
2432-5		99.16	0.066	0.934	856.00	582.85
2432-6		98.83				
2432-10		98.60				
2432-11		98.70				
2432-12		98.77				
2432-13		99.78	0.043	0.957	772.65	499.50
2432-14	beam into a dol	100.39				
2432-15	cracks	99.23				
2432-16		99.51	0.065	0.935	854.28	581.13
2432-17		99.23	0.056	0.944	823.50	550.35
2432-18		99.22	0.043	0.957	772.30	499.15
411-1		99.95	0.064	0.936	850.04	576.89
411-2		99.51	0.062	0.938	844.59	571.44
411-3		100.07	0.059	0.941	833.36	560.21
411-4		101.04				
411-5		100.30	0.062	0.938	844.37	571.22
411-6		99.54	0.046	0.954	785.43	512.28
411-7		99.89	0.059	0.941	833.62	560.47

Label	rim (r); core (c) midway (m) inclusion (incl)	restandardised Mg+Ca=1			T calc: Anovitz & Essene	
		oxide sum	NbCat st Mg	NbCat st Ca	T/K	T/C
411-8		100.73	0.060	0.940	836.63	563.48
411-9		100.53	0.060	0.940	837.33	564.18
411-10		100.11	0.058	0.942	829.14	555.99
411-11		100.21	0.042	0.958	767.49	494.34
411-12		99.33	0.061	0.939	841.03	567.88
411-13		99.92	0.062	0.938	844.02	570.87
411-14		100.28	0.062	0.938	842.23	569.08
411-15		99.96	0.059	0.941	834.45	561.30
411-16		99.56	0.060	0.940	836.04	562.89
411-17		99.71	0.064	0.936	848.94	575.79
411-18		99.16	0.061	0.939	841.83	568.68
411-19		100.03	0.064	0.936	849.70	576.55
832-1		100.13	0.066	0.934	857.36	584.21
832-2		100.30	0.059	0.941	834.88	561.73
832-3		100.52	0.060	0.940	837.58	564.43
832-4		100.59	0.063	0.937	848.37	575.22
832-5		100.82	0.066	0.934	855.50	582.35
832-6		100.41	0.056	0.944	824.34	551.19
832-7		101.18				
832-10		101.12				
832-11		100.73	0.047	0.953	787.93	514.78
832-12		100.26	0.045	0.955	780.21	507.06
832-13		101.50				
832-14		100.00	0.063	0.937	847.26	574.11
832-16		100.61	0.039	0.961	752.22	479.07
832-17		99.12	0.043	0.957	770.05	496.90
832-18		101.48				
833-1		100.82	0.049	0.951	798.24	525.09
833-2		99.67	0.055	0.945	820.25	547.10
833-3		100.14	0.053	0.947	810.67	537.52
833-4		99.43	0.055	0.945	817.74	544.59
833-5		100.63	0.053	0.947	812.83	539.68
833-6		101.33				
833-7		100.04	0.050	0.950	800.98	527.83
833-9		99.50	0.059	0.941	834.65	561.50
833-8		100.19	0.055	0.945	817.87	544.72
833-10		99.29	0.043	0.957	769.99	496.84
833-11		99.80	0.038	0.962	749.09	475.94
833-12		100.27	0.052	0.948	808.41	535.26
833-13		100.70	0.058	0.942	828.71	555.56
833-14		100.16	0.059	0.941	833.41	560.26
2233-1		99.33	0.057	0.943	826.55	553.40
2233-2		98.91				
2233-3		99.24	0.056	0.944	822.43	549.28
2233-4		99.22	0.044	0.956	775.10	501.95
2233-5		98.51				
2233-6		99.56	0.037	0.963	741.21	468.06
2233-7		98.77				
2233-8		98.85				
2233-10		99.07	0.062	0.938	842.97	569.82
2233-11	along vein	99.59				
2233-12	(Tr-Cal /no dol contact)	98.08				
2233-13		98.73				
2233-15	"	99.14				
2233-17	"	98.54				
2233-19	"	98.97				
2233-20	"	99.36				
2233-21	"	99.33				
2233-22		98.64				
2233-23		98.71				
2233-24		98.99				

Label	rim (r); core (c) midway (m) inclusion (incl)	oxide sum	restandardised Mg+Ca=1		T calc: Anovitz & Essene	
			NbCat st Mg	NbCat st Ca	T/K	T/C
2233-25		98.91				
2233-27		98.84				
2233-28		98.83				
2233-29		98.80				
2233-31		98.61				
2233-32		98.51				
2211-1		99.67	0.058	0.942	831.38	558.23
2211-2		100.14	0.058	0.942	831.33	558.18
2211-3		99.21	0.056	0.944	823.06	549.91
2211-4		100.25	0.054	0.946	816.55	543.40
2211-5		100.33	0.059	0.941	831.98	558.83
2211-6		99.75	0.054	0.946	814.36	541.21
2211-7		99.85	0.056	0.944	821.50	548.35
2211-8		99.85				
2211-9		99.99				
2211-10		100.00	0.058	0.942	829.82	556.67
2211-11		100.05	0.061	0.939	840.24	567.09
2211-12		100.47	0.057	0.943	827.26	554.11
2211-13		99.56	0.058	0.942	830.39	557.24
2211-14		100.94	0.057	0.943	826.83	553.68
2213-37		98.61				
2213-38		100.45	0.056	0.944	823.97	550.82
2213-39		99.02	0.048	0.952	792.88	519.73
2213-40		99.88				
2213-41		99.45	0.050	0.950	800.97	527.82
2213-42		99.63	0.057	0.943	825.69	552.54
2213-43		99.43	0.049	0.951	795.84	522.69
2213-44		99.12	0.041	0.959	762.98	489.83
2213-45		100.10	0.041	0.959	761.65	488.50
2213-46		100.06	0.042	0.958	765.91	492.76
2111-1		99.75	0.017	0.983	585.14	311.99
2111-2		99.78	0.038	0.962	748.43	475.28
2111-3		99.68	0.021	0.979	633.78	360.63
2111-4		100.02	0.046	0.954	785.85	512.70
2111-5		100.07	0.037	0.963	743.22	470.07
2111-6		100.07	0.052	0.948	807.78	534.63
2111-7		100.73	0.052	0.948	809.97	536.82
2111-8	in vein (cal-tlc-tr-cat)	101.16				
2111-9	in vein (cal-tlc-tr-cat)	99.96				
2111-10	in vein (cal-tlc-tr-cat)	101.35				
2111-12		100.73	0.050	0.950	798.91	525.76
2111-11		100.36	0.016	0.984	576.14	302.99
2111-13		100.97	0.021	0.979	636.85	363.70
2111-14	area beside vein, no Dio	100.24				
2111-15		100.66	0.052	0.948	806.34	533.19
2111-16		100.61	0.053	0.947	810.73	537.58
2111-17		100.41	0.054	0.946	815.19	542.04
2111-18		100.36	0.035	0.965	729.94	456.79
2111-19		99.78	0.036	0.964	736.96	463.81
2111-20		100.63	0.046	0.954	784.77	511.62
2111-21		99.79	0.053	0.947	810.06	536.91
1313-2	vein	101.41				
1313-5	vein	100.33	0.007	0.993	211.82	-61.33
1313-6		100.44	0.012	0.988	500.01	226.86
1313-7	Ksp-Cal intergrowth	101.04				
1313-8	Ksp-Cal intergrowth	100.70	0.009	0.991	401.66	128.51
1313-10		100.35	0.037	0.963	740.57	467.42
1313-13	veinlet (Cal)	101.40				
1313-14	"	101.33				
1313-17	vein (Dol-Cal)	101.39				
1313-18	"	101.40				

dolomite free sample

rim (r);  
core (c)  
midway (m)  
inclusion (incl)

restandardised Mg+Ca=1

T calc: Anovitz & Essene

Label	oxide sum	NbCat st Mg	NbCat st Ca	T/K	T/C
251-1	100.45	0.049	0.951	796.20	523.05
251-2	101.10				
251-3	101.43				
251-4	100.35	0.047	0.953	789.88	516.73
251-5	100.98	0.045	0.955	778.93	505.78
251-6	100.44	0.050	0.950	799.62	526.47
251-7	101.31				
251-8	102.65				
251-9	100.81	0.046	0.954	783.91	510.76
251-10	101.35				
251-11	101.03				
251-12	101.11				
251-13	101.03				
251-14	100.42	0.046	0.954	784.99	511.84
251-15	101.20				
251-16	100.84	0.046	0.954	783.26	510.11
251-17	101.73				
251-18	101.33				
251-19	101.03				

**APPENDIX B**

**XRF DATA**

## Whole rock analyses - Method and Raw Data

Rock chips of about 4.5 x 2.5 x 2.0 cm were cut, crushed and ground to powder in a ring-mill.

The powders were used for whole rock analyses as well as stable isotope analyses. Powders were thoroughly mixed to make sure that grains were homogeneously distributed. The powders were sent to the Geochemical Laboratories at McGill University, Montreal where they were analyzed by X-ray fluorescence.

Estimates of mineral abundance in the analyzed samples are given below. They are listed in decreasing grade.

**Table B1:** Rough volume percentage of carbonates versus hydrous versus non-hydrous silicates in rocks analyzed

	<b>carbonates</b> calcite and/or dolomite	<b>hydrous silicates</b> tremolite                      phlogopite		<b>non-hydrous silicates</b> Forsterite/Diopside/ K-feldspar
95 Ho 2/5-1	45%			55%
96 Ho 24/2-1	55%		10%	35%
96 Ho 23/2-1	30%		5%	65%
96 Ho 23/2-2	25%		5%	70%
96 Ho 23/2-3	35%		5%	60%
96 Ho 24/3-2	40%		15%	45%
96 Ho 24/1-4	70%		10%	20%
95 Ho 6/2-1	40%		5%	55%
96 Ho 25/1-2	30%		15%	55%
96 Ho 25/2-2	50%		5%	45%
95 Ho 3/1-1	45%	40%	15%	
96 Ho 3/1-2	40%		10%	50%
95 Ho 3/3-1	45%	40%		15%
96 Ho 27/3-2	60%	35%	5%	
95 Ho 19/3-1	55%		5%	50%
96 Ho 10/2-5	25%	75%		
96 Ho 22/4-1	65%	25%		10%
96 Ho 22/3-1	50%	50%		
96 Ho 22/1-2	65%	30%	5%	
95 Ho 12/1-4	55%	40%		5%
95 Ho 12/2-1	20%	80%		
96 Ho 21/3-2	30%	70%		
96 Ho 28/1-2	mostly dolomite with little Ksp - Qtz - Phl			
95 Ho 13/2-2	mostly dolomite with little Ksp - Qtz - Phl			
95 Ho 13/2-1	mostly dolomite with little Ksp - Qtz - Phl			
96 Ho 18/1-1	mostly dolomite with little Ksp - Qtz - Phl			

**Table B2:** XRF results for whole rock carbonate analyses

Sample	SiO <sub>2</sub>	TiO <sub>2</sub>	Al <sub>2</sub> O <sub>3</sub>	Fe <sub>2</sub> O <sub>3</sub>	MnO	MgO	CaO	Na <sub>2</sub> O	K <sub>2</sub> O	P <sub>2</sub> O <sub>5</sub>	BaO	Cu	V	Zn	LOI	Total
2/5-1	39.86	0.063	1.54	0.75	0.062	18.13	27.79	0.12	0.74	0.037	205	38	13	16	10.24	99.36
24/2-1	19.98	0.126	3.23	1.53	0.062	19.89	27.25	0.13	2.27	0.039	254	46	16	47	23.34	97.88
23/2-1	40.83	0.061	1.47	0.90	0.053	18.16	27.22	0.05	0.97	0.027	438	36	12	22	10.22	100.01
23/2-2	43.33	0.058	1.44	0.88	0.046	18.97	25.93	0.06	0.87	0.039	475	19	17	19	8.37	100.05
23/2-3	36.87	0.064	1.55	0.74	0.045	16.81	29.27	0.04	1.03	0.037	585	32	17	16	13.28	99.80
24/3-2	28.06	0.093	2.22	1.20	0.050	19.81	27.55	0.16	1.44	0.037	245	31	17	25	18.96	99.61
24/1-4	18.74	0.060	1.63	1.74	0.229	21.32	29.40	0.18	0.81	0.027	607	46	17	69	25.32	99.53
6/2-1	24.15	0.065	1.82	0.95	0.040	19.79	28.61	0.11	1.16	0.025	489	34	14	37	21.14	97.92
25/1-2	28.95	0.102	2.70	1.06	0.057	18.12	27.05	0.10	1.97	0.052	538	46	22	23	17.78	98.00
25/2-2	40.46	0.042	0.96	1.21	0.061	17.15	28.60	0.08	0.50	0.025	199	33	11	17	10.40	99.51
3/1-1	41.14	0.127	2.89	2.11	0.114	15.23	26.92	0.03	1.49	0.047	312	32	20	47	9.31	99.45
3/1-2	31.44	0.099	2.32	1.46	0.123	18.19	26.97	0.05	1.40	0.038	479	56	16	64	16.37	98.52
3/3-1	29.55	0.121	3.17	0.99	0.062	14.72	28.10	0.10	1.79	0.036	353	40	16	45	20.05	98.73
27/3-2	30.58	0.067	1.71	1.14	0.058	17.33	27.17	0.14	0.45	0.029	38	41	17	20	20.87	99.56
19/3-1	29.81	0.121	2.97	0.98	0.044	15.67	27.37	0.05	2.16	0.048	154	68	16	14	20.03	99.28
10/2-5	46.87	0.091	1.90	1.00	0.041	19.51	20.51	0.30	0.19	0.021	<d/l	23	17	33	9.39	99.83
22/4-1	21.17	0.140	2.69	0.86	0.051	14.59	30.49	0.04	0.14	0.045	24	35	21	18	26.94	97.17
22/3-1	43.60	0.058	1.13	0.88	0.036	18.80	22.79	0.26	0.52	0.035	40	24	11	51	12.30	100.42
22/1-2	24.92	0.094	2.93	0.75	0.043	16.90	27.21	0.13	1.36	0.036	235	29	11	21	24.61	99.01
12/1-4	41.72	0.100	3.44	0.84	0.040	15.56	22.87	0.29	1.55	0.052	2824	44	21	78	13.38	100.14
12/2-1	42.25	0.014	0.23	1.06	0.057	18.25	23.27	0.05	0.05	0.021	51	29	<d/l	33	13.53	98.79
21/3-2	41.84	0.215	5.61	0.72	0.033	12.36	21.52	0.49	3.42	0.046	2030	27	23	22	13.58	100.04
28/1-2	25.29	0.093	2.99	0.71	0.034	14.73	21.16	0.15	2.25	0.034	726	39	19	3	32.22	99.74
13/2-2	11.31	0.053	1.15	0.92	0.042	18.13	26.38	0.09	0.87	0.016	89	30	10	3	40.17	99.14
13/2-1	8.04	0.023	0.45	0.94	0.051	19.37	28.47	0.10	0.35	0.011	47	24	11	4	39.50	97.31
18/1-1	8.95	0.052	1.25	0.81	0.043	18.76	27.45	0.10	0.96	0.013	378	29	<d/l	6	39.40	97.83

\*\*\*\*\*  
 Detection Limits for all oxides and elements (ppm): 60,35,120,30,30,95,15,75,25,35,17,2,10,2,100,

Note: The results are expressed as weight percent, the trace elements (BaO to Zn) as ppm ( $\mu\text{g/g}$ ). Total iron present has been recalculated as  $\text{Fe}_2\text{O}_3$ . In cases where most of the iron was originally in the ferrous state (usually the case with unaltered rocks) a higher total is the result.

<d/l : below detection limit.

Analyses done on fused beads prepared from ignited samples.

Detection limits are based on three times the background sigma values.

Note: regarding low totals in some carbonate analysis:

Low totals are usually a result of incomplete volatilization of  $\text{CO}_2$  from carbonates during a Loss on Ignition (LOI) determination because of its high percentage in them.

In any case the determination of Loss on Ignition is fraught with considerable errors and variations.

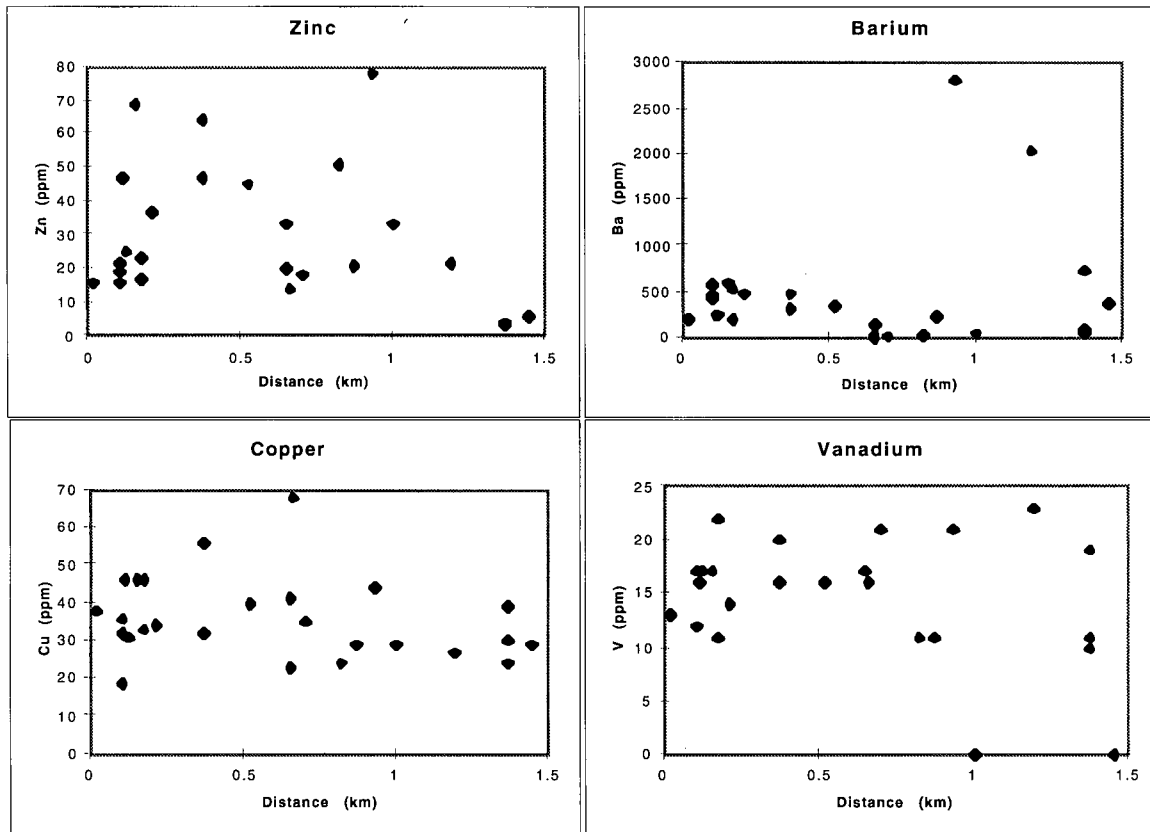


**Figure B1:** Plots of distribution of trace elements Zn, Ba, Cu and V which show a generally homogeneous distribution. A noteworthy exception are two Barium values at  $\approx 1000\text{m}$  distance which are three times the average values. These results coincide with the petrographic observation of Ba-rich feldspars in the same area. Source of the barium might be (late) magmatic fluids from underlying igneous bodies of unknown form or extent. Such a presence of igneous bodies below the contact-metamorphosed rocks may also explain the unusual  $\approx 550^\circ\text{C}$  plateau in the temperature profile recorded in the Horsethief Creek siliceous dolomites.

**APPENDIX C**

**STABLE ISOTOPE DATA**

## C1 Stable Isotopes - Methods - Data - Interpretation of $\delta^{13}\text{C}$ signature

Powders (whole rock carbonate - see appendix B) were sent out to the Stable Isotope Laboratory at Texas A&M university. Analyses are done with a Finnigan Kiel II analysis system using a Finnigan MAT 251 isotope mass spectrometer.

The isotopes were measured against standard NBS-19 and converted into Vienna-PDB (VPDB) values by using  $\delta^{18}\text{O}_{\text{NBS 19/VPDB}} = -2.2\text{‰}$  and  $\delta^{13}\text{C}_{\text{NBS 19/VPDB}} = +1.95\text{‰}$ . The oxygen data was subsequently converted into VSMOW scale by the relation:

$$\delta^{18}\text{O}_{\text{a/VSMOW}} = \delta^{18}\text{O}_{\text{a/b}} + \delta^{18}\text{O}_{\text{b/VSMOW}} + 10^{-3} \delta^{18}\text{O}_{\text{a/b}} \delta^{18}\text{O}_{\text{b/VSMOW}}$$

as recommended by Coplen (1994).

**Table C1-1:** Stable isotope analyses data, samples sorted in increasing grade.

sample #	$\delta^{18}\text{O}$ (NBS 19)	$\delta^{13}\text{C}$ (NBS 19)	$\delta^{18}\text{O}$ (VSMOW)	$\delta^{13}\text{C}$ (VPDB)
2/5-1	-12.39	-3.45	18.17	-5.40
23/2-3	-11.45	-4.73	19.13	-6.68
23/2-2	-12.02	-5.08	18.55	-7.03
23/2-1	-11.43	-4.53	19.16	-6.48
24/2-1	-9.96	-0.91	20.67	-2.86
24/3-2	-9.69	-1.33	20.95	-3.28
24/1-4	-17.04	-4.66	13.38	-6.61
25/1-2	-13.16	-4.14	17.38	-6.09
25/2-2	-12.42	-5.02	18.14	-6.97
6/2-1	-13.60	-2.33	16.92	-4.28
3/1-2	-13.92	-5.78	16.59	-7.73
3/1-1	-13.19	-5.74	17.34	-7.69
3/3-1	-13.52	-4.89	17.01	-6.84
10/2-5	-12.40	-2.61	18.16	-4.56
27/3-2	-11.93	-2.33	18.64	-4.28
19/3-1	-12.27	-3.62	18.29	-5.57
22/4-1	-12.10	-1.55	18.47	-3.51
22/3-1	-10.07	-2.26	20.55	-4.21
22/1-2	-10.64	-1.93	19.97	-3.88
12/1-4	-10.19	-1.25	20.43	-3.20
12/2-1	-12.90	-3.45	17.64	-5.40
21/3-2	-10.55	-1.23	20.06	-3.18
13/2-2	-8.32	-0.18	22.35	-2.13
13/2-1	-8.17	0.18	22.51	-1.77
28/1-2	-8.59	0.66	22.07	-1.29
18/1-1	-8.43	0.21	22.24	-1.74

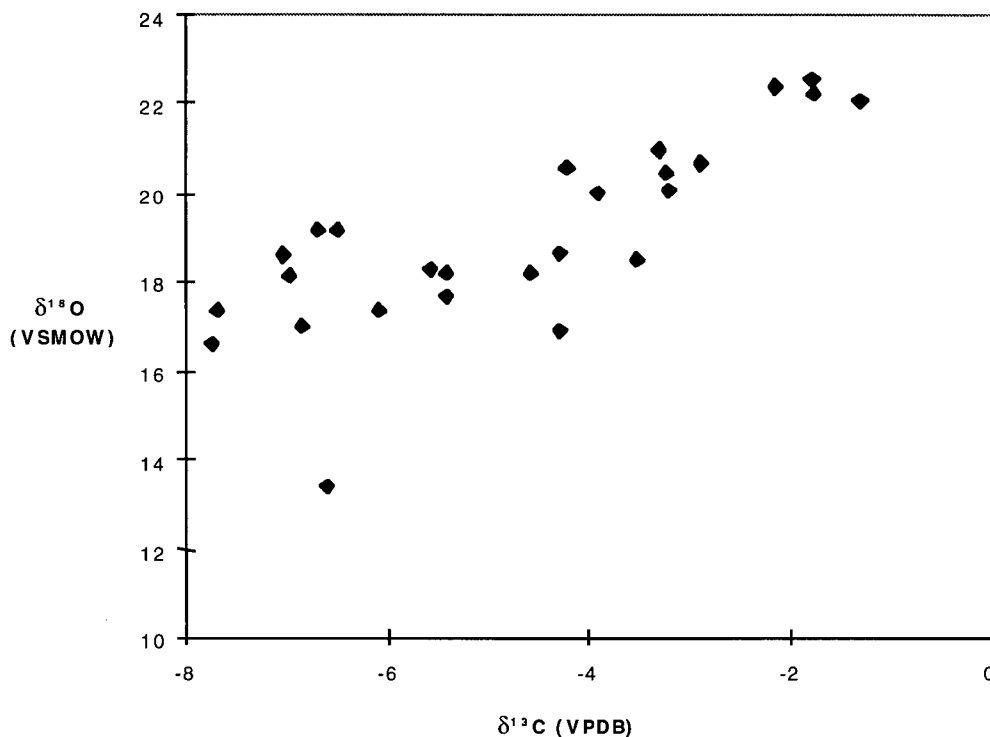


**Figure C1:** This plot shows that not only  $\delta^{18}\text{O}$  but also  $\delta^{13}\text{C}$  values were considerably lowered during contact metamorphism. Possible explanations for the  $\delta^{13}\text{C}$  depletion of  $\approx 6\%$  from  $\approx -2\%$  to  $-8\%$  are Rayleigh fractionation with or without infiltration of an igneous fluid ( $\delta^{13}\text{C} \approx -4$  to  $-6$ ) (see review by Valley 1986). Although no quantification of the amount of carbon remaining in the system ( $F$ ) was done, a rough estimate of these values is considered to be  $F \approx 0.3-0.5$  (for 25-55vol% calcite remaining in the system). For these values of  $F$ , Rayleigh fractionation seems sufficient to explain the lowering in  $\delta^{13}\text{C}$  values. The outlier could reflect either interaction with an igneous fluid which would simultaneously lower both isotope values or it could reflect a lowering of the carbon isotope signature by Rayleigh fractionation analogous to the other samples and subsequent lowering of the oxygen isotope values by low-temperature alteration with involvement of surface waters (see text for more details). The physical meaning of Rayleigh fractionation is one of a fairly open system where evolving fluids are basically constantly removed from the system. This agrees with petrographic observations of closely spaced veins that act as conduits. The linear correlation between  $\delta^{18}\text{O}$  and  $\delta^{13}\text{C}$  is in contrast to the basically missing correlation of oxygen or carbon with distance (cf. Figure 13 and Table C1-1). The reason for this is not clear.

## C2 Silica Weight Percent (whole rock) versus $\delta^{18}\text{O}$ - Evidence for Silica Metasomatism

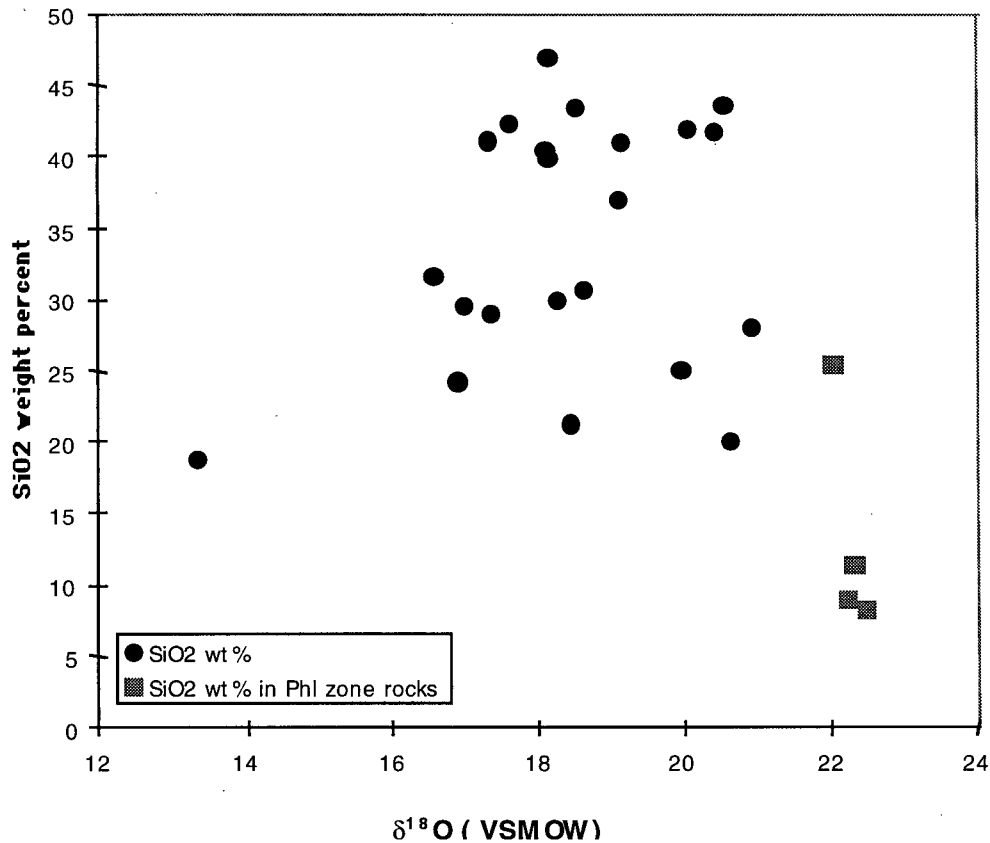


**Figure C2-1:** This  $\text{SiO}_2$  weight percent versus whole rock carbonate oxygen isotope plot shows that there is basically no correlation between the oxygen data and the whole rock XRF data except for a step function at  $\delta^{18}\text{O} \approx 22$ . This step coincides with the step in silica content over distance at  $\approx 1250\text{m}$  (see figure 7) which also is the location of the petrographic break. Hence, there is no correlation between silica content and oxygen isotope data in rocks that record pervasive infiltration ( $\leq 1250\text{m}$ ) but because all of these rocks have significantly higher silica contents than the average phlogopite zone rock ( $\geq 1250\text{m}$ ) it shows that the fluid influx is somehow coupled with silica increase. The random correlation within infiltrated rocks reflects the complex infiltration pattern suggested for the Horsethief Creek aureole.

**APPENDIX D**

**MINERAL FORMULAS**

**AND**

**MOLAR VOLUMES**

**Mineral formulas and molar at standard state 1bar, 298.15 K**

**(after Berman, 1988):**

dolomite	$\text{CaMg}(\text{CO}_3)_2$	$64.32 \text{ cm}^3\text{mol}^{-1}$
calcite	$\text{CaCO}_3$	$36.90 \text{ cm}^3\text{mol}^{-1}$
tremolite	$\text{Ca}_2\text{Mg}_5\text{Si}_8\text{O}_{22}(\text{OH})_2$	$272.68 \text{ cm}^3\text{mol}^{-1}$
diopside	$\text{CaMgSi}_2\text{O}_6$	$66.20 \text{ cm}^3\text{mol}^{-1}$
talc	$\text{Mg}_3\text{Si}_4\text{O}_{10}(\text{OH})_2$	$136.10 \text{ cm}^3\text{mol}^{-1}$
phlogopite	$\text{KMg}_3(\text{AlSi}_3\text{O}_{10})(\text{OH})_2$	$149.77 \text{ cm}^3\text{mol}^{-1}$
K-feldspar	$\text{KAlSi}_3\text{O}_8$	$108.69 \text{ cm}^3\text{mol}^{-1}$
forsterite	$\text{MgSiO}_3$	$43.66 \text{ cm}^3\text{mol}^{-1}$
periclase	$\text{MgO}$	$11.25 \text{ cm}^3\text{mol}^{-1}$
brucite	$\text{Mg}(\text{OH})_2$	$24.68 \text{ cm}^3\text{mol}^{-1}$
quartz	$\text{SiO}_2$	$22.69 \text{ cm}^3\text{mol}^{-1}$

**APPENDIX E**

**SAMPLE NUMBER CONVERSION**

**Table E 1:** List of original and modified sample numbers, including location distances from contact

originally used sample numbers	modified sample numbers	distance from pluton (m)	originally used sample numbers	modified sample numbers	distance from pluton (m)
95Ho18-2	18/2-1	1520	96Ho27-3/2	27/3-2	610
95Ho18-1/1	18/1-1	1440	95Ho3-4	3/4-1	540
95Ho18-1/2	18/1-2	1415	95Ho3-3	3/3-1	540
95Ho13-2/1	13/2-1	1355	95Ho9-1/1	9/1-1	530
95Ho13-2/2	13/2-2	1355	95Ho9-1/2	9/1-2	530
96Ho28-2/1	13/2-3	1355	96Ho23-3/1	23/3-1	505
96Ho28-2/2	13/2-4	1355	96Ho23-3/2	23/3-2	505
96Ho28-1/1	28/1-1	1350	95Ho3-1	3/1-1	365
96Ho28-1/2	28/1-2	1350	95Ho8-3/1	8/3-1	360
96Ho28-1/3	28/1-3	1350	95Ho8-3/2	8/3-2	360
95Ho13-1/2	28/1-4	1350	95Ho8-3/3	8/3-3A	360
95Ho13-1/3	28/1-5	1350	ditto	8/3-3B	360
95Ho15-1/3	15/1-3	1250	95Ho8-4/1	8/4-1A	320
95Ho15-1/4	15/1-4	1250	ditto	8/4-1B	320
95Ho15-1/2a	15/1-5	1250	95Ho8-2	8/2-1	305
95Ho15-1/2b	15/1-6	1250	95Ho8-1/1	8/1-1	270
95Ho15-1/2c	15/1-7	1250	96Ho25-2/1	25/2-1	260
95Ho12-3/1	12/3-1	1240	96Ho25-2/2	25/2-2	260
95Ho12-3/2	12/3-2	1240	96Ho25-2/3	25/2-3A	260
96Ho21-3/1	21/3-1	1150	ditto	25/2-3B	260
96Ho21-3/2	21/3-2A	1150	96Ho25-2/4	25/2-4	260
ditto	21/3-2B	1150	96Ho25-1/1	25/1-1	240
95Ho12-4/1	12/4-1	1125	96Ho25-1/2	25/1-2	240
95Ho12-4/2b	12/4-2	1125	95Ho6-3/1	6/3-1	220
95Ho12+4/1	12/4-3	1125	95Ho6-2	6/2-1	220
96Ho21-2/1	21/2-1	1075	95Ho4-1/1	4/1-1A	215
96Ho21-2/2	21/2-2A	1075	ditto	4/1-1B	215
ditto	21/2-2B	1075	95Ho4-1/2	4/1-2	215
96Ho21-1/1	21/1-1	1010	95Ho4-1/3	4/1-3A	215
96Ho21-1/2	21/1-2	1010	ditto	4/1-3B	215
96Ho21-1/3	21/1-3	1010	96Ho23-1/1	23/1-1	165
95Ho12-2/1	12/2-1	990	96Ho23-1/2	23/1-2	165
95Ho12-1/1	12/1-1	920	96Ho23-1/4	23/1-4	165
95Ho12-1/3a	12/1-3	920	96Ho24-1/1	24/1-1	160
95Ho12-1/4	12/1-4	920	96Ho24-1/2	24/1-2	160
95Ho12-1/5	12/1-5	920	96Ho24-1/3	24/1-3	160
96Ho22-1/1	22/1-1	865	96Ho24-1/4	24/1-4	160
96Ho22-1/2	22/1-2	865	95Ho7-1	7/1-1A	140
96Ho22-1/3	22/1-3A	865	ditto	7/1-1B	140
ditto	22/1-3B	865	96Ho24-3/1	24/3-1	115
96Ho22-2/1	22/2-1	815	96Ho24-3/2	24/3-2	115
96Ho22-2/2	22/2-2	815	96Ho24-3/3	24/3-3	115
96Ho22-2/3	22/2-3	815	95Ho4-3	4/3-1	115
96Ho22-3/1	22/3-1	800	95Ho4-3b	4/3-2	115
96Ho22-3/2	22/3-2A	800	96Ho23-2/1	23/2-1	110
ditto	22/3-2B	800	96Ho23-2/2	23/2-2	110
96Ho22-3/3	22/3-3	800	96Ho23-2/3	23/2-3	110
96Ho22-3/4	22/3-4	800	96Ho24-2/1	24/2-1	100
95Ho17-1	17/1-1	760	96Ho24-2/2	24/2-2	100
96Ho22-4/1	22/4-1	700	96Ho2'-5/1	2/5-1A	25
96Ho22-4/2	22/4-2	700	ditto	2/5-1B	25
95Ho11-1	11/1-1	680	96Ho2'-5/2	2/5-2	25
95Ho10-2/1	10/2-1	670	96Ho2'-5/3	2/5-3	25
95Ho10-2/2	10/2-2	670	96Ho2'-5/4	2/5-4	25
96Ho10+1/1	10/2-3	670	96Ho2'-5/5	2/5-5	25
96Ho10+1/2	10/2-4	670	96Ho2-5	2/5-6	25
96Ho10+1/3	10/2-5	670	96Ho2'-4/1	2/4-1	20
95Ho19-3/1	19/3-1	655	96Ho2-4	2/4-2	20
95Ho19-3/2	19/3-2	655	96Ho2-4+	2/4-3A	20
95Ho14-2/1b	14/2-1	615	ditto	2/4-3B	20
96Ho27-3/1	27/3-1	610	96Ho2-2	2/2-1	20